POLITECNICO DI TORINO

Master Course in Civil Engineering

Master Thesis

Developing Fragility Curves for Earth-Retaining walls due to Dynamic loads

Supervisors:

Prof. Foti Sebastiano

Dr. Cosentini Renato Maria

Candidate

Raslan Alainia

December,2019

ABSTRACT

Studying the influence of the earthquake on different structures interacting with soil has become a priority, due to the devastating damage caused by the earthquake on these types of constructions. In this thesis, the effects of the dynamic load on earth retaining walls have been studied. In particular, the aim of this study is to develop fragility curves for these structures. They describe the probability of a structure being damaged beyond a specific damage state for several levels of ground shaking. In this respect, several numerical models were built to carry out advanced numerical simulations by using a plain strain commercial software *FLAC* (Fast Lagrangian Analysis of Continua), based on the finite difference method.

Models of wall used in analyses are trapezoid shape gravity earth retaining wall with different height. For each wall two main configurations of backfill have been used: in the first one, the surface of backfill is horizontal while in the second one the backfill is inclined of 30°. The geometry of each wall satisfies the safety static condition according to the Italian Technical Code prescription. A non-linear hysteretic model with Mohr-Coulomb failure criterion and viscous damping has been adopted for the foundation and backfill soils, while an elastic model has been used for the wall and bedrock. Literature standard values for soil geotechnical parameters have been assumed. Consistent soil-wall interfaces parameters have been selected, as well. Advanced numerical analyses have been carried out using a set of 18 acceleration time histories selected among real accelerograms recorded at rock outcropping sites for a return period of 475 years. The results of the simulations in terms of permanent relative displacement of the wall and its tilting have been analysed at the first with respect the intensity measures (IMs) of each accelerogram to identify which of IMs are best correlated with the seismic damage of wall. A practically, efficiency and proficiency criteria available in the literature have been adopted. Finally, fragility functions for the earth retaining walls were evaluated.

ACKNOWLEDGMENTS

I acknowledge the university of Politecnico di Torino, Turin, and the DISEG - Department of Structural, Construction and Geotechnical Engineering, especially the Geotechnical engineering department for allowing me access to their facilities in accomplishing this work.

I am deeply indebted to Dr. Cosentini Renato Maria for all the support and guidance he has provided me throughout the course of study and the work on this thesis.

I would also like to thank Prof. Foti Sebastiano for giving me the opportunity of working on this thesis that was a real chance to evolve my research skills.

CONTENTS

List of Tables

CHAPTER1

CHAPTER2

CHAPTER3

List of Figures

CHAPTER1

CHAPTER2

CHAPTER3

Appendix-A

Appendix-B

Appendix-C

INTRODUCTION

One of the oldest issues in geotechnical engineering is understanding the behavior of earth retaining wall structures in seismic events. Earthquake's devastating effects make the issue more significant. Despite many studies over the years, it was not well understood the complex response of earth retaining structures under seismic actions. As a consequence, the current engineering experience therefore, lacks reliable data that can be used in accurate design and development of the earth retaining walls in terms of seismic loads.

The most widely used methods of retaining walls seismic design are equilibrium-based pseudo static analysis (e.g., Mononobe-Okabe 1926, 1929), was the first explicit application for retaining walls, that was too approximate, as it was based on Coulomb's earth pressure analysis under static conditions. Another method that is displacement-based design criteria (e.g., Richard and Elms1979), last but not least time dependent method used is pseudo-dynamic analysis (Steedman and Zeng 1990), that still has some approximations.

As understanding the real reaction of a retaining wall under the static loads is not that easy as it involves a lot of parameters that could vary and still not defined perfectly, as it is too hard to understand deeply the effect of each parameter on the other, an evidence of that is having a lot of constitutive models for the soil itself, which in order make the thinking about the phenomena of interaction between the soil and the wall, and on the other hand the behaving of the wall itself, the study will be much harder when dealing with a dynamic load that is a time dependent load.

This thesis consists the study of eight earth retaining walls that varies in geometry, and divided into two categories of backfills, where the first four walls have flat backfills, the other four have a slope backfills, and a dynamic load of eighteen different accelerograms, that have several intensity measures (IMs), have been applied separately on each wall.

The simulation has been done through implementing a numerical model for each wall on FLAC software, after verifying the static local conditions, the model has been built in the software according to specific properties that are discussed in this thesis, to be analysed initially in its static situation. Then the dynamic loads are applied as mentioned, according to the dynamic characteristics of the software.

The main concentration of this study was to have a simulation for the difference between the real interaction between these earth retaining walls and the soil backfills that is supposed to be supporting a highway and the walls deformations in terms of relative horizontal displacement and tilting of the walls that will be used in developing the fragility curves in terms of the best correlated IMs of the seismic loads based on the probabilistic seismic demand model (PSDM).

Organization of the thesis

This thesis is divided into three chapters, converting from one chapter to the other through the demands the thesis simultaneously.

The first chapter starts by the definition of the numerical models of the walls were done according to the specific properties chosen for this study, then a comparison between software's were done in order to validate the software's and the numerical model, verifying the static conditions of the wall, the numerical model that has been described and defined in its static and dynamic situations at the beginning is statically analysed and the static deformation are saved in order to start the next chapter. The second chapter consists applying the dynamic loads and reading the composite deformation from both the analysis according to each applied load and according to each wall case.

Finally, the last chapter that is the third chapter is including the main comparison criteria that are developing fragility curves for earth-retaining walls, discovered according to the selected IM from the probabilistic seismic demand model study and having some combinations of several cases of the walls that can lead to a better prediction of the selected IM, according to two damage states.

After getting the results of all the analysis, we can conclude our work and the results that we obtained in this thesis, and what further development could be done in order to have a better results and study.

CHAPTER 1: The Definition of Numerical Models of the walls

Several types of earth retaining walls could be used in this study that could have several response according to its type, a gravity retaining wall has been chosen as the general shape of all the walls as shown in Figure 1.1, that has been in this study analysed in two soil backfill cases, flat backfill that is shown in Figure 1.2 and slope backfill that has the same layers as the flat one but with an increment in the last layer with 25º angle, for each case four different walls geometry have been assigned that are shown in Table 1.1, the first step in this chapter was to satisfy the local static verification then has been done for all the walls before analysing them statically on FLAC, then to make a validation of the model by a comparison between FLAC 2D software and DEEPSOIL 1D software in term of dynamic applied load, for a unit grid model, at the end of this chapter a discussion on the static and the dynamic characterisations of the model according to FLAC software has been done.

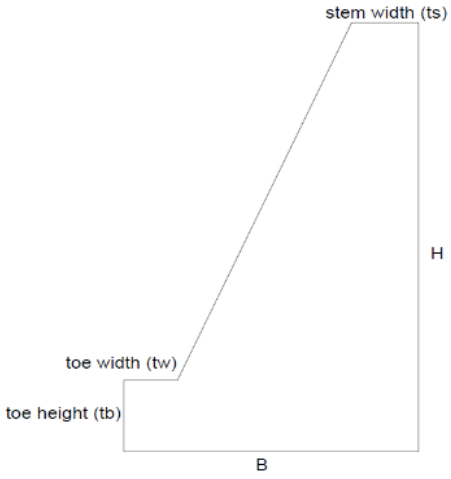

Figure1.1 General shape of walls

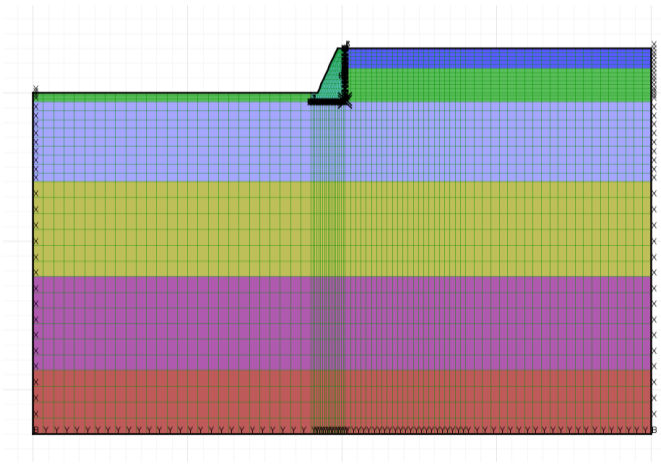

Figure1. 2 Numerical model for the flat case

Table1. 1 Geometries of the walls

Wall Geometry	First wall	Second wall	Third wall	Fourth wall
Stem Width (t_s)	0.5 m	0.65m	0.75m	0.8m
H	3.6 m	4.5 m	5.5 m	6.5 m
B	2.2 m	2.8 m	3.35 m	4 m
Toe Height (t_b)	0.6 m	0.75m	0.8 m	0.8 m
Toe Width (t_w)	0.4 m	0.5 m	0.6 m	0.8 m
γ interaction soil	17(kN/m^3)	17(kN/m^3)	17(kN/m^3)	17(kN/m^3)
γ soil under wall	20(kN/m^3)	20(kN/m^3)	20(kN/m^3)	20(kN/m^3)

1.1 Static design of the wall

In order to analyse the seismic response of the retaining walls, whose geometric characteristics were assigned based on the information chosen as the general shape of the wall as shown in Figure 1.1 and relating to the two cases of the backfill that included one flat case (Figure 1.2) where the other is slope. The modelling of the earth retaining walls was implemented using the FLAC (explicit finite difference software), with the aim of evaluating the mechanical response of the structure both in static conditions and in dynamic conditions. The model has been carried out by assigning the geometric and mechanical characteristics for the first wall are shown in Table 1.1,1.2, and a non-linear visco-elastic stress / strain law and appropriate boundaries to the boundary.

An initial step was done at the beginning which was deciding the geometry of the walls that are going to be modelled and making sure that they fulfil the static verifications which are sliding, tilting and bearing capacity in both cases flat backfill and slope backfill.

The earth retaining walls are constructed as an elastic material for which bulk modulus, shear modulus and mass density are the effective properties. These properties have been given in Table1.2.

Table1.2 Mechanical properties of the models

Layers	Thickness(m)		γ (kN/m^3)	K (MPa)	G (MPa)	c' (kPa)	φ' (º)	Ψ (º)	Models
	Flat	Slope							
Foundation (*purple layer*)	6.3		24	4000	2000	-	-	-	Non-linear hysteretic and Mohr-Coulomb failure criterion and viscous damping
Foundation (*yellow layer*)	6.4		20	378	175	0	37.5	5	
Foundation (*blue layer*)	6		20	270	125	0	37.5	5	
Backfill & foundation (*green layer*)	2.1	4.4	17	126	58.2	0	30	5	
Backfill (*violet layer*)	1.5	3.8	17	72	33.6	0	30	5	
Wall	-		24	3000	3200	-	-	-	Linear viscoelastic

The geometry of the walls satisfies the verifications under static conditions with reference to both the EQU ultimate limit state of static equilibrium (loss of structural equilibrium such as sliding) and the GEO limit state (failure or extreme ground deformation) according to the Italian standards (NTC18) and that is shown for the first wall in (Table 1.6,1.7,1.8), in which an appropriate earth pressure coefficient was calculated according to the slope angle if available and soil friction angle, for both

cases flat and slope, then finding the design friction angle (φ_d) by dividing it by the material partial coefficients for soil geotechnical parameters (γ_φ) that is related to the Italian standards (NTC08) (Table 1.3),

Table1.3 Partial coefficients for soil geotechnical parameters

Parametro	Grandezza alla quale applicare il coefficiente parziale	Coefficiente parziale γ_M	(M1)	(M2)
Tangente dell'angolo di resistenza al taglio	$\tan \varphi'_k$	$\gamma_{\varphi'}$	1,0	1,25
Coesione efficace	c'_k	$\gamma_{c'}$	1,0	1,25
Resistenza non drenata	c_{uk}	γ_{cu}	1,0	1,4
Peso dell'unità di volume	γ_γ	γ_γ	1,0	1,0

After that calculating the actions effecting the wall starting from the design thrust from earth pressure ($K_{a,\beta}$),to compute the horizontal component of design thrust (H_{Ed}), Factorized with the partial coefficients for actions , taking into account the slope case angle $H_{Ed}$is equal to $E_{a,d}\cos(\beta)$ in both action cases favourable and unfavourable factors (Table 1.4), then calculating the stabilizing forces, starting with the total weight of the wall ($W_{total,Gk}$) ,then the vertical/normal component of design weight and thrust (N_{Ed}) for the design sliding resistance (H_{Rd}) is used in the verification of safety against sliding dividing it by the Partial coefficients γ_R for verifying the ultimate limit states of retaining walls (Table 1.5) .

Table1.4 Partial coefficients for actions or the effect of actions

	Effetto	Coefficiente Parziale γ_F (o γ_E)	EQU	(A1)	(A2)
Carichi permanenti G_1	Favorevole	γ_{G1}	0,9	1,0	1,0
	Sfavorevole		1,1	1,3	1,0
Carichi permanenti G_2 [1]	Favorevole	γ_{G2}	0,8	0,8	0,8
	Sfavorevole		1,5	1,5	1,3
Azioni variabili Q	Favorevole	γ_{Qi}	0,0	0,0	0,0
	Sfavorevole		1,5	1,5	1,3

Table1.5 Partial coefficients γ_R for verifying the ultimate limit states of retaining walls

Verifica	Coefficiente parziale (R3)	
Capacità portante della fondazione	$\gamma_R = 1,4$	Bearing capacity of the foundation
Scorrimento	$\gamma_R = 1,1$	Sliding
Ribaltamento	$\gamma_R = 1,15$	Overturning
Resistenza del terreno a valle	$\gamma_R = 1,4$	

Table1.6 Sliding verification for first wall

effect of actions	Formula	Flat(β=0)		Slope(β=25°)		unit
		A1=1.3	A1=1	A1=1.3	A1=1	
Appropriate earth pressure coefficient	$K_{a,\beta}=\left(\frac{cos\beta-\sqrt{cos^2\beta-cos^2\varphi}}{cos\beta+\sqrt{cos^2\beta-cos^2\varphi}}\right)cos\beta$	0.33	0.41	0.49	0.82	-
Design friction angle	$\varphi_d = atan\left(\frac{\tan(\varphi_k)}{\gamma_\varphi}\right)$	0.52 30	0.43 24.79	0.52 30	0.43 24.79	Rad ◦
Design thrust from earth pressure	$E_{a,Gd} = \gamma_G K_{a\beta,d}\left(\frac{1}{2}\gamma_k H^2\right)$	47.73	45.07	69.52	90.65	(kN/m)
Horizontal component of design thrust	$H_{Ed} = E_{a,d}\cos(\beta)$	47.73	45.07	63.19	82.39	(kN/m)
Stem weight of the wall	$W_{stem,Gk}=\gamma_{c,k}.t_s$.H	31.68	31.68	31.68	31.68	(kN/m)
base weight of the wall	$W_{base,Gk}=\gamma_{c,k}.t_b$.B	36	36.00	36	36	(kN/m)
Triangle area weight of the wall	$W_{traingle,Gk}=\gamma_{c,k}\cdot\frac{1}{2}$.(H - t_b).(B - t_s- t_w)	46.8	46.80	46.8	46.8	(kN/m)
Total weight of wall	$W_{total,Gk} = W_{stem,Gk} + W_{base,Gk} + W_{traingle,Gk}$	114.48	114.48	114.48	114.48	(kN/m)
Vertical/normal component of design weight and thrust	$N_{Ed}=\gamma_G W_{Gk} + E_{a,d}\sin(\beta)$	148.82	114.48	177.80	152.27	(kN/m)
Design sliding resistance	$H_{Rd} = \gamma_{G1,fav} N_{Ed}\tan(\delta_d)$	168.57	133.19	188.43	159.73	(kN/m)
Verification of resistance to sliding	ODF = $\frac{H_{Rd}}{\gamma_R H_{Ed}}$	2.01	1.69	1.70	1.11	-

The second verification was the overturning (Table 1.7) in which is the moments about wall toe and the summation of them are the design overturning moments (M_{Gd}), destabilizing moments, about wall toe then calculating the stabilizing forces, having the total weight of the wall, as a design restoring moments(M_{Rd}), stabilizing moments, about wall toe,to get the overdesign factor that is the stabilizing moments to the destabilizing moments factorized with the partial coefficients as in the sliding verification but factors that are related to overturning.

Table1.7 Overturning verification for first wall

effect of actions	Formula	Flat(β=0)		Slope(β=25°)		unit
		A1=1.3	A1=1	A1=1.3	A1=1	
Moments about wall toe - Design overturning moments (destabilizing) about wall toe	$M_{Gd}=\frac{1}{3}E_{a,Gd}$H cos(β)	56.71	53.54	75.07	97.88	(kN.m/m)
Centroid of wall on x-axis from the toe	$\bar{X} = \frac{\bar{x_s}A_{stem} + \bar{x_b}A_{base} + \bar{x_{tra}}A_{traingle}}{A_{total}}$	1.435	1.435	1.435	1.435	(m)
Design restoring moments (stabilizing) about wall toe	$M_{Rd}= \bar{X}. W_{Gk}$	213.63	164.32	213.63	164.33	(kN.m/m)
Verification of overturning resistance	ODF = $\frac{M_{Rd}}{\gamma_R M_{Gd}}$	3.28	2.67	2.47	1.46	-

Then finding the bearing capacity of soil if it is sufficient, going from line of action of resultant force according to the distance from the toe, to find the eccentricity of actions from centre line of base, to get the effective width of base, so it could be used in calculating the total design bearing resistance in terms of force, but in order to find it the bearing resistance from overburden and body mass should be computed that are effected by the design bearing capacity factors (Table 1.8).

Table1.8 Bearing capacity verification for first wall

effect of actions	Formula	Flat(β=0)		Slope(β=25°)		unit
		A1=1.3	A1=1	A1=1.3	A1=1	
Line of action of resultant force is a distance from the toe	$X = \frac{M_{Rd}-M_{Gd}}{N_{Ed}}$	0.723	0.74	0.78	0.37	(m)
Eccentricity of actions from center line of base	$e_d = \frac{B}{2} - X$	0.376	0.36	0.32	0.73	(m)
Effective width of base	$B'_d = B - 2e_d$	1.44	1.49	1.56	0.75	(m)
Design bearing capacity factors	$N_{q,d} = e^{\pi \tan(\varphi_d)}\left(tan\left(45° + \frac{\varphi_d}{2}\right)\right)^2$	18.17	10.33	18.18	10.33	-
	$N_{\gamma,d} = 2(N_{q,d}-1)tan(\varphi_d)$	19.83	8.62	19.83	8.62	-
Shape factors (for an infinitely long footing)	s_q	1	1.00	1.00	1.00	-
	s_γ	1	1.00	1.00	1.00	-
Inclination factors: (using m_B= 2 for an infinitely long footing)	$i_q = \left(1 - \frac{H_{Ed}}{N_{Ed} - A c'_d \cot(\varphi_d)}\right)^{m_B}$	0.461	0.37	0.42	0.21	-
	$i_\gamma = i_q^{\frac{m_B+1}{m_B}}$	0.313	0.22	0.27	0.10	-
Design bearing resistance from overburden	$q_{Rvq,d} = \gamma_k t_b N_{q,d} s_q i_q$	71.88	32.55	90.64	46.98	(kN/m^2)
Design bearing resistance from body-mass	$q_{Rv\gamma,d} = \frac{1}{2} B'_d \gamma_k N_{\gamma,d} s_\gamma i_\gamma$	298.76	91.65	309.12	115.94	(kN/m^2)
Total design bearing resistance	$q_{lim} = q_{Rvq,d} + q_{Rv\gamma,d}$	370.64	124.19	124.19	162.92	(kN/m^2)
Characteristic bearing resistance (in terms of force)	$N_{Rd} = q_{lim} B'_d$	781.59	184.90	184.90	121.76	(kN/m)
Vertical/normal component of design weight and thrust	$N_{Ed} = \gamma_G W_{Gk} + E_{a,d}\sin(\beta)$	148.82	114.48	177.80	152.27	(kN/m)
Design sliding resistance	$H_{Rd} = \gamma_{G1,fav} N_{Ed} \tan(\delta_d)$	105.73	83.55	118.44	100.54	(kN/m)
Verification of bearing resistance	$\text{ODF} = \frac{N_{Rd}}{\gamma_R N_{Ed}}$	3.75	2.26	2.50	1.12	

1.2 Validation of numerical model

Two phases are involved in the "numerical design" sequences,initially this part includes an overview of FLAC, the software that is used in this study, at the beginning a comparison between the response due to a Ricker function, that is applied on both 1D soil software which is DEEPSOIL, where a linear analysis was carried out in the time domain and considering a linear visco-elastic model, and 2D software which is the main program FLAC ,but to compare with a 1D software, a 1D mesh model on FLAC also has been modelled, by consisting only the foundations, one time for the right side of the full model and the other time for the left side, implemented on FLAC, analysing it statically and dynamically, comparing then the response on FLAC with the response of the same model made with the DEEPSOIL software (Figure 1.6) to guarantee that the analysis are going right and not having any software problems.

After that, taking into account the considerations and the general problems, such as applied loading conditions, types of soil damping models, boundaries and interface element in the modelling of soil structure system. All of that will be analysed in both cases, static and dynamic loading.

The properties of the materials of the soil, backfill and the retaining wall were given as shown in Table 1.2, from there the model of Deepsoil was designed as a linear model and a time domain solution, also one of the important things is that the simulation has been done for the foundation layers only on the boundary of the whole 2D model with a rigid bedrock for the model in Deepsoil.

As mentioned previously, modelling on 1D DEEPSOIL has been done for the left side of the 2D model, then the same model was done on FLAC as a 1D mesh model as shown in Figure 1.3,1.4 respectively:

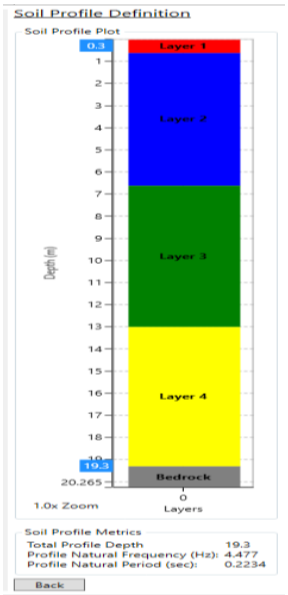

Figure1.3 1D DEEPSOIL model left side

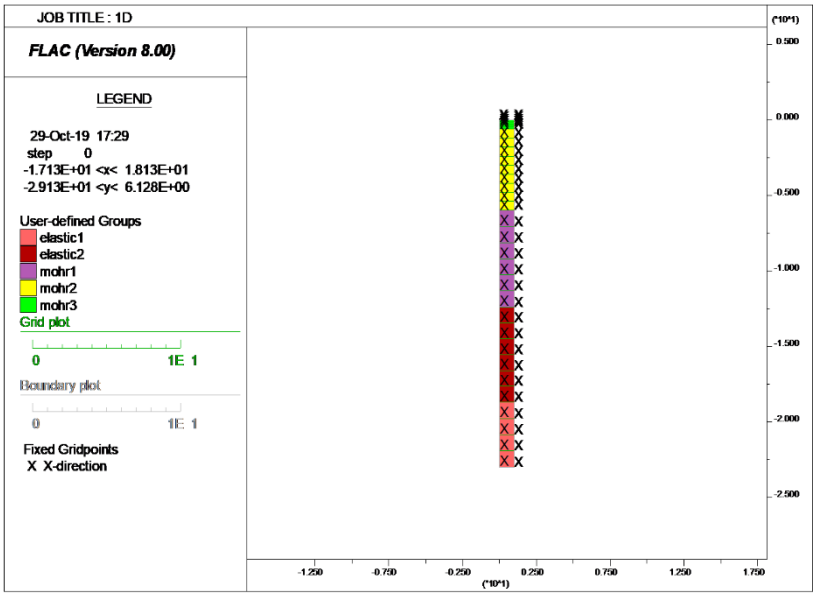

Figure1.4 1D FLAC model left side

A Ricker function as shown in Figure 1.5 was applied for the 1D models to compare between the response of the model on different softwares mentioned in Figures 1.3,1.4. This Ricker wave is simulating seismic input, defined in the time domain, and having a central frequency of about 3 Hz. In this case, considering a rigid base, the seismic input is provided as an acceleration history.

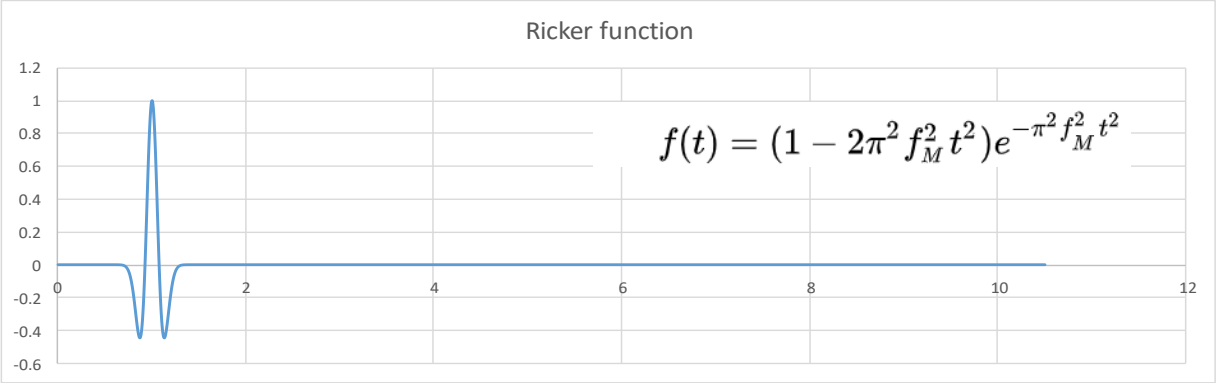

Figure1.5 Ricker function

As it is shown in Figure 1.6 in which it is possible to notice that the results obtained through the two softwares in terms of acceleration history, recorded at the surface layer have a similar trend. In particular, with reference to the same figure, it can be noticed how in FLAC model, the response tends to be damped quicker than the model done on DEEPSOIL. The interesting thing that could be seen is that how the shape of the response is perfectly overlapping, having an exclusion of the maximum acceleration value recorded which, is underestimated in FLAC with respect to the results obtained by DEEPSOIL. This perception could be due to the different theoretical solution methods used in the analysis executed by the two softwares.

This was the response of both softwares of the 1D left side layers on the top layer of the whole model:

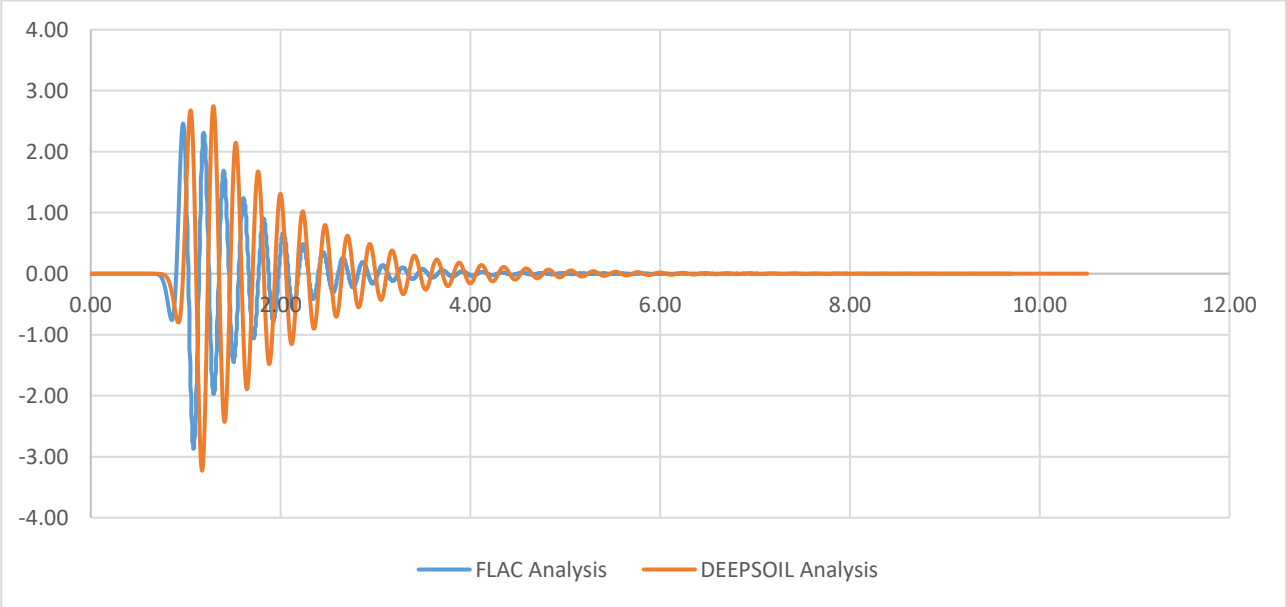

Figure1.6 Response of 1D models due to Ricker function of the left side

Then the same thing was done for the right side of the model (Figure 1.7,1.8):

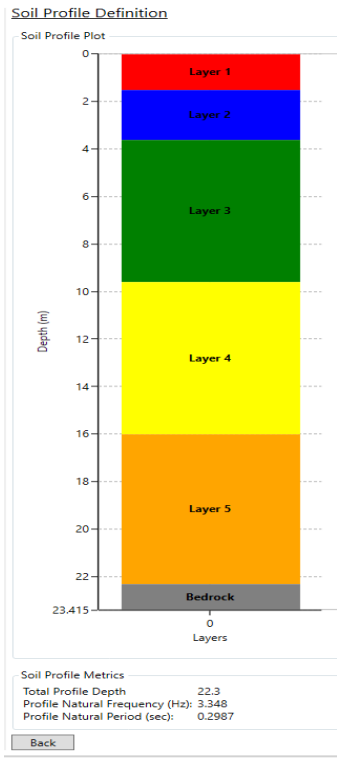

Figure1.7 1D DEEPSOIL model right side

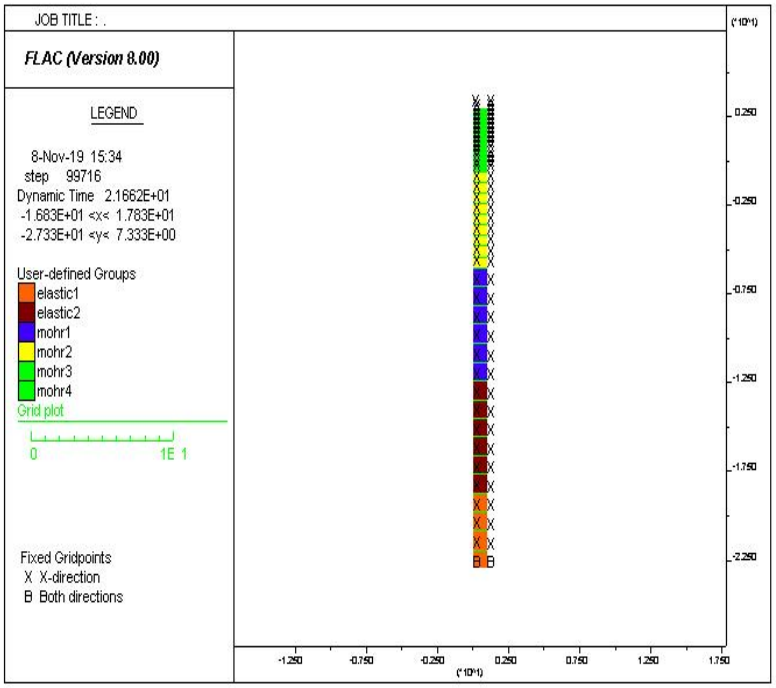

Figure1.8 1D FLAC model right side

This was the response of both softwares of the 1D left side layers on the top layer of the whole model (Figure 1.9):

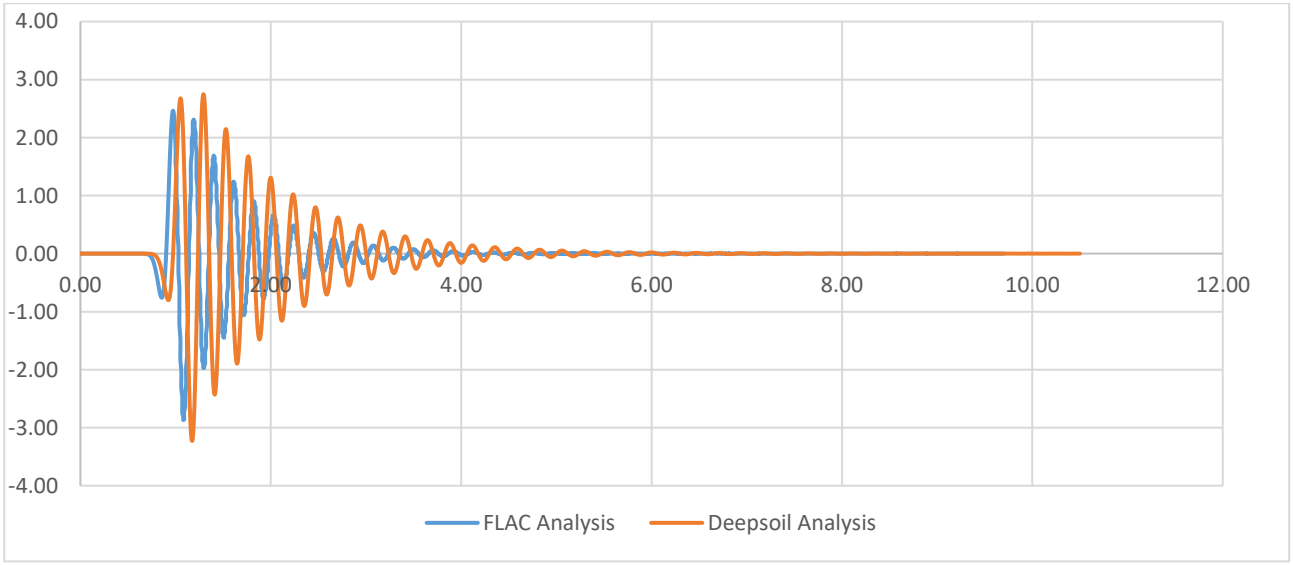

Figure1.9 Response of 1D models due to Ricker function of the right side

1.3 Definition of numerical model

Static characterization of the model:

As done in numerical analysis softwares, the realization of the section was necessary to define a Mesh that allows the division of the model into zones. The choice of the grid was made so as to guarantee the adequate discretization of the model, on the other hand a limited analysis time.

Figures 1.10 and 1.11 show the sections of the retaining wall model, the backfill and the foundation soil model built on FLAC; the model refers to the static equilibrium of the retaining wall, for which the following boundaries have been assigned to the boundary, in order to prevent rigid movements:

- Roller constraints to the base in vertical direction to prevent any movement
- Horizontal rollers on the edges, right and left, to prevent horizontal movement and allow vertical movement.

The materials that were in touch with the retaining wall were assigned a denser mesh than the one attributed to the foundation system, so as to be able to analyse phenomena affecting the retaining wall with greater accuracy, such as the interaction boundary of retaining wall with soil and the reaction of the structure due to the applied load.

After defining the mesh, the different materials making up the retaining wall and their properties were assigned. The Non-linear hysteretic &Mohr-Coulomb failure criterion and viscous damping was attributed to the backfill and to the foundation levels, while a linear elastic model was assigned to the retaining wall.

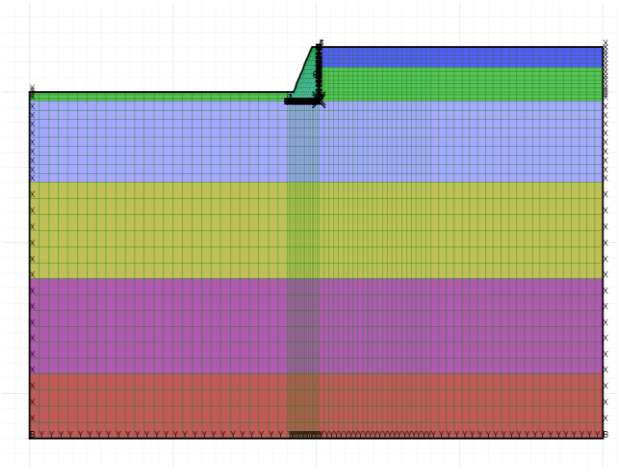

Figure1.10 Flat backfill model

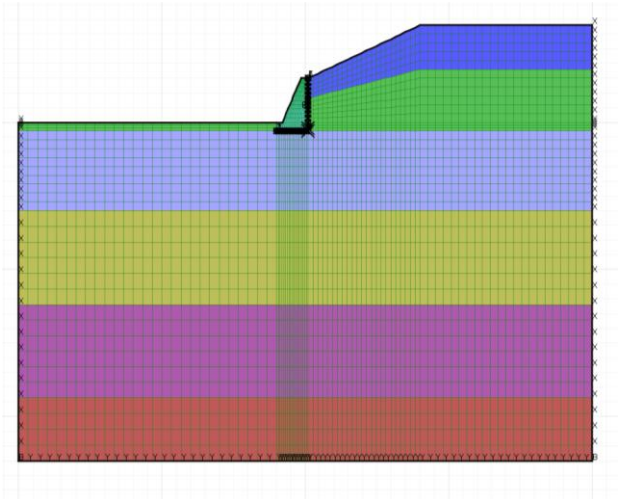

Figure1.11 2D Slope backfill model

An interface is defined in terms of normal and shear stiffness between two planes that may contact each other as shown in Figure 1.12

k_n= normal stiffness

k_s= shear stiffness

In this case study the glued interfaces have been used in both static and dynamic situations in which no slip or opening is allowed, but elastic displacement still occurs, according to the given stiffness's. The soil-wall interface parameters and stiffness's are shown in Table1.9.

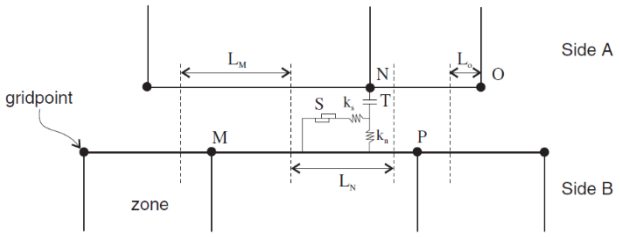

Figure1.12 Interface element model (ITASCA 2015)

Table1.9 Soil-wall interfaces parameters

Interface	K_n(MPa)	K_s (MPa)	c(kPa)	δ(°)	Ψ(°)
Backfill	5500	5500	0	20	0
Foundation	1000	10000	0	23	0

After setting the grid mesh, applying the material properties for each layer and the boundaries in the static conditions by setting the gravity as 9.81 m/s^2,for each model, then they were analysed statically and the static displacement was measured for each case by placing a set of points on the boundary of the wall on FLAC. These displacements were used after the dynamic analysis to get the permanent horizontal displacement of the wall by adding them to the residual dynamic displacements as shown in Figure 1.13 as an example.

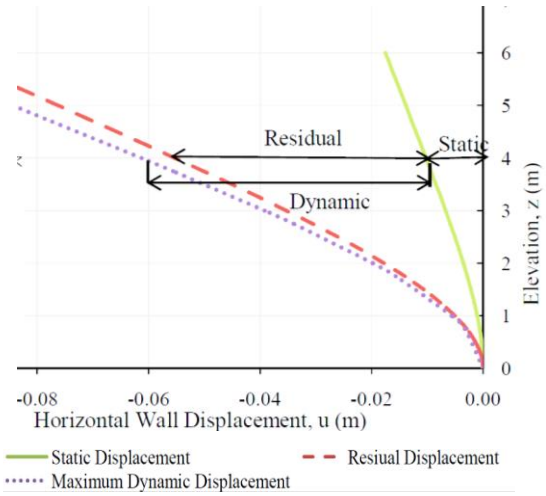

Figure1.13 Permanent horizontal displacement

Dynamic characterization of the model:

As mentioned in the introduction the most effective parameters that should be taken into account while applying a numerical dynamic soil-structure models in detail are:

- Boundaries conditions:

Boundary conditions is one of the main aspects that should be considered while running a dynamic analysis as it plays an important role in the response of the seismic wave and gives the wave the ability or the disability of extending:

Free Field Boundaries: In this study a free field boundary has been used they simulate the behaviour of an infinitely extended medium preventing the reflection of the waves on the boundaries of the mesh. Actually, once this consideration is imposed, the nodes of the grid are connected to viscous dampers that absorb the energy of the applied waves (Figure1.14).

Quiet Boundaries: The viscous dashpots that are connected to the free fields are simulating a quiet boundary that does not reflect the applied waves.

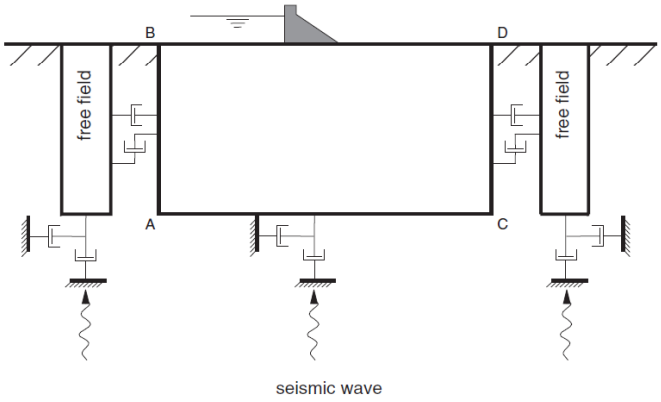

Figure1.14 Seismic analysis model for surface structure and free field mesh (ITASCA, FLAC manual, 2015)

- Dynamic input motions:

Dynamic input can be applied either in the *x* or *y* direction with respect to the *xy*-axes of the model, or in the normal and shear directions according to the model boundary. Some boundary conditions cannot be merged at the same boundary element, an important notice while applying velocity or acceleration input to model boundaries is that these boundary conditions cannot be applied along the same boundary as a quiet boundary condition, because the effect of the quiet boundary would be revoked. To input seismic motion at a quiet boundary, a stress boundary condition is used, as done in

this study velocity record is transformed into a stress record and applied to a quiet boundary as shown in Figure 1.17.a.

A velocity wave may be converted to a stress wave using the equation 1.1.

$$\sigma_s = 2(\rho\, C_s)\, v_s \qquad \textit{(equation 1.1)}$$

σ_s = applied shear stress;

ρ = mass density;

C_s = speed of *s*-wave propagation through medium;

where $C_s = \sqrt{\frac{G}{\rho}}$

v_s = input shear particle velocity.

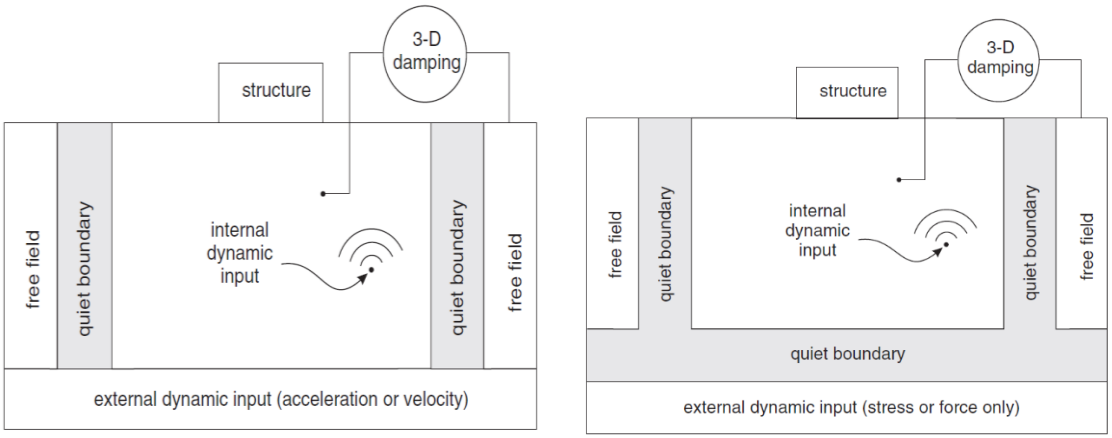

(a)Rigid base (b)flexible base

Figure1.15 Types of dynamic loading boundary conditions available in FLAC (ITASCA, FLAC manual, 2015)

- Soil damping models that could be applied for the model in FLAC:

Dynamic Damping: Damping in general is the phenomenon produced by processes that dissipate the energy stored in the oscillation system. Usually, different forms of energy dissipation can happen in materials, especially in rocks and soils the damping is hysteretic, therefore independent of frequency, therefore it would be difficult to reproduce this behaviour numerically by hysteretic damping function for two reasons, the first reason that it is not damping all the numerical elements equally when several waves are applied, where the second reason is that this functions lead to a path –dependence which makes the prediction of the results too hard . So for the modelling of the phenomenon a Rayleigh damping is used, in the time domain, in addition to the hysteretic damping that is assigned initially to the model, in case of noting that it is better not to use Rayleigh damping in contribution with hysteretic damping, unless as in our case that a Rayleigh damping is used in a small value in order to avoid high frequency noise.

The hysteretic damping is assigned in FLAC as a secant modulus of the shear stress/strain cycles that is applied in our case as a sigmoidal model 4 that depends on four input parameters that are implemented in the software as (a, b, x_0, y_0) respectively that x_0 and y_0 are the initial values of the tangent of the secant modulus of first cycle, where a and b are the regression parameters of the first tangent line of shear stress/strain cycles (Figure 1.16), to represent the secant modulus as shown in equation 1.2. Another parameter that is defined by the software automatically in the equation according to the parameters and cyclic load is the logarithmic strain L.

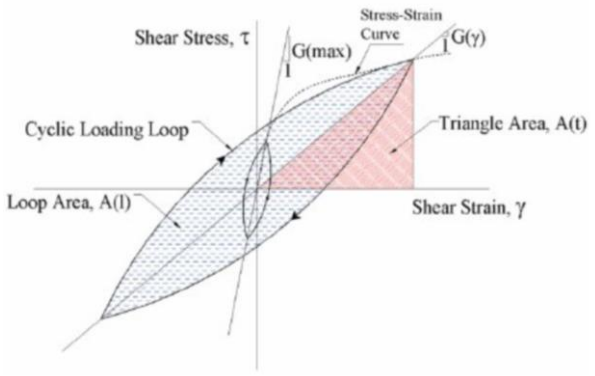

Figure1.16 Hysteretic shear stress-shear strain relationship (MEIDANI, M., et, 2008)

$$M_s = y_0 + \frac{a}{1+\exp\left(-\frac{L-x_0}{b}\right)} \qquad \text{(equation 1.2)}$$

Two different hysteretic damping has been assigned for the backfill layers that differs in the initial shear strain value x_0, according to a selected ideal type of clay that is expected to well presents the backfill properties as shown in Table 1.10.

Table1.10 Secant modulus parameters that represents the hysteretic damping

parameters	a	b	x_0	y_0
Backfill & foundation (*green layer*)	1	-0.473	-1.612	0
Backfill (*violet layer*)	1	-0.473	-1.774	0

In FLAC the Rayleigh damping is defined by assigning two parameters that are:

- f_{min}, first resonance frequency of the system (4.48Hz) in our case
- ξ_i, fraction of critical damping corresponding to the generic pulsation ω_i (0.1%)

Where in a multi degree of freedom system the two parameters defined according to (Bathe and Wilson 1976) in equation 1.3.

$$\alpha + \beta\, \omega_i^2 = 2\omega_i \xi_i \qquad \text{(equation 1.3)}$$

Where α and β are the mass-proportional damping constant; and the stiffness-proportional damping constant respectively for the damping matrix C shown in equation 1.4 and the first resonance frequency is defined in terms of minimum frequency ω_{min}.

$$C = \alpha M + \beta K \qquad \text{(equation 1.4)}$$

$$f_{min} = \omega_{min} / 2\pi \qquad \text{(equation 1.5)}$$

Damping Ratio, ξ_{min}

For geological materials, damping generally ranges from 2 to 5% of critical; for structural systems, 2 to 10% is for recommended damping values for different materials. In this analyses a Mohr-Coulomb plasticity constitutive model has been used, in which a large amount of energy dissipation can occur during plastic flow. That's why, for many dynamic analyses that include large-strain, only a minimal percentage of damping (e.g., 0.5%) may be required. That is why in our case we have considered 0.1%.

Dynamic analysis consumes a lot of time as it depends on the stiffness and the mass of a single-mass spring system that express the critical time step Δt_{crit} as the minimum over all grid points. However, the more general form is used in deriving the dynamic timestep, Δt_d , using a safety factor of 0.5 (to allow for the fact that the calculation of timestep is an estimate only). So, it is mostly affected by the dynamic time step and the dense of the mesh. Thus, equation 1.6 and equation 1.7 shows the time step of the dynamic analysis.

$$\Delta t_{crit} = 2\sqrt{\frac{M}{k}} \qquad \text{(equation 1.6)}$$

$$\Delta t_d = \min.\left\{\sqrt{\frac{\Sigma M}{\Sigma k}}\right\} * 0.5 \qquad \text{(equation 1.7)}$$

Chapter 2: Dynamic Analysis

This chapter describes the numerical dynamic analysis that has been done for all the four walls in both backfill cases (flat and slope), that leads to have eight different models, by applying eighteen different acceleration time histories selected among real accelerograms recorded at rock outcropping sites for a return period of 475 years. At the end of this chapter a comparison between all the walls response of each backfill case is done and the results are discussed in terms of the relation between the walls geometries and their reactions.

2.1 Input motions

The accelerograms were given in the form of acceleration time histories and with different amplitudes, varying from the small ranges nearly to the high amplitude ranges, this accelerograms range from 0.26 m/s^2 the highest acceleration value approximately in the first accelerogram which lasts for 60 seconds duration (Figure 2.1), to reach 6.5 m/s^2acceleration the highest velocity magnitude approximately in the last accelerogram that lasts for 238 seconds duration.

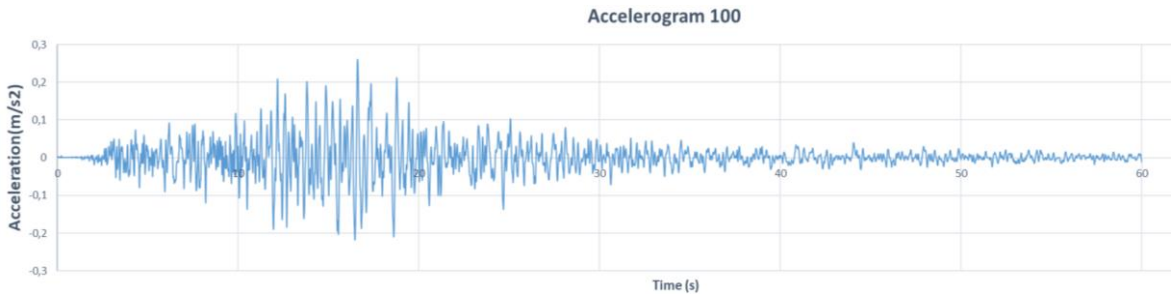

Figure2.1 First accelerogram of the input motions

The input motions were presented in different forms of intensity measures (IMs) that will play an important role in the next chapter in which the best fit intensity will be measured according to specified parameters, this issue will be discussed in details after discussing the dynamic analysis results in this chapter for all the walls.

One of the important things that should be also mentioned is that the IMs that are listed in table are not all the IMs that has been compared in the study, but these are the most important and effected in our case study. The other IMs are shown in Appendix-B.

To show the difference excitation of the input motions clearly, a Frequency-Fourier Amplitude is shown in (Figure 2.2) that shows how the input motions are approximately increasing in amplitude and similarly the duration that is not shown in this figure but according to the data of the accelerograms given it can be read that the it is also increasing.

Another clearer graph that shows the difference between the input motions is elastic acceleration spectrum (Figure2.3), were it is obvious that the first accelerogram has an elastic spectrum acceleration of nearly 2 m/s^2, were it ranges between 20 m/s^2 and 22 m/s^2 for the last two accelerograms and a 4 second ending period has been chosen as the value of mostly all the spectrums are tending to approximately zero.

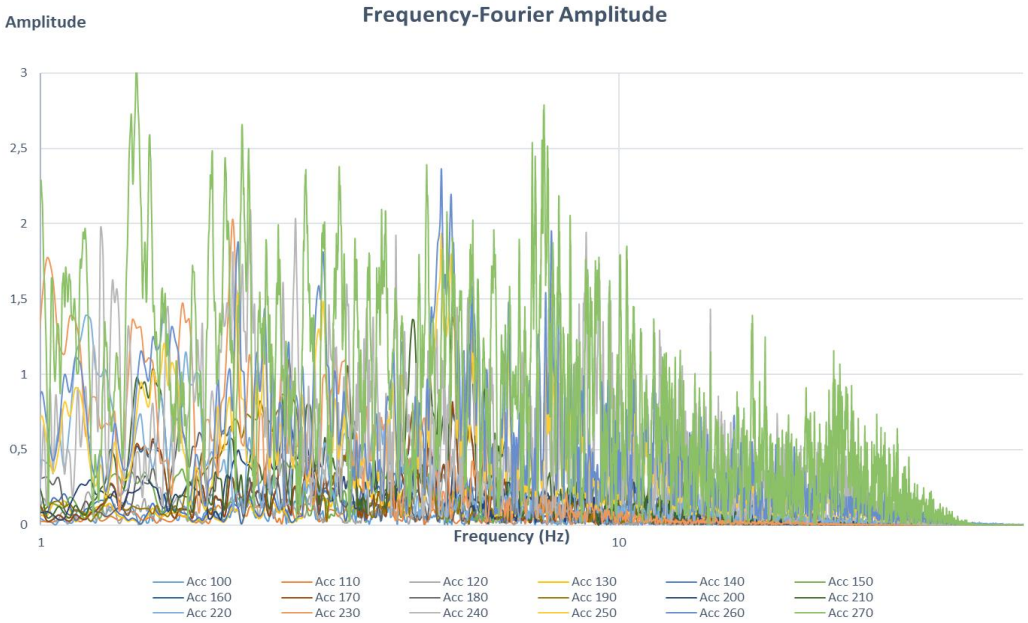

Figure 2.2 Frequency-Fourier Amplitude for all motions

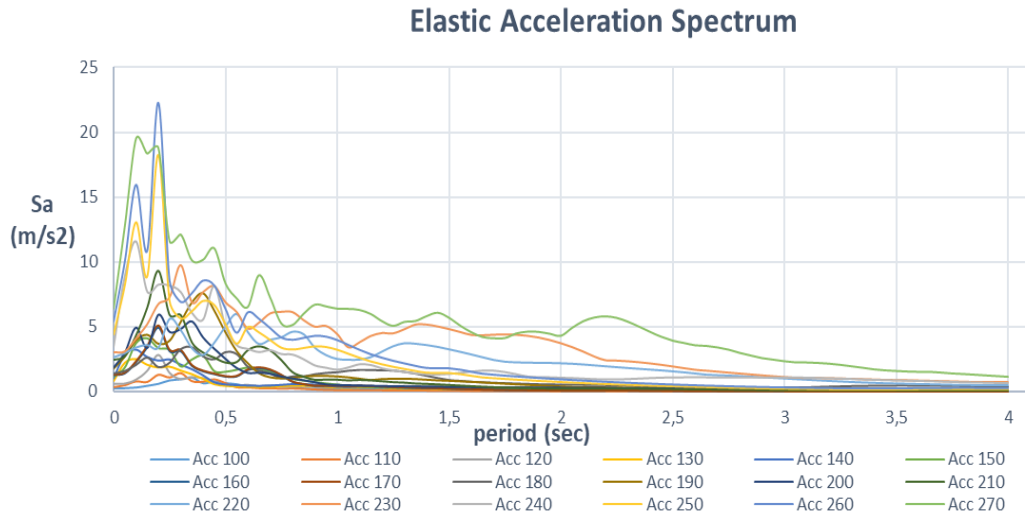

Figure 2.3 Elastic acceleration spectrum for all motions

The information and the sources of the input motions is shown in (Table 2.1), this table represents also the magnitude of this motions in different intensity measures (IMs),

Table 2.1 Input motions characteristics and intensity measures (IMs)

Earthquake ID	Site	ID Node	ID Acc site	ID	Mw	Depi	Source	PGA (m/s^2)	Arms (m/s^2)	I_a (m/s)	I_c (-)	CAV (cm/s)	ASI (m/s)	EDA (m/s^2)
Acc_100	TRAPANI	ID46049	5	96	6.46	69.09	NGA	0.2599	0.042	0.017	0.066	150.37	0.288	0.263
Acc_110	MILANO	ID11366	*5*	103	5.8	21.00	ITACA	0.3580	0.067	0.016	0.082	91.59	0.395	0.353
Acc_120	TRAPANI	ID46049	*1*	92	5.3	37	ESD	0.5742	0.058	0.034	0.112	184.32	0.513	0.560
Acc_130	BOLZANO	ID8073	*4*	88	6.19	38.63	NGA	0.7934	0.123	0.073	0.237	205.661	0.555	0.722
Acc_140	TARANTO	ID34359	*4*	81	6.19	38.63	NGA	1.0270	0.160	0.122	0.349	266.22	0.718	0.935
Acc_150	BERGAMO	ID11380	*6*	76	5.8	9.3	ITACA	1.1383	0.199	0.158	0.442	240.44	1.116	1.118
Acc_160	PALERMO	ID44949	*6*	69	6	33	ITACA	1.2959	0.208	0.200	0.510	339.81	1.090	1.311
Acc_170	FIRENZE	ID19836	*6*	62	6	33	ITACA	1.3376	0.214	0.213	0.534	350.73	1.125	1.353
Acc_180	TREVISO	ID11859	*3*	52	6.93	92.21	NGA	1.4124	0.148	0.140	0.360	311.41	1.030	1.426
Acc_190	RIMINI	ID18968	*5*	47	6.93	28.64	NGA	1.7910	0.199	0.253	0.561	283.86	2.126	1.705
Acc_200	PERUGIA	ID23185	*4*	39	6.93	28.64	NGA	1.8631	0.188	0.226	0.515	304.96	1.759	1.990
Acc_210	ATELETA	ID28537	*6*	34	6	33	ITACA	2.4216	0.388	0.699	1.302	634.98	2.037	2.450
Acc_220	LAMEZIA	ID41668	*3*	24	6.93	94.31	NGA	2.6644	0.301	0.580	1.045	646.27	1.550	2.610
Acc_230	CATANIA_SF	ID47866	*3*	10	6.93	103.91	NGA	3.0302	0.430	1.181	1.780	895.60	2.768	3.023
Acc_240	CATANIA_SF	ID47866	*5*	12	7	50.5	KNET2	3.4797	0.471	2.847	2.895	2083.98	2.998	3.395
Acc_250	CATANIA	ID47866	*2*	16	6.61	24.19	NGA	4.4107	0.551	1.793	2.484	1069.20	3.461	4.153
Acc_260	CATANIA_SF	ID47866	*2*	9	6.61	24.19	NGA	5.3840	0.673	2.672	3.350	1305.12	4.224	5.070
Acc_270	GIOIA TAURO	ID43661	*6*	6	6.9	23.05	KNET2	6.4126	0.447	7.625	4.615	3498.72	5.096	6.062

The previous table contains the most important intensity measures that had been selected among 34 IMs where the other IMs are attached in (Appendix-2), after showing the details of our input motions the next step is to apply these motions to the numerical models of the walls that has been done through FLAC.

2.2 Dynamic Analysis

The dynamic analysis was done on the models that had been analysed statically, in order to have a cumulative displacement. As mentioned in the first chapter the motions were applied to the models on FLAC after having them in velocity time history and transferring them to a stress through the equation 1.1, then this stress was applied separately and sequentially going from one motion to the other by changing the velocity time history. One important thing should be mentioned that in this study that polarity was not taken in consideration which means that the dynamic load has been applied in one direction but not the other and this was because in order to do the dual cases, it consumes a lot of time as each response of a model due to an applied motion numerically analysed was taking 4 to 5 hours and this was because of the dynamic time step and the dense of the mesh mentioned in chapter1. The eighteen motions were applied separately for each wall and the displacement was measured by combining them with the static analysis.

The analysis was done by placing certain points according to the grid mesh that has been done on the boundaries of the retaining wall, and read the response of each point, as it is asked in the program such as displacement in x and y direction then having a text file that contains the history of this response for each point in each direction. This files have been used in the next step of data analysis to have the full reaction of the wall after both numerical analysis, statically and dynamically has been done

2.3 Dynamic response of wall

The histories that have been saved after the dynamic analysis represents the history of displacement of each selected point, in this step these histories of the several points has been arranged in a way that they could give an obvious response according to the demanded reaction, considering the demand of this case study two main things were measured that are the relative horizontal displacement and the tilting angle of the walls.

In order to have this two demands several points were placed at the base, vertical side and the barycentre of the retaining wall, then these points are gathered as a whole continuous line in FLAC, the maximum values of both displacements, absolute displacement that represents the maximum dynamic displacement of the wall base without considering the displacement of the foundation, and the relative horizontal displacement that represents the displacement of the wall with respect to the displacement of the foundation and another important thing was done which is taking into account the static displacement files and having the maximum static displacements in order to have a cumulative effect of dynamic and static analysis, then the tilting angle was measured by subtracting

the initial base displacement of the wall from the final displacement of the base and then dividing it by the base width.

The same steps were done separately for all the models with the different geometries of the walls, and at the end a comparison between the flat backfill walls relative horizontal displacements and tilting, and a similar comparison for the slope backfill case.

Walls with flat backfills

The analysis of the first wall with flat backfill shows that the first ten dynamic load applied that have a small magnitudes and short duration in comparison with the other dynamic loads have less effect than the other loads as their relative horizontal displacement is less than 2cm in the first wall as the others that in the fourth wall also did not exceeds the value of approximately 7cm.

As the other loads have greater displacement starting from Acc-210 that has a displacement of 10cm where Acc-230 shows a lesser displacement of about 5cm, although that it has a higher peak ground acceleration(PGA) value than Acc-210, and that is may because has a higher frequency, for this two intermediate PGA in comparison with the other motions, the response of the second wall was as the first wall with a little bit increment, while for the other two walls the higher motion starts to have a higher response as usual with same increment range of the first two walls.

Another thing that could be seen in the relative horizontal displacement of the loads is that the displacement is increasing gradually until a specific timing then it is becoming approximately constant for a while of time except for the last load Acc-270, and Acc-240, it could be seen that the displacement was nearly constant at the beginning but a sudden shock in displacement happened and it increased dramatically to reach a relative horizontal displacement of 28cm for Acc-270 which is the maximum overall relative horizontal displacement where it reach 5cm for Acc-240, for the first wall, while it is increasing for the other walls the phenomena of constant displacement after a specific time is happening for all the motions.

According to the tilting value it is obvious that a small tilting angle has appeared at the end of the analysis of the first wall which ranges from 0.2 to 1.2 degrees, the tilting value for the second wall unlike the relative horizontal displacement, instead of increasing, it decreases to the values that ranges from 0 to 0.5 degree which approximately means no noticed final tilting appears, where it again increases for the third wall more than the two walls, the fourth wall final tilting was unpredicted as it

decreases to reach a low value that is approximately near to the second wall. The dynamic analysis results of all the walls with slope backfills are shown in Figure 2.4 to Figure 2.11 respectively from the first wall to the fourth wall.

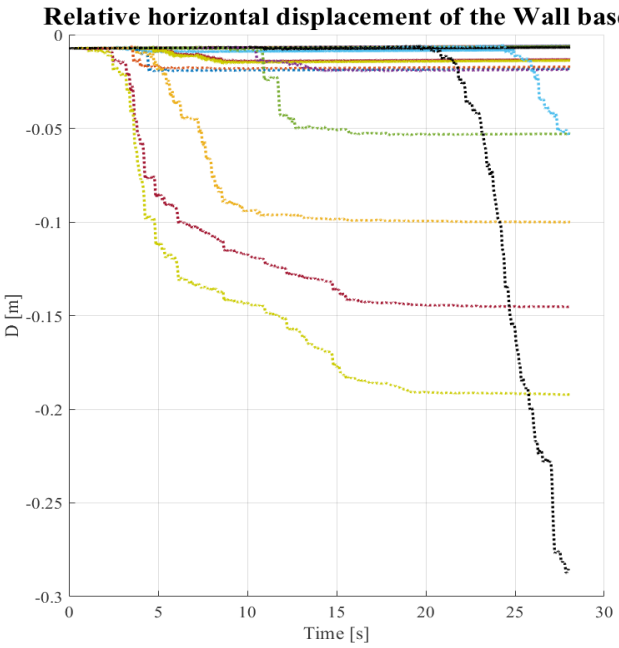

Figure 2.4 Relative horizontal displacement of first wall flat backfill

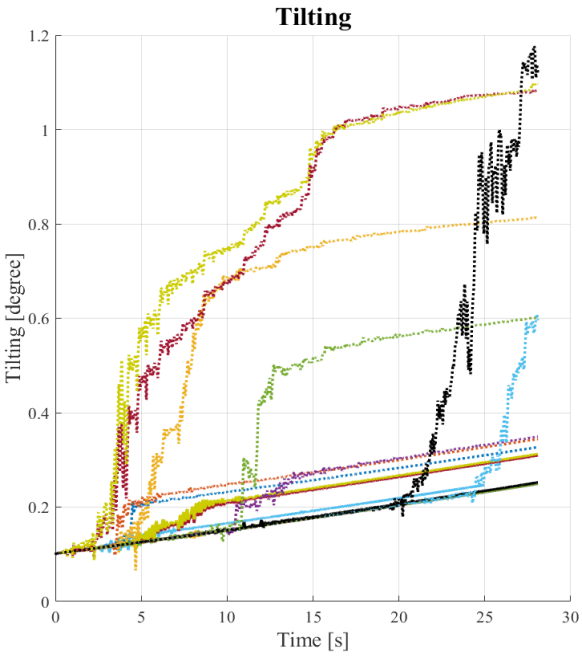

Figure 2.5 Tilting of first wall flat backfill

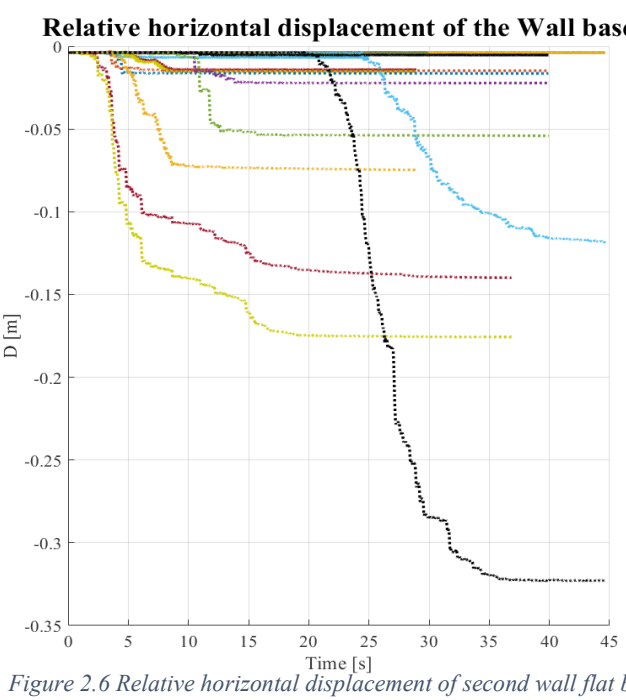

Figure 2.6 Relative horizontal displacement of second wall flat backfill

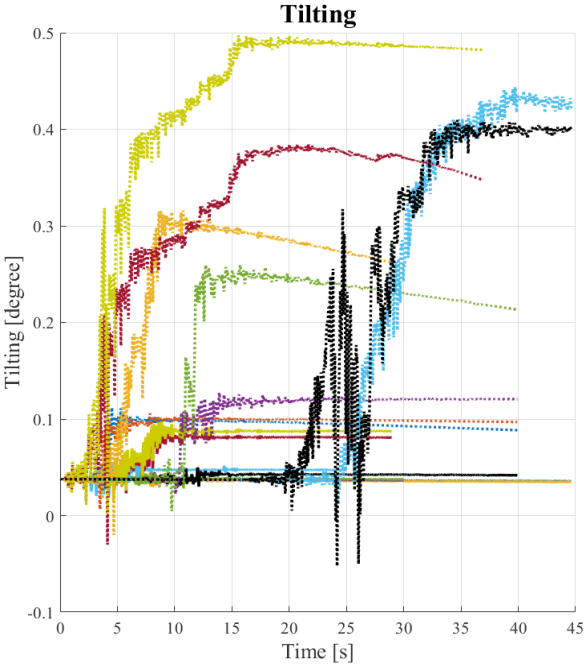

Figure 2.7 Tilting of second wall flat backfill

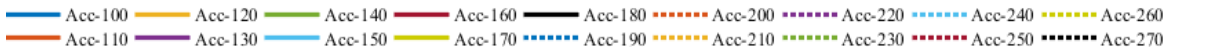

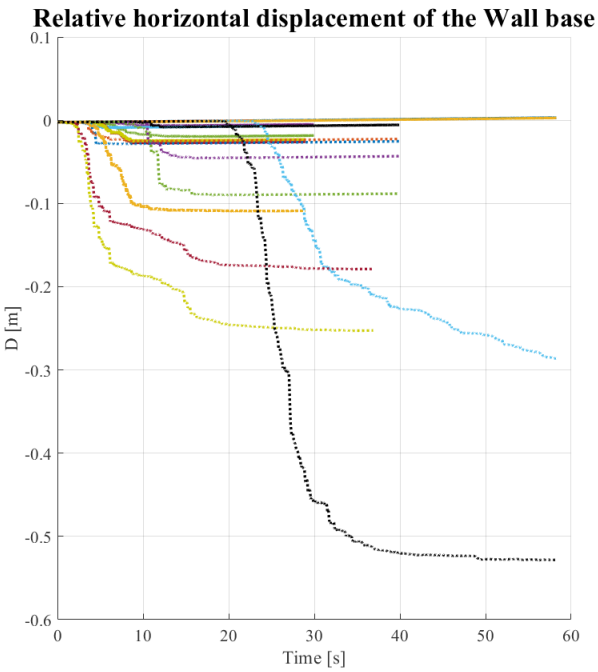

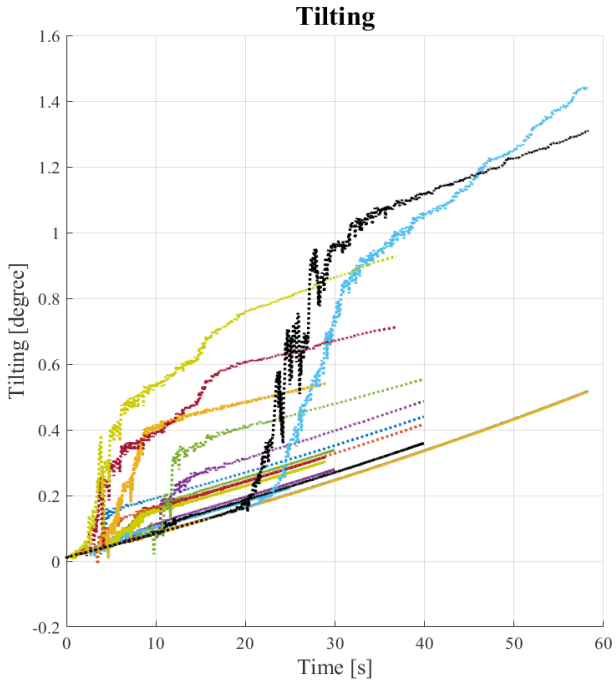

Figure 2.8 Relative horizontal displacement of third wall flat backfill

Figure 2.9 Tilting of third wall flat backfill

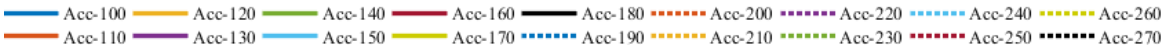

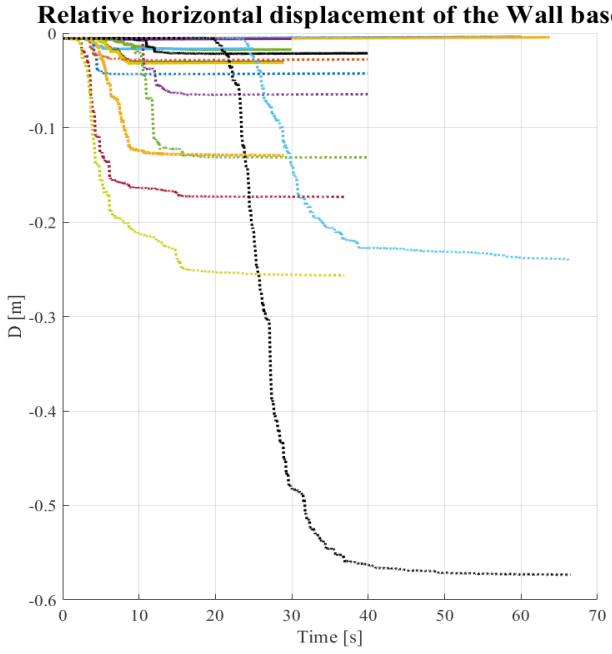

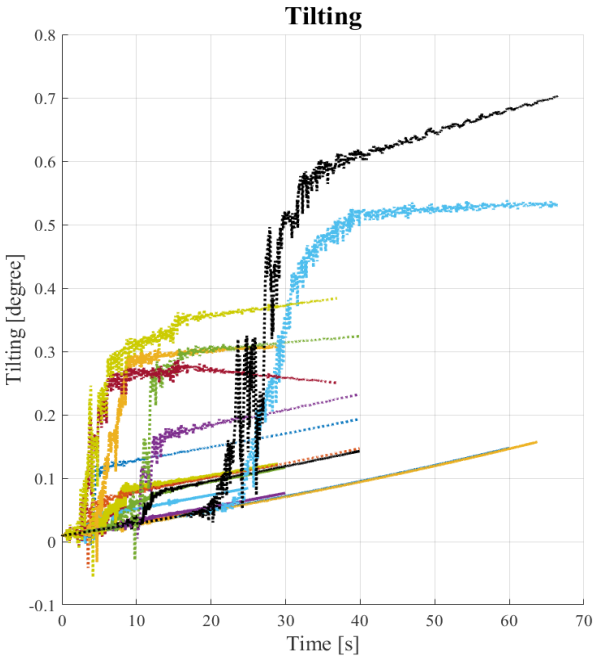

Figure 2.10 Relative horizontal displacement of fourth wall flat backfill

Figure 2.11 Tilting of fourth wall flat backfill

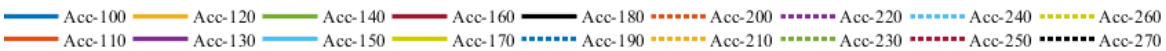

2.4 Comparison between all the flat backfill walls curves

As it is obvious in Figure 2.12 that combines all the walls with flat backfill, it could be seen that how the relative horizontal displacement is increasing monotonically with respect to the geometry of the wall, while there is no specific relation between the geometry of the wall and the tilting angle as it is shown in Figure 2.13, as it decreases when going from the first to the second, while getting larger when transferring from the second to the third to reach the highest value and decreasing for the last wall.

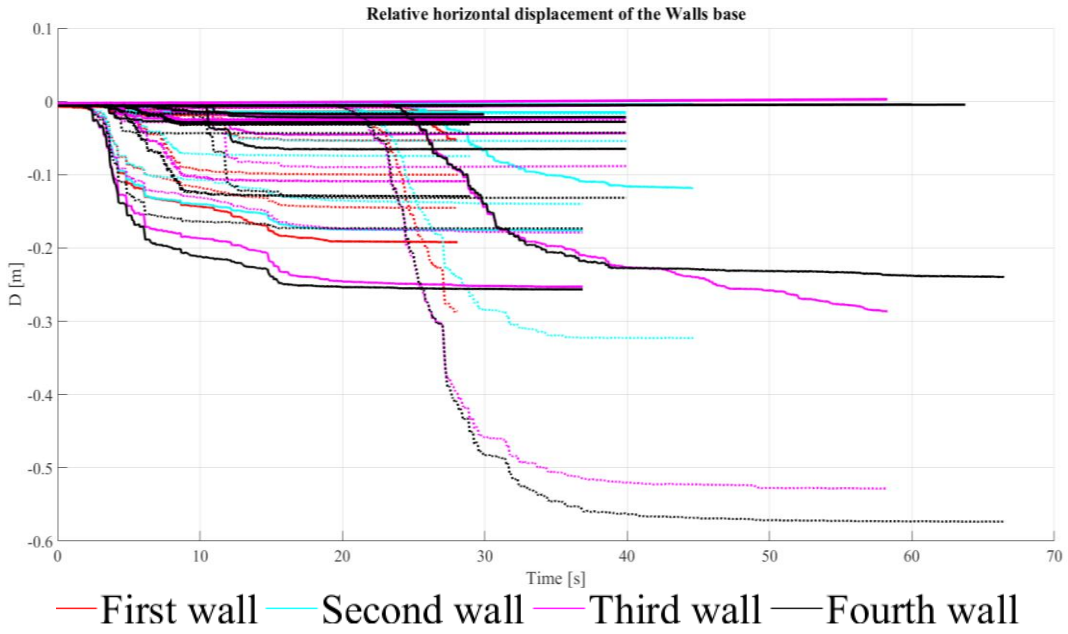

Figure 2.12 All Flat backfill walls relative horizontal displacement curves

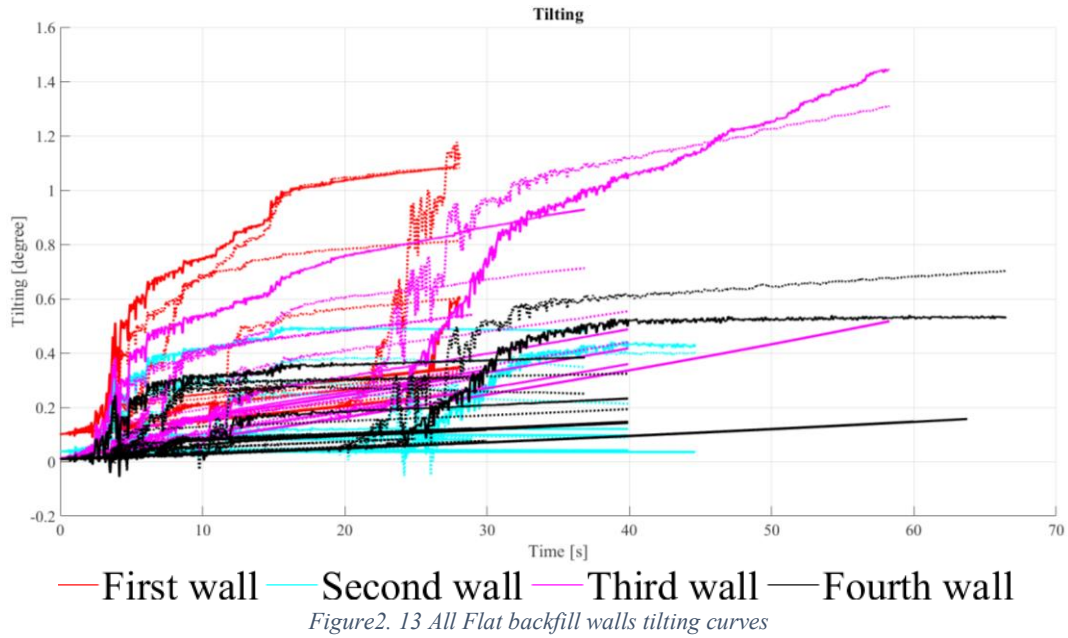

Figure2. 13 All Flat backfill walls tilting curves

Walls with slope backfills

The slope backfill case has been considered with same geometry cases of the previous analysis, in this first wall case with the same applied dynamic loads. An overall greater response than the first wall with flat case but the general response shape is approximately still similar, the first ten dynamic load applied that have a small magnitudes and short duration in comparison with the other dynamic loads have less effect than the other loads as their relative horizontal displacement is less than 5cm,but nearly more than double the values of the flat case for all the other walls with a proportional increment with wall geometry and backfill as the slope backfill was having a greater response than the flat ones.

Where the other loads have greater displacement starting from Acc-210 that has a displacement of 14cm where Acc-230 is immediately showing a bigger reaction of about 17cm, where in the flat case it was having a smaller reaction than Acc-210 for the first wall, then all the other reactions of the other motions is greater than the flat case in which the last load Acc-270 has a displacement of 45cm for the first wall. It continues in increasing for the other walls as the flat case to reach a value that is 72cm that is the higher overall value for all the walls in both backfill cases.

According to the tilting angle it has a bigger response than all the previous walls in flat case which reaches 2.6 degree in the first case, while it has a non-uniform response according to the wall geometries in the slope case but a higher overall value than the flat case.

The dynamic analysis results of all the walls with slope backfills are shown in Figure 2.14 to Figure 2.21 respectively from the first wall to the fourth wall.

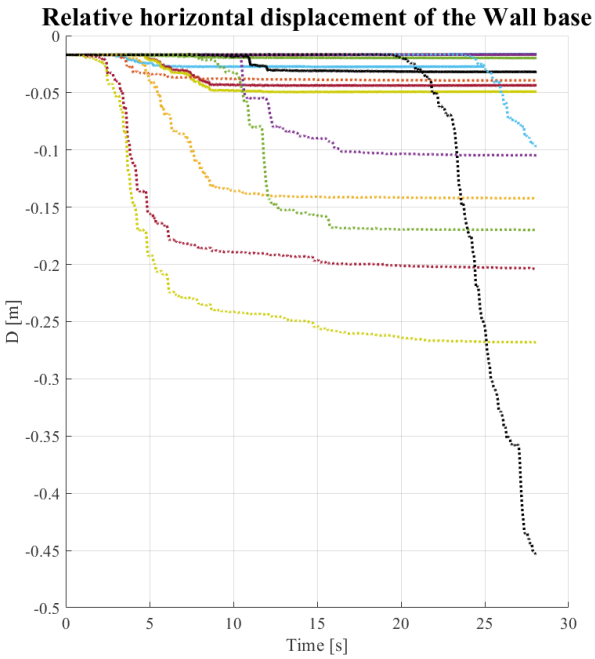

Figure 2.14 Relative horizontal displacement of first wall slope backfill

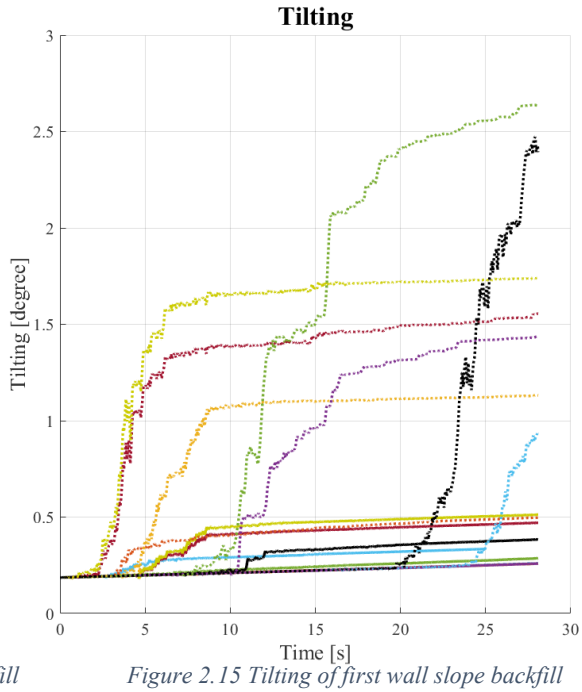

Figure 2.15 Tilting of first wall slope backfill

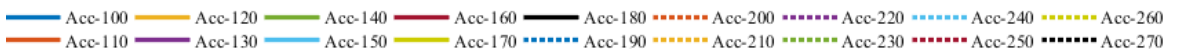

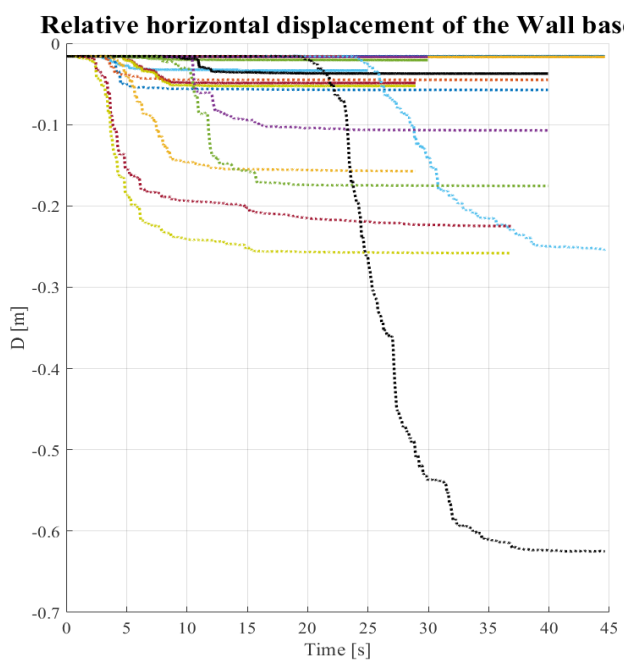

Figure 2.16 Relative horizontal displacement of second wall slope backfill

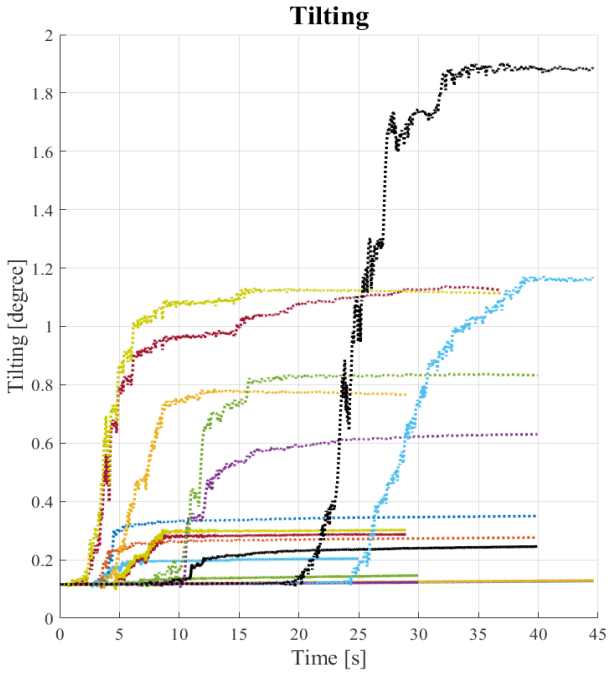

Figure 2.17 Tilting of second wall slope backfill

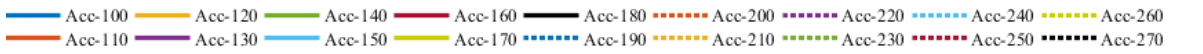

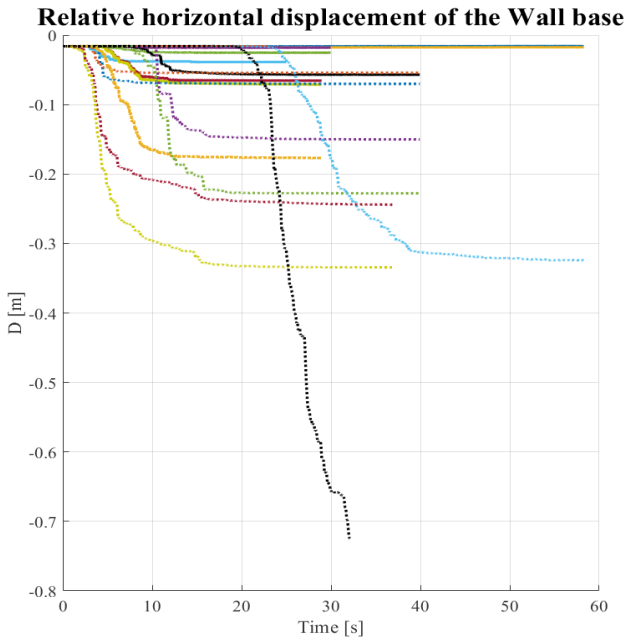

Figure 2.18 Relative horizontal displacement of third wall slope backfill

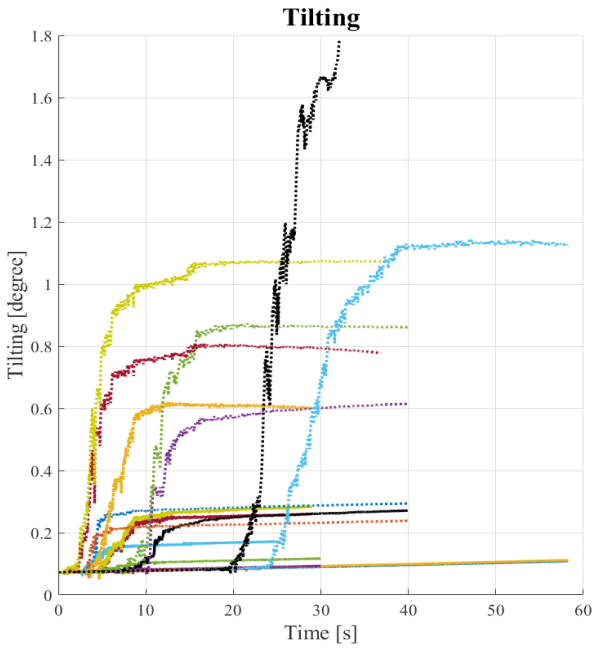

Figure 2.19 Tilting of third wall slope backfill

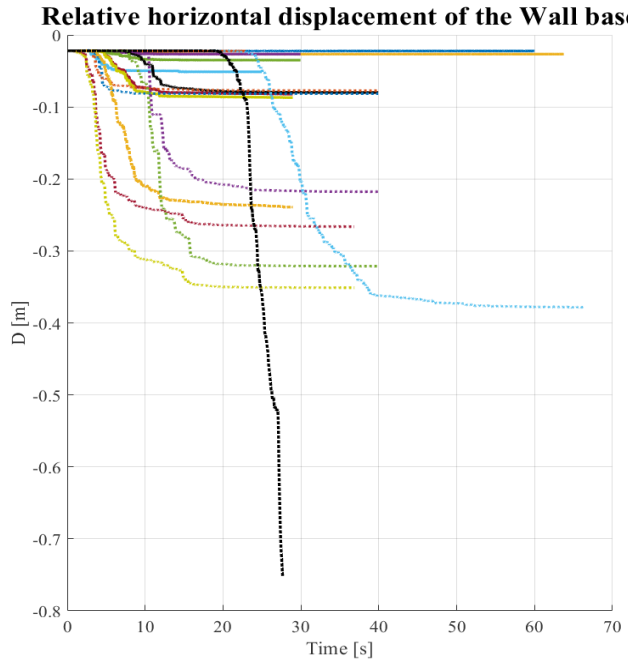

Figure 2.20 Relative horizontal displacement of fourth wall slope backfill

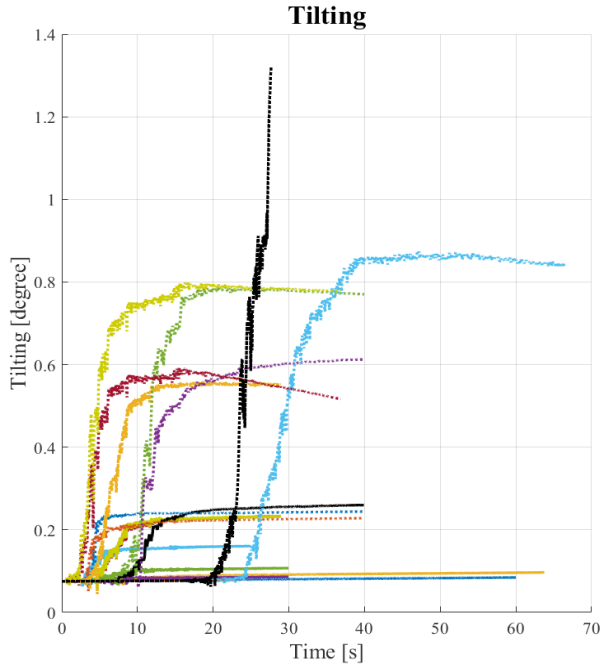

Figure 2.21 Tilting of fourth wall slope backfill

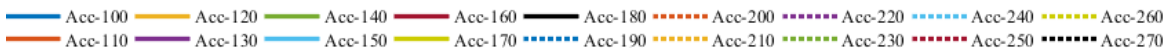

2.5 Comparison between all the slope backfill walls curves

In this case in Figure 2.22 that combines all the walls with slope backfill, mostly the same relation between the curves of different geometries happened that as the geometry increased the relative horizontal displacement is increasing monotonically, on the other hand a decreasing relationship could be distinguished between the geometry of the wall and the tilting angle in this case as it is shown in Figure 2.23, as it decreases when going from the first to reach the fourth to reach the smallest value for the fourth wall in comparison with others, the same thing could again be noticed that is the time increment with respect to the geometry.

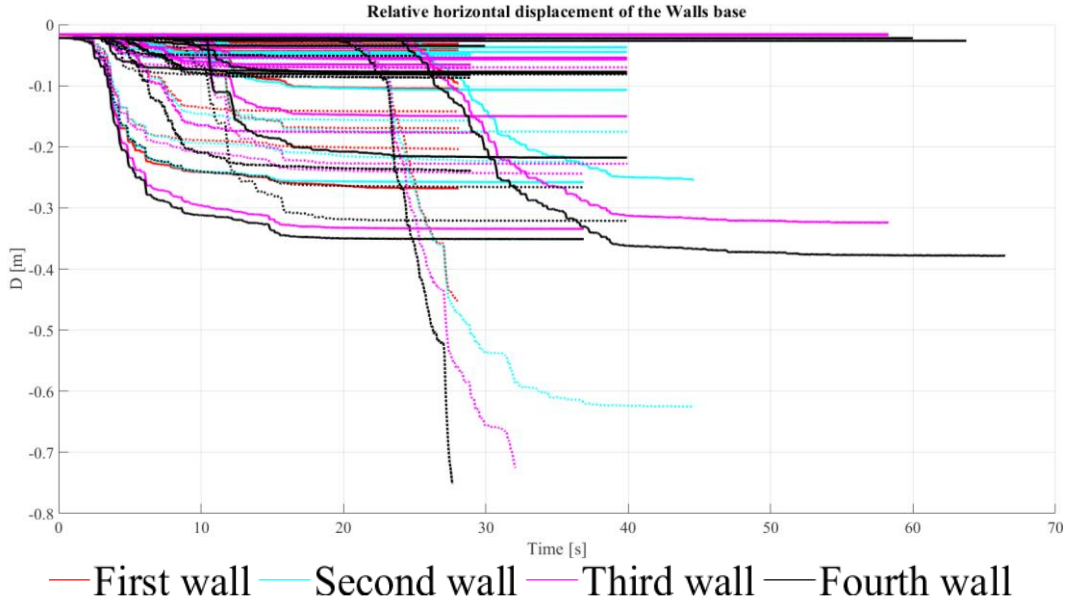

Figure 2.22 All slope backfills walls relative horizontal displacement curves

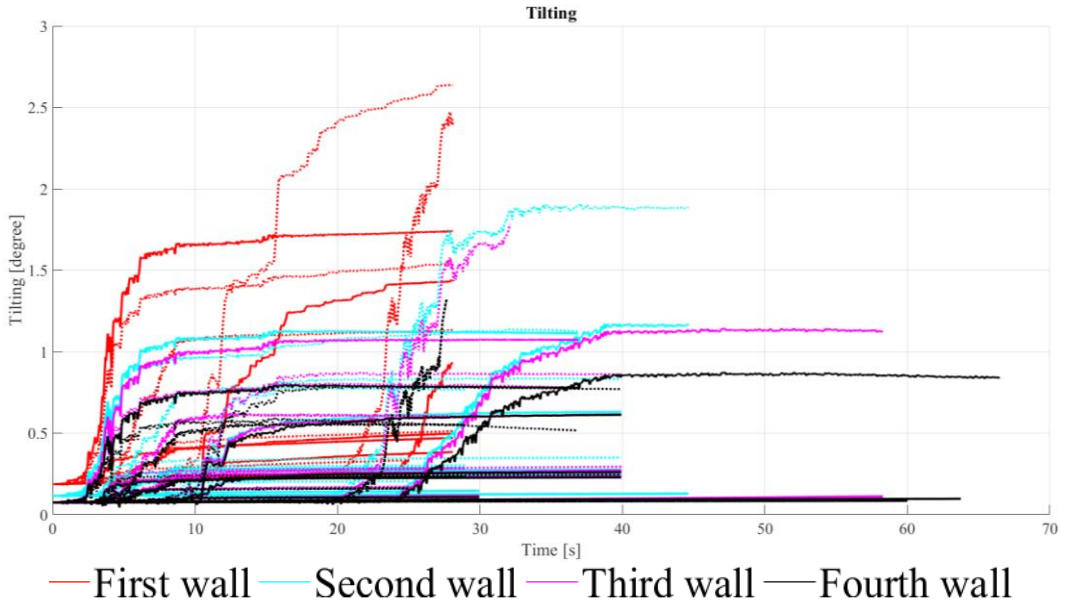

Figure 2.23 All slope backfills walls tilting curves

Chapter 3: Developing fragility curves for earth-retaining walls

The most important work that is related to the developing of the fragility curves has been done in this chapter and this work has passed through two main stages that are**:**

- Evolution of the intensity measure better correlated with the retaining wall response.
- Developing fragility curves with respect to the best intensity measure selected.

These steps have been done for each wall separately, then for each geometry combining the two cases of backfills together and at the end for all the walls together regardless to their various cases.

3.1 Evolution of the intensity measure better correlated with the retaining wall response.

The first step of developing the fragility curves was the evolution of the intensity measure better correlated with the retaining wall response, in which the results of the numerical analysis that are the deformation data according to the response of the retaining wall due to the seismic load applied have been used in their normal logarithmic form with respect to this input motion in its different forms of intensity measures that was also in the form of normal logarithmic.

These data were represented as points, and to find the best relationship as a regression line that has been found for this data that fits them and gives a correlation between the response demand and the intensity measure.

After the previous step has been done we have 34 different graphs for the same damages state that have been decided with respect to the 34 intensity measures that were available in this study shown in previous chapter and in Appendix-B , in this thesis this demand response were selected in the form of the optimal relative horizontal displacement for the several cases mentioned in the second paragraph and the other selection was the final tilting of the wall, the main aspect of this step was to select the best correlated IMs with the damage state according to some statistical parameters that represents the practicality (b), efficiency (σ), and proficiency (ξ) criteria, of the data on this graphs.

Practicality (b):Starting with the practicality that is measured by the regression parameter (b) of the regression line shown in equation 3.1 that is shown later with the Figure 3.1 that represents the parameter in a clear way, and as this parameter represents the fitting line of the distribution of the damage states with respect to the intensity measure IM, so as the line inclines more as the value of practical will increase which means the IM contributes well with damage state and as the inclination will decrease the value of practical will decrease to reach the worst case which is a horizontal line with a practical parameter equal to zero.

$$\ln(S_D) = \ln(a) + b.\ \ln(IM) \qquad \text{(equation 3.1)}$$

Efficiency (σ): The second parameter is the easier best examined parameter that describes the ideal IM that is efficiency, that as much reduction of the amount of variation in the evaluated damage state for a certain IM as it could be said more efficient, where it is shown in Figure 3.1 as the dispersion about the median threshold which is the standard deviation of the regression line that fits the structural demand with the intensity measure, efficiency mathematical formula is as shown in equation 3.2.

$$\beta_{D|IM} = \frac{\sum((ln(d_i) - \ln(aIM^b))^2}{N-2} \qquad \text{(equation 3.2)}$$

Proficiency (ξ):The last parameter is just a composition of the previous two parameters that involves a better selection of the IM, in which the dispersion is adjusted into a smaller value by taking into account the uncertainty of the study carried out by a specific intensity measure through its practicality parameter, this parameter gives a better prediction of the best correlated intensity measure than only depending on one parameter that may lead to incorrect selection of the intensity measure, this expression is shown in the equation 3.3.

$$\xi = \frac{\beta_{D|IM}}{b} \qquad \text{(equation 3.3)}$$

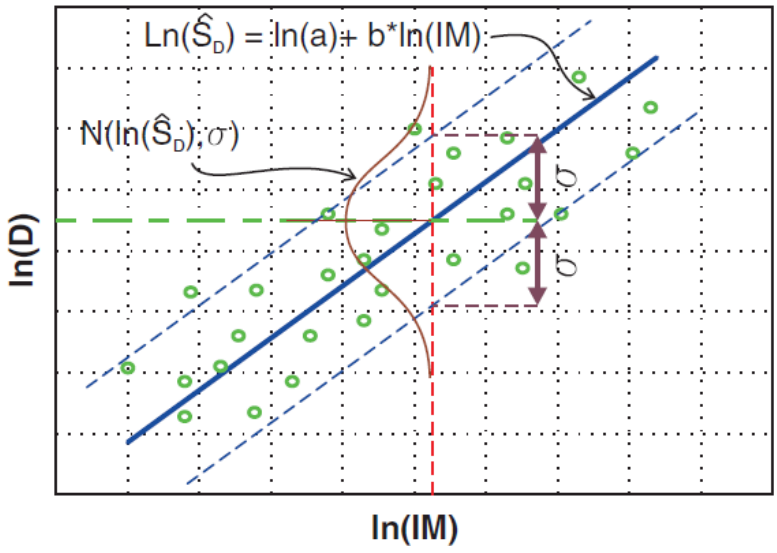

Figure 3. 2 Explanation of the parameters of the probabilistic seismic demand model (PADGETT, 2008)

3.2 Developing fragility curves with respect to the best intensity measure selected.

Final step that leads to the development of the fragility curves, where fragility curves are the probability of exceedance of that damage that is represented mathematically in equation 3.4 as the lognormal probability distribution function with respect to this intensity measure median value and the total standard deviation β_{tot}.

$$P_f(d_s \geq d_{si}|S)=\phi\left(\frac{1}{\beta_{tot}}.\ln\left(\frac{IM}{IM_{mi}}\right)\right) \qquad \text{(equation 3.4)}$$

After selecting the best intensity measures for each demand response discussed in the previous steps, it is time to define a limit damage states that will give the level of danger that the wall reaches according to its deformation.

Then using the median threshold parameter from the previous step of the regression line of the graph selected to have the specific intensity measure value of that damage state, that is one of the parameters shown in the equation 3.4.

The other parameter, which is the total standard deviation of the natural logarithm of spectral displacement for damage state shown in equation 3.5, that is a combination of three normal logarithmic parameters that are, the uncertainty in the estimate of the median value of the threshold of structural damage state (β_{ds}), variability in the capacity (response) properties of the model building type of the case study(β_C), and uncertainty in response due to the variation in space of ground motion demand spectrum (β_D), the last two parameters were taken from literature (Hazus-MH 2.1) but as there is no specific values for this value for a retaining wall, this values for a building similar in properties for a retaining wall.

These parameters are combined together by the SRSS method (square root squares summation) to get the total standard deviation of the data. The probability of exceedance function represents the fragility curve for each damage state level, the equation of this probability could be written as shown.

$$\beta_{tot} = \sqrt{(\beta_{ds})^2 + (\beta_C)^2 + (\beta_D)^2} \qquad \text{(equation 3.5)}$$

In this study case as mentioned before the study of the fragility curves has been done for two different limit damage states, one was in terms of displacement in which the limit damages of displacement levels were in terms to the wall height percentages, according to Huang et (2009) study given in (Table 3.1), as can be seen the damage levels has been divided into three levels listed as minor level

in which the serviceability of the highway supported by the retaining wall will be opened with certain speed limits, the second level of the damage state was the moderate level that if reached the highway either will be closed or some repairing works should be done, the third level is the extensive damage of the structure in which there are no more serviceability of the highway and it should be reconstructed.

Table 3.1 Definition of damage states for earth-retaining walls in terms of horizontal displacement

Damage state ds	Threshold for horizontal displacement D	Serviceability
Minor ds	2%.H	Open, reduce speeds
Moderate ds	5%.H	Closed or partial during repair works
Extensive ds	10%.H	Closed during reconstruction works

The second limit damage state was defined in terms of tilting angle in which the maximum angle that satisfy the static equilibrium has been discovered and used to evaluate a limit damage state, for each wall separately according to that angle.

This study two thresholds for the damage states were specified according to this angle, the damage states were again the same as the displacement one, but instead of using H value the angle that had been calculated (θ), starting with the minor damage state, reaching the extensive damage state passing through the moderate state, the first threshold was exactly as the Huang et (2009) percentages shown in Table 3.2.

Table 3.2 Definition of damage states for earth-retaining walls in terms of tilting angle

Damage state ds	Threshold for tilting angle θ	Serviceability
Minor ds	2%. θ	Open, reduce speeds
Moderate ds	5%. θ	Closed or partial during repair works
Extensive ds	10%. θ	Closed during reconstruction works

Another approach was used to compare between the two thresholds that was estimated as 20%, 50% and 80% according to each damage state respectively shown in (Table 3.3).

Table 3.3 Definition of damage states for earth-retaining walls in terms of tilting angle

Damage state ds	Threshold for tilting angle θ	Serviceability
Minor ds	20%. θ	Open, reduce speeds
Moderate ds	50%. θ	Closed or partial during repair works
Extensive ds	80%. θ	Closed during reconstruction works

The maximum inclination angle that satisfies the equilibrium of the retaining wall while tilting was found as shown in Figure 3.2. The forces that are affecting the wall are the active thrust of the backfill and the weight of the wall that is initially analysed into a vertical component and the resultant force for these two forces was found through the tangent of interaction angle (δ), which is the interaction angle between the wall and the soil.

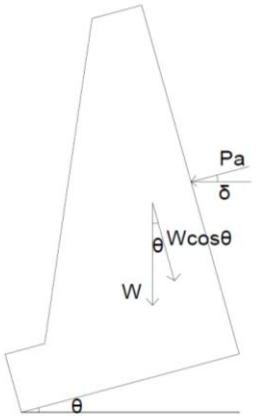

Figure 3.3 free body diagram of detecting the tilting angle

According to the walls geometry each wall has different forces as computed in chapter 1 with respect to its geometry and the type of the backfill, that leads to eight different static angles shown in Table 3.4 that are computed according equation 3.6.

$$\tan(\delta) = \frac{W.cos(\theta)}{P_a}, \qquad \theta = cos^{-1}\left(\frac{\tan(\delta).P_a}{W}\right) \qquad \text{(equation 3.6)}$$

Table 3.4 Static tilting angle for each wall case

Static tilting angle in degrees	Flat backfill	Slope backfill
First wall	28.20	20.1819
Second wall	30.61	22.70881
Third wall	25.88	17.65198
Fourth wall	20.18	10.73009

As the best correlated IM variated from one demand response to the other, a common better intensity measure that was PGA has been selected for all the models to have a comparison between the last fragility curves for all walls geometry of the same backfill case for both cases in order to see if we could have a certain relationship between the geometries of the walls and the fragility curves.

3.3 Evolution of the intensity measure better correlated with the retaining wall response for each wall.

3.3.1 The first wall of height 3.6m according to each backfill

The study was done according to the listed steps at the beginning of this chapter, the first step was to draw the evolution of damage with intensity measure and having the graphs of all the specific damage for each wall case and all the 34 damage states, which leads us to 34 graph for each case, in which the best correlated ones among all the IMs that has been decided as a second step according to the PSDM (probabilistic seismic demand model).

These parameters are shown for all the IMs in this case in Appendix C, Tables C1, C2, where here only the best correlated graphs are shown in this study, and the others were not represented, as the development of the fragility curves were done for only the best IMs.

In this case the best IMs, of retaining wall height of slope and flat cases, for each damage index of relative horizontal displacement and tilting were shown in Figure 3.3,3.4, and the selected IMs for discovering the fragility curves where listed in Table 3.5.

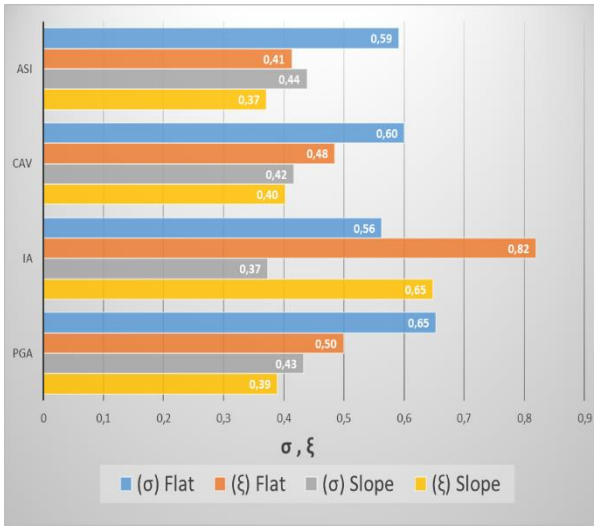

Figure 3.4 Comparing the best selected IMs with respect to efficiency (σ), and proficiency (ξ) for the first wall in terms of relative horizontal displacement

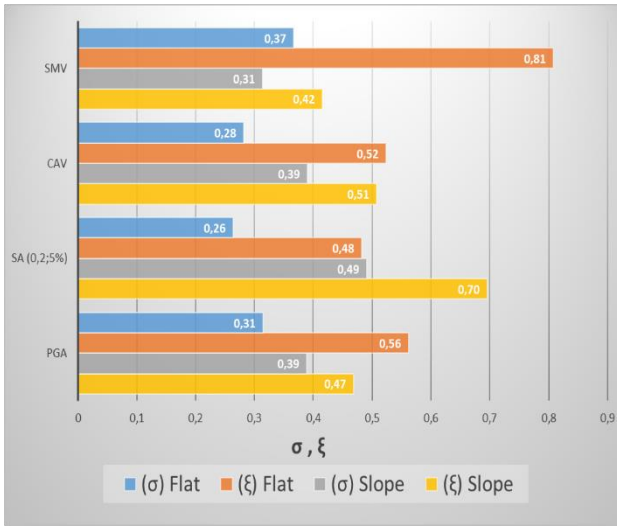

Figure 3.5 Comparing the best selected IMs for the with respect to efficiency (σ), and proficiency (ξ) first wall in terms of tilting

As it could be seen that the best PSDM parameters for the IMs in the first wall case of relative horizontal displacement damage index, were for the flat case represented by the blue bars for the efficiency (σ) and by the orange bars for the proficiency (ξ), that according to the efficiency in this case the best IM is the I_a, where after modifying it to proficiency we can see that it turns to be the ASI intensity measure, the same relation was for the slope case as the most efficient IM was the I_a but taking into account the practicality of the IMs, the best IM correlated to this case is the ASI again.

On the other hand, the other graph in terms the tilting damage state appears another result as the most efficient IM was the $S_{a(0,2;5\%)}$, which was again the proficient IM in the case of flat backfill, where this time the best intensity measure in the slope case was different from the flat case as the best IM for both parameters was the SMV.

Table 3.5 Best correlated IMs for the first wall case

The best four selected IMs	Flat		slope	
In terms of relative horizontal displacement	***PGA*** (m/s^2)	***ASI*** (m/s)	***PGA*** (m/s^2)	***ASI*** (m/s)
In terms of tilting	***PGA*** (m/s^2)	$S_{a(0,2;5\%)}(m/s^2)$	***PGA*** (m/s^2)	***SMV*** (cm/s)

Then the graphs were shown in Figures 3.5 to 3.12.

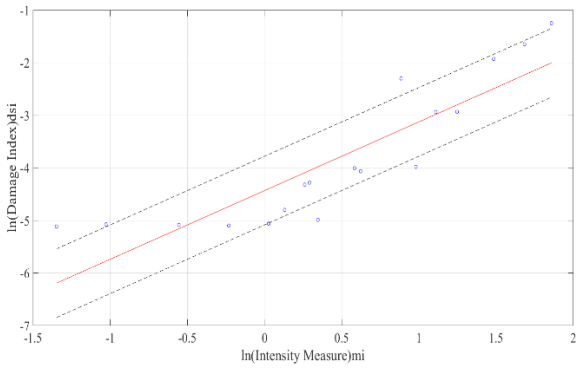

Figure 3.6 PGA flat relative horizontal displacement

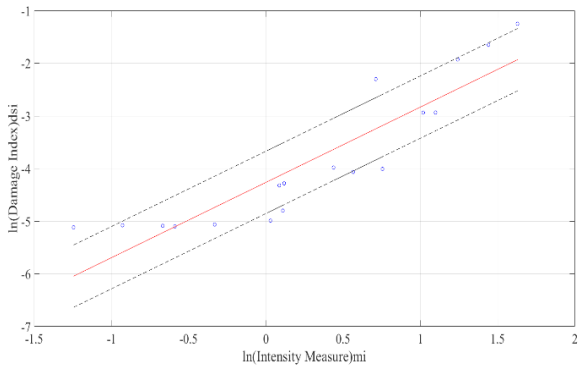

Figure 3.7 ASI flat relative horizontal displacement

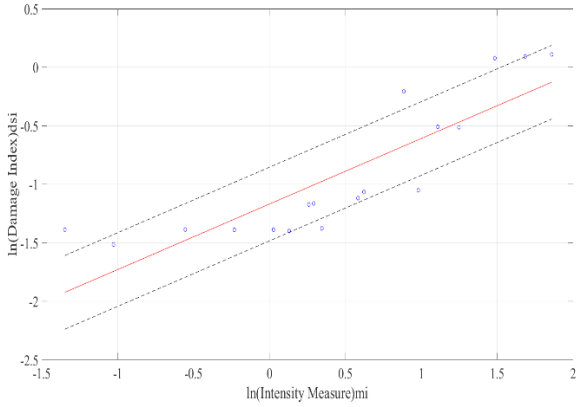

Figure 3.8 PGA flat Tilting

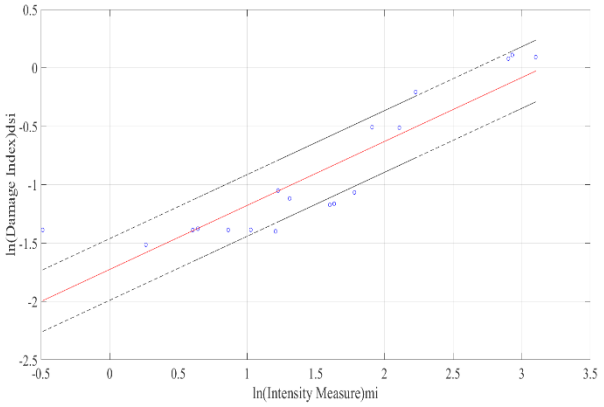

Figure 3.9 $S_{a(0,2;5\%)}$ flat Tilting

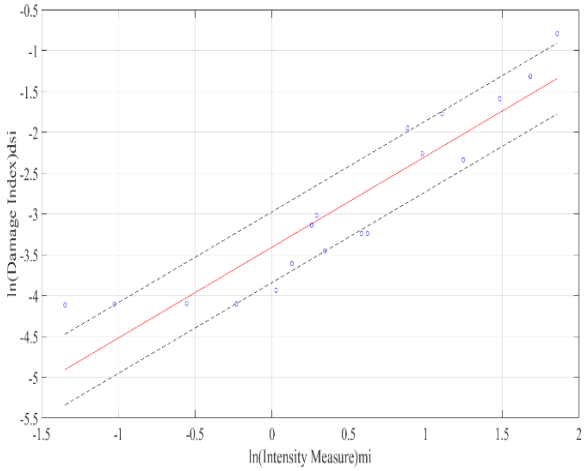

Figure 3. 10 PGA slope relative horizontal displacement

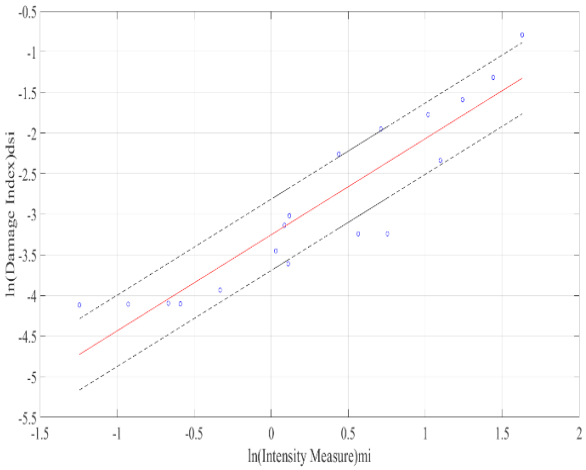

Figure 3.11 ASI slope relative horizontal displacement

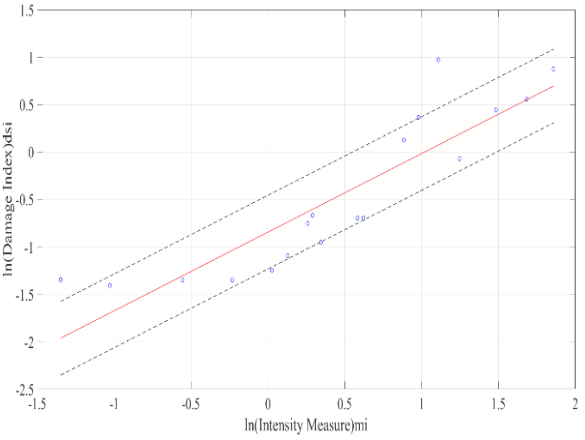

Figure 3.12 PGA slope Tilting

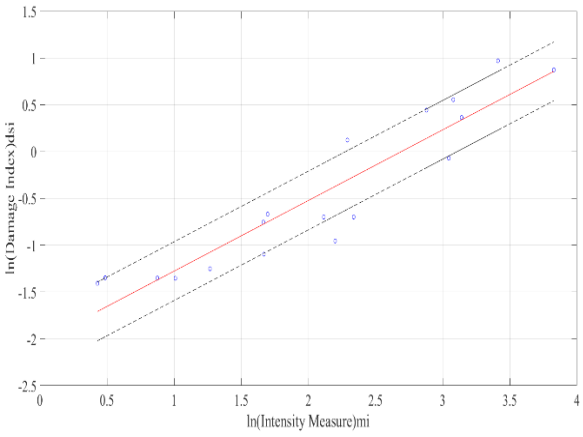

Figure 3.13 SMV slope Tilting

These graphs represent the best correlated IMs with the damage index according to the PSDM and in order to show the difference between the best four IMs a bar chart has been discussed to show the difference among the efficiency and the modified efficiency (proficiency).

3.3.2 The second wall of height 4.5m according to each backfill

The same steps that has been done for the first wall has been done for the second wall, the only thing that has changed is the results of choosing the best fitting IMs Table 3.6 that are shown as a bar chart comparison in Figures 3.13, 3.14and discussed according to the results of PSDM studies.

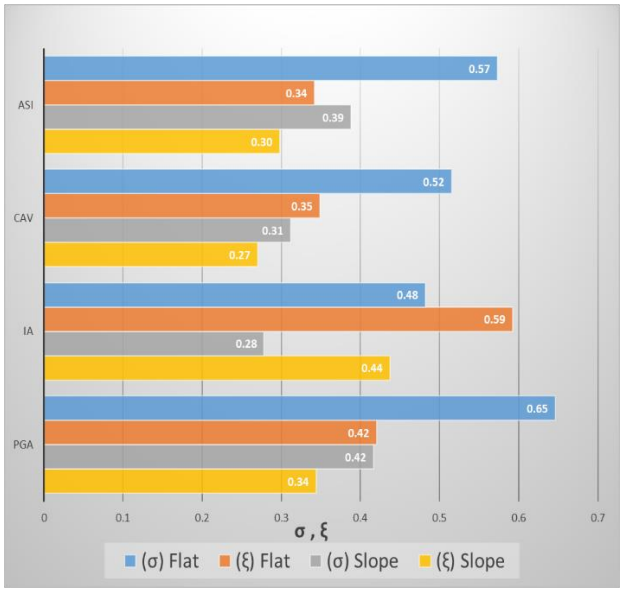

Figure 3.14 Comparing the best selected IMs with respect to efficiency (σ), and proficiency (ξ) for the second wall in terms of relative horizontal displacement

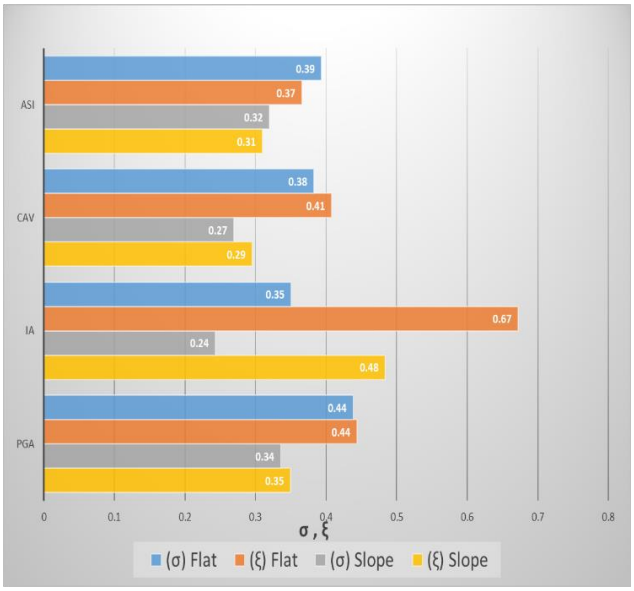

Figure 3.15 Comparing the best selected IMs for the with respect to efficiency (σ), and proficiency (ξ), second wall in terms of tilting

After the studies of PSDM for the second wall the best parameters for the IMs in the second wall case of relative horizontal displacement damage index, were for the flat case represented by the blue bars for the efficiency (σ) and by the orange bars for the proficiency (ξ), that according to the efficiency in this case the best IM is the I_a, where after modifying it to proficiency we can see that it turns to be the ASI intensity measure again as the first wall, the same relation was for the slope case as the most efficient IM was the I_a but taking into account the practicality of the IMs, the best IM correlated to this case is the CAV.

Where in this time the other graph in terms of tilting damage state appears different from the first wall but totally the same as the relative horizontal displacement which wasn't the same as the first wall, as the most efficient IM was the ASI, which was again the proficient IM in the case of flat backfill, where this time the best intensity measure in the slope case was not same as the flat case but the same as the slope case as for the previous damage state which is CAV.

Table 3.6 Best correlated IMs for the second wall case

The best four selected IMs	flat		slope	
In terms of relative horizontal displacement	***PGA (m/s^2)***	***ASI (m/s)***	***PGA (m/s^2)***	***CAV (cm/s)***
In terms of tilting	***PGA (m/s^2)***	***ASI (m/s)***	***PGA (m/s^2)***	***CAV (cm/s)***

These graphs represent the best correlated IMs with the damage index according to the PSDM and after selecting the best four IMs in Figures 3.15 to 3.22.

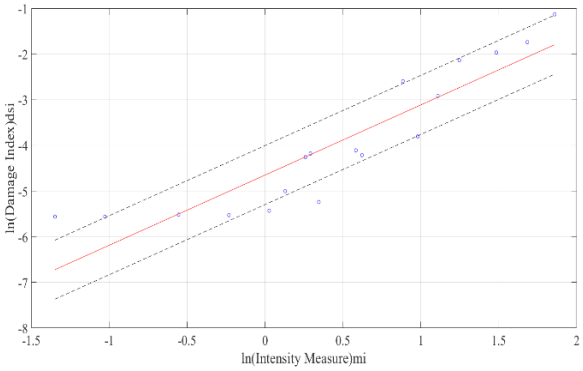

Figure 3.16 PGA flat relative horizontal displacement

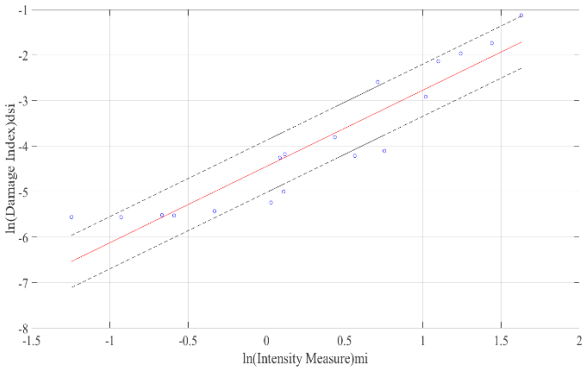

Figure 3.17 ASI flat relative horizontal displacement

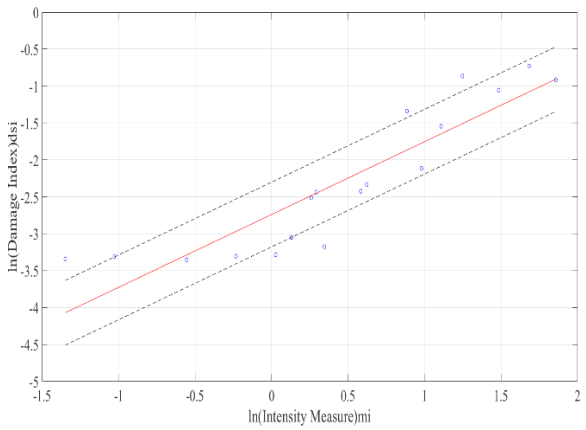

Figure 3.18 PGA flat Tilting

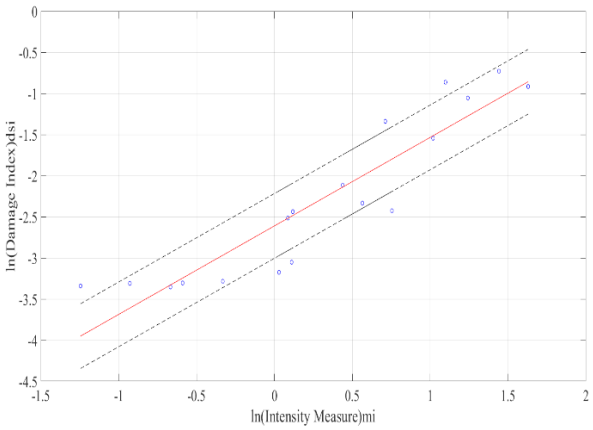

Figure 3.19 ASI *flat Tilting*

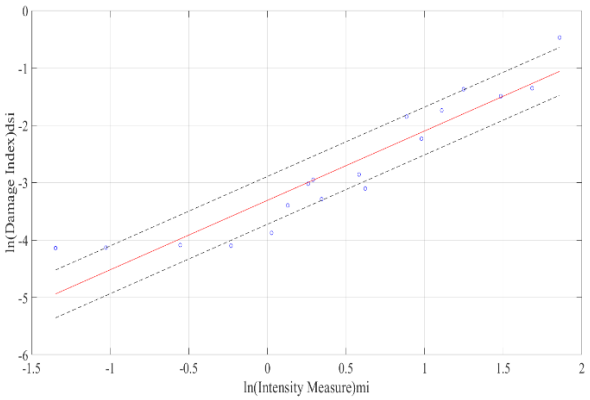

Figure 3. 20 PGA slope relative horizontal displacement

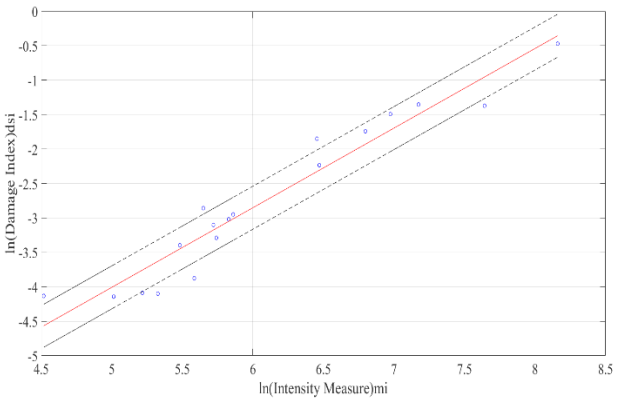

Figure 3.21 CAV slope relative horizontal displacement

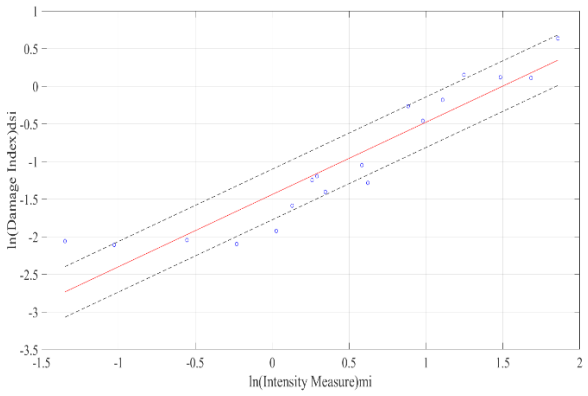

Figure 3.22 PGA slope Tilting

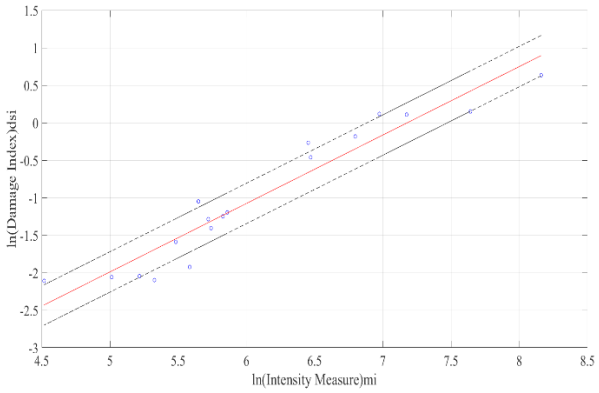

Figure 3.23 CAV slope Tilting

3.3.3 The third wall of height 5.5m according to each backfill

Again, the repetition of the previous steps has been done and the results are discussed according to the best 4 correlated IMs as bar charts in Figure 3.23, 3.24.

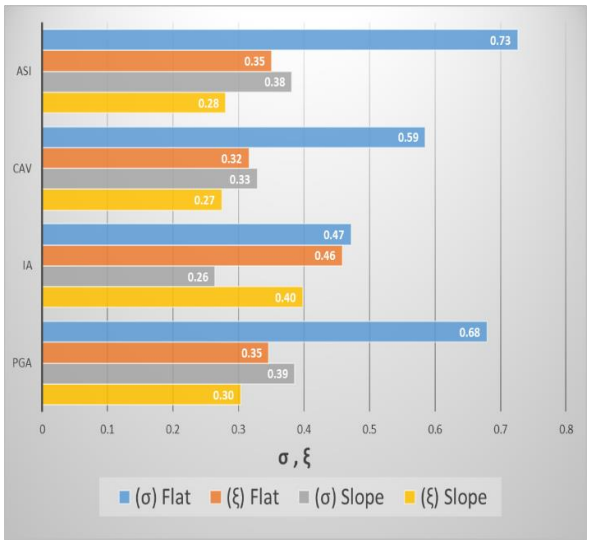

Figure 3.24 Comparing the best selected IMs with respect respect to efficiency (σ), and proficiency (ξ) for the third wall in terms of relative horizontal displacement

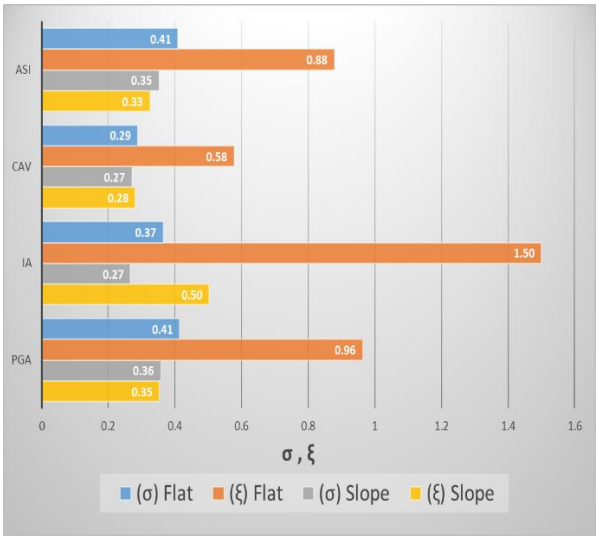

Figure 3.25 Comparing the best selected IMs for the with to efficiency (σ), and proficiency (ξ) third wall in terms of tilting

After the studies of PSDM for the third wall, the best parameters for the IMs in the third wall case of relative horizontal displacement damage index, were for the flat case represented by the blue bars for the efficiency (σ) and by the orange bars for the proficiency (ξ) as previous, that according to the efficiency in this case the best IM is the I_a, where after modifying it to proficiency we can see that it turns to be the CAV intensity measure, the same relation was for the slope case as the most efficient IM was the I_a but taking into account the practicality of the IMs, the best IM correlated to this case is the CAV that mean that CAV fits the best for both cases slope and flat for the third wall.

While in terms the tilting damage state appears exactly the same as the relative horizontal displacement case as the most efficient IM was the CAV, in both backfill cases which means that the

third wall is fitting totally with CAV intensity measure, so the best IMs are listed in Table 3.7.

Table 3.7 Best correlated IMs for the third wall case

The best four selected IMs	flat		slope	
In terms of relative horizontal displacement	***PGA (m/s^2)***	***CAV (cm/s)***	***PGA (m/s^2)***	***CAV (cm/s)***
In terms of tilting	***PGA (m/s^2)***	***CAV (cm/s)***	***PGA (m/s^2)***	***CAV (cm/s)***

These graphs represent the best correlated IMs with the damage index according to the PSDM and after selecting the best four IMs in Figures 3.25 to 3.32.

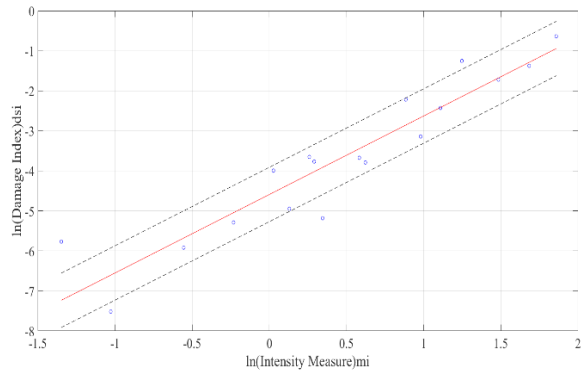

Figure 3.26 PGA flat relative horizontal displacement

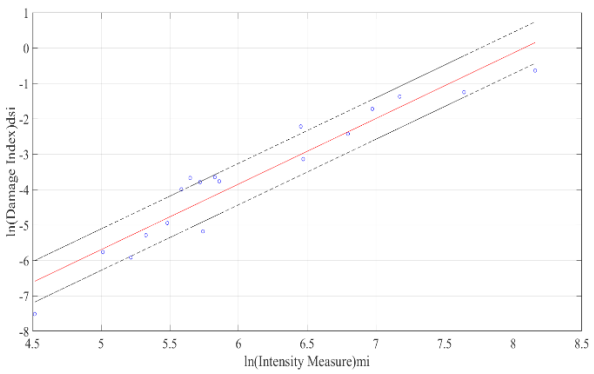

Figure 3.27 CAV flat relative horizontal displacement

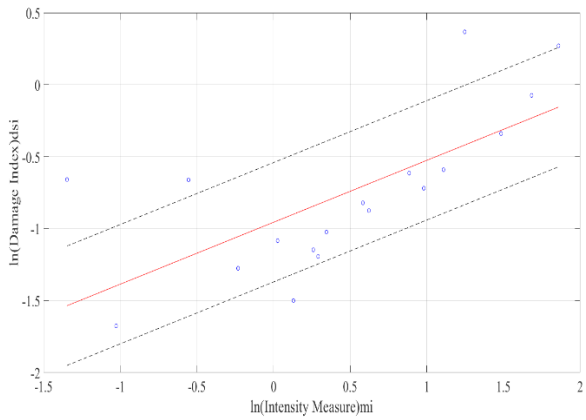

Figure 3.28 PGA flat Tilting

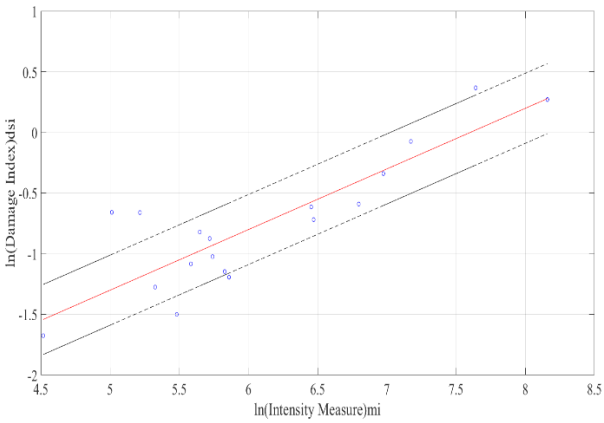

Figure 3.29 CAV flat Tilting

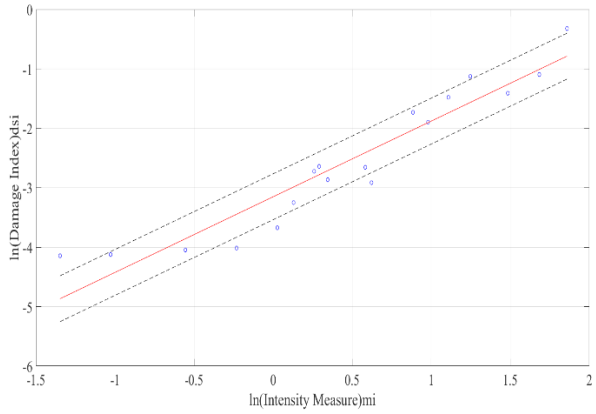

Figure 3. 30 PGA slope relative horizontal displacement

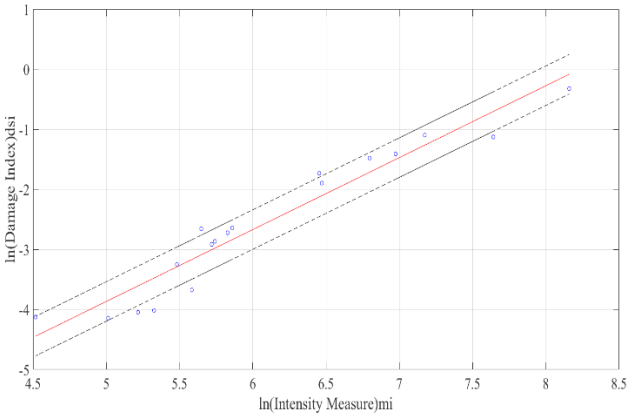

Figure 3.31 CAV slope relative horizontal displacement

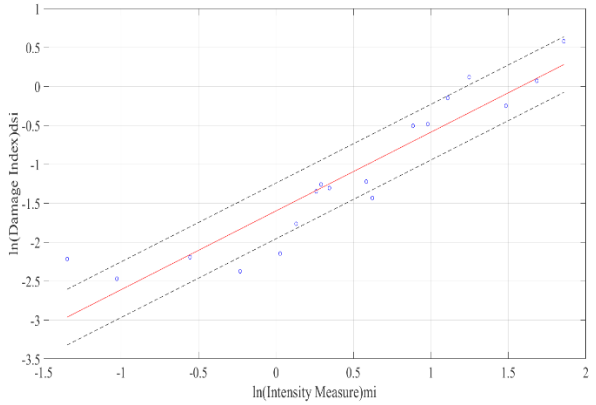

Figure 3.32 PGA slope Tilting

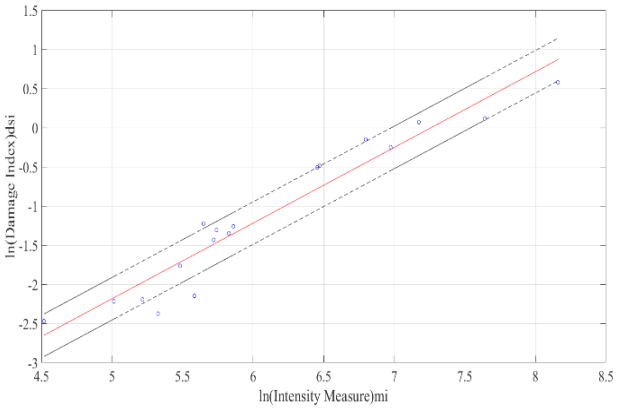

Figure 3.33 CAV slope Tilting

3.3.4 The fourth wall of height 6.5m according to each backfill

The last wall was again derived through similar steps as before and the initial step of PSDM studies, that in which the best fitting IMs has been compared for all the cases are shown in Figures 3.33, 34.

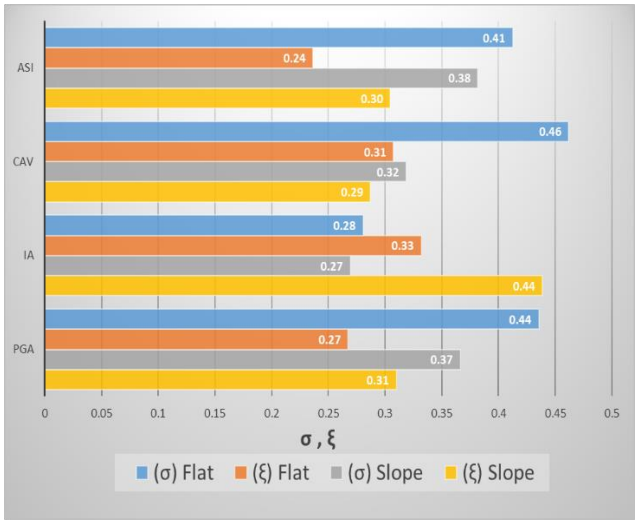

Figure 3.34 Comparing the best selected IMs with respect to efficiency (σ), and proficiency (ξ) for the fourth wall in terms of relative horizontal displacement

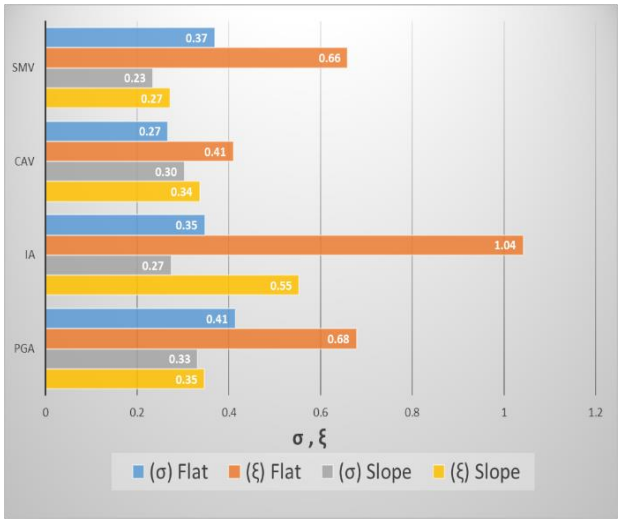

Figure 3.35 Comparing the best selected IMs for the with respect to efficiency (σ), and proficiency (ξ) fourth wall in terms of tilting

The fourth wall best parameters for the IMs case of relative horizontal displacement damage index, were for the flat case represented by the blue bars for the efficiency (σ) and by the orange bars for the proficiency (ξ) as previous, that according to the efficiency in this case the best IM is the I_a, where after modifying it to proficiency we can see that it turns to be the ASI intensity measure, the slope case was different as the most efficient IM was the I_a but taking into account the practicality of the IMs, the best IM correlated to this case is the CAV.

While in terms the tilting damage state, the most efficient IM was the CAV, for the flat case while it was SMV as the first wall in this study. The selected IMs in Table 3.8.

Table 3.8 Best correlated IMs for the fourth wall case

The best four selected IMs	flat		Slope	
In terms of relative horizontal displacement	***PGA (m/s²)***	***ASI (m/s)***	***PGA (m/s²)***	***CAV (cm/s)***
In terms of tilting	***PGA (m/s²)***	***CAV (cm/s)***	***PGA (m/s²)***	***SMV (cm/s)***

These graphs represent the best correlated IMs with the damage index according to the PSDM and after selecting the best four IMs in Figures 3.35 to 3.42.

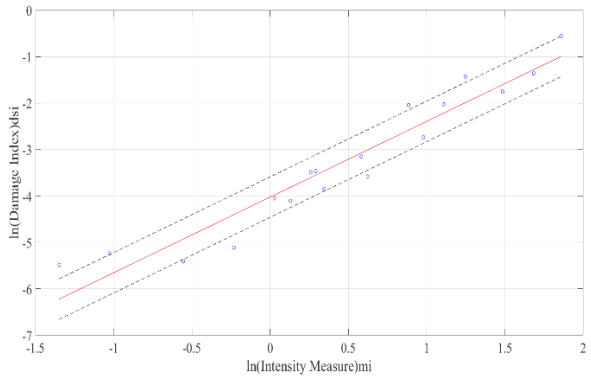

Figure 3.36 PGA flat relative horizontal displacement

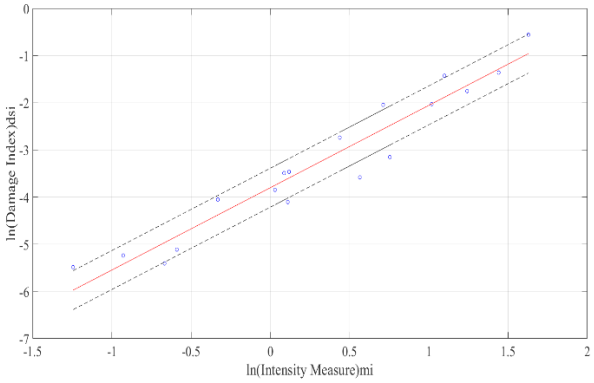

Figure 3.37 ASI flat relative horizontal displacement

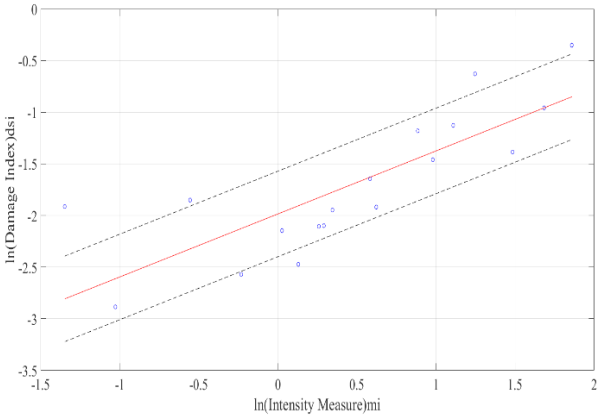

Figure 3.38 PGA flat Tilting

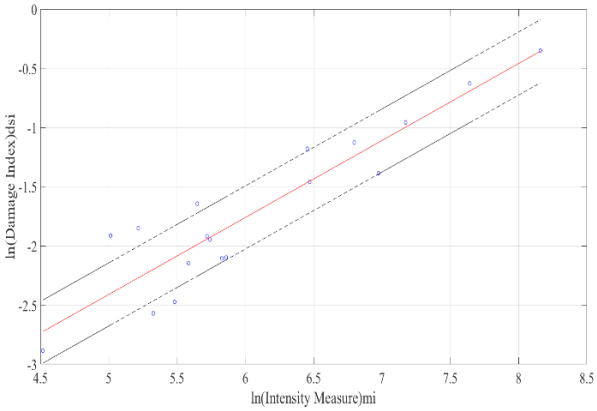

Figure 3.39 CAV flat Tilting

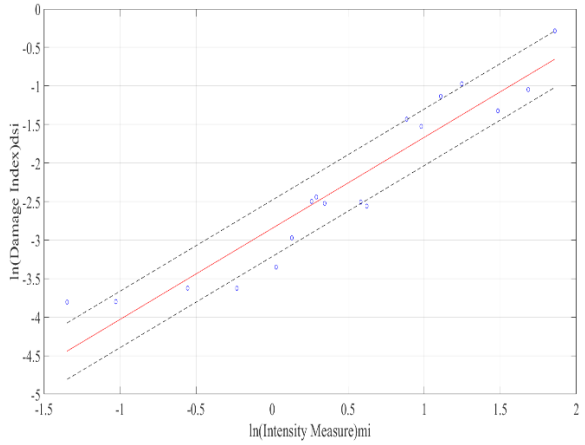

Figure 3. 40 PGA slope relative horizontal displacement

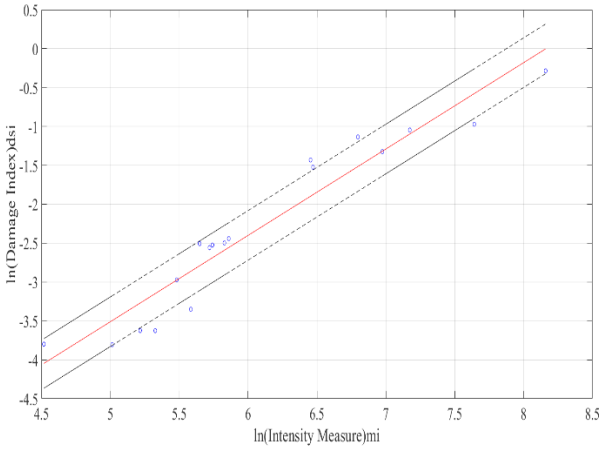

Figure 3.41 CAV slope relative horizontal displacement

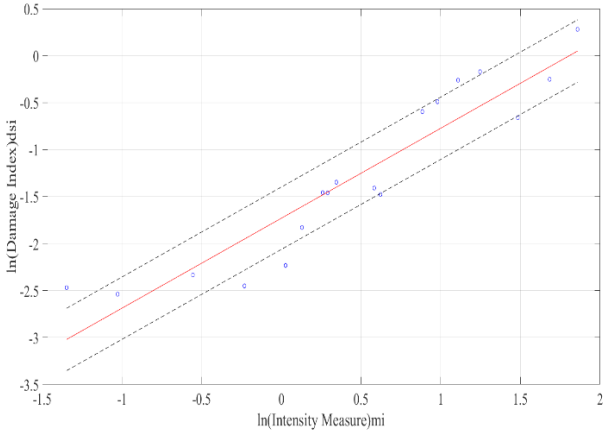

Figure 3.42 PGA slope Tilting

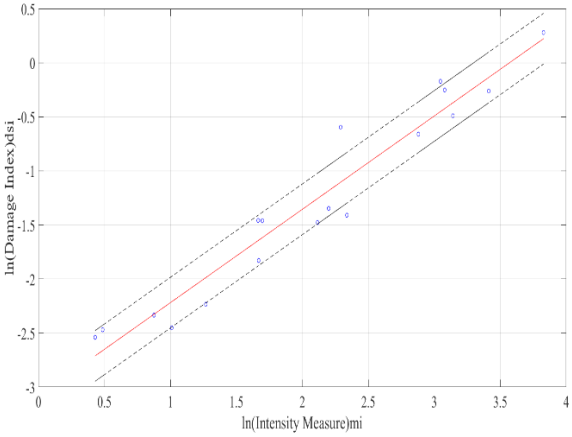

Figure 3.43 SMV slope Tilting

3.4 Developing fragility curves with respect to the best intensity measure selected for each wall.

3.4.1 The first wall of height 3.6m according to each backfill

After knowing the best correlated IMs the last step was to develop the fragility curves according to each case IMs selected, which was done as written in paragraph 3.3 which in order to do it the total logarithmic standard deviation has been calculated and the logarithmic median IM with respect to the damage state values according to the threshold was also computed as shown (Appendix C Table C.14), in order to make the cumulative lognormal function that gives the probability of exceedance according to these parameters. Surely that each fragility curves graph that are shown in Figures 3.43 to 3.54 are done for each case as mentioned in their references.

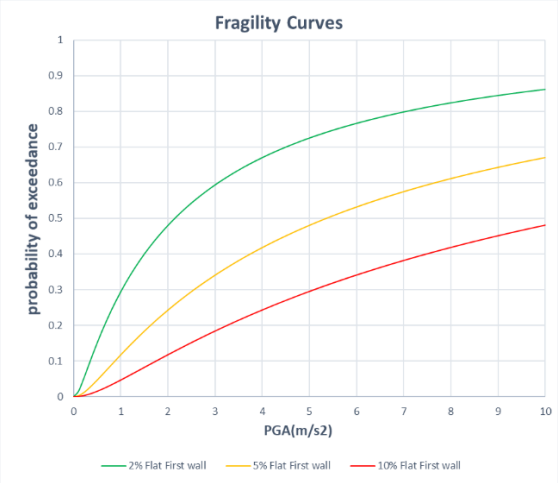

Figure 3.44 First wall flat backfills fragility curves in terms of PGA with respect to relative horizontal displacement

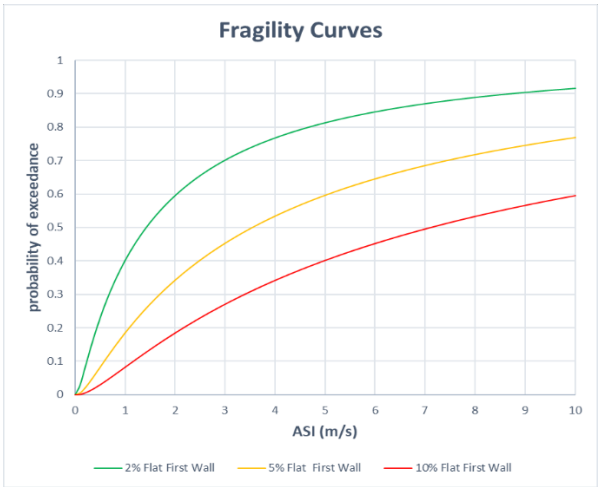

Figure 3.45 First wall flat backfills fragility curves in terms of ASI with respect to relative horizontal displacement

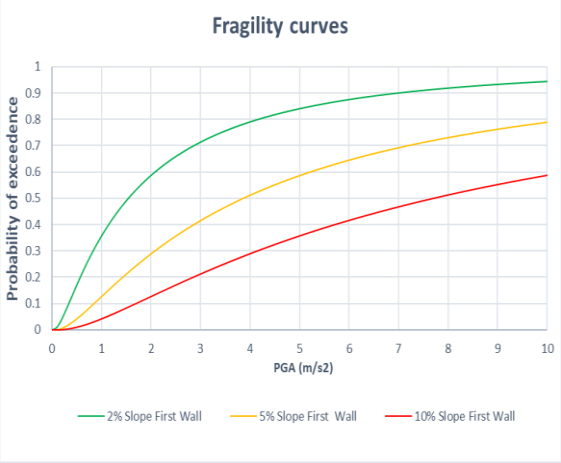

Figure 3.46 First wall slope backfills fragility curves in terms of PGA with respect to relative horizontal displacement

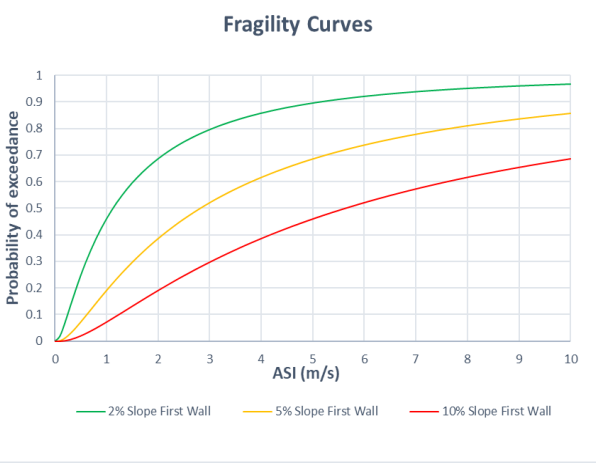

Figure 3.47 First wall slope backfills fragility curves in terms of ASI with respect to relative horizontal displacement

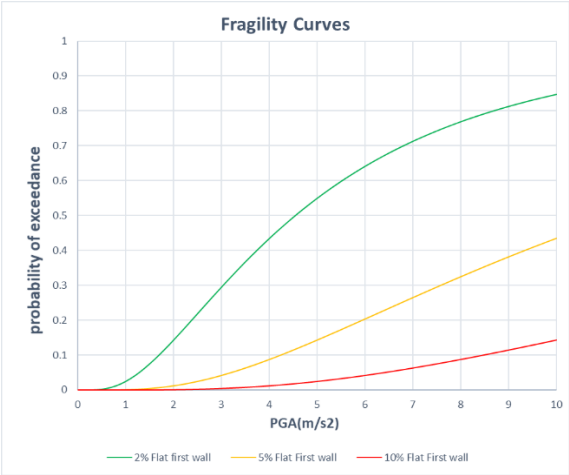

Figure 3.48 First wall flat backfills fragility curves in terms of PGA with respect to tilting angle first threshold

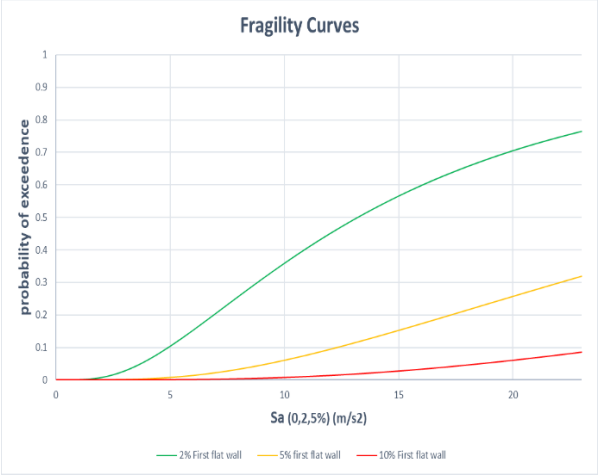

Figure 3.49 First wall flat backfills fragility curves in terms of $S_{a(0,2;5\%)}$ with respect to tilting angle first threshold

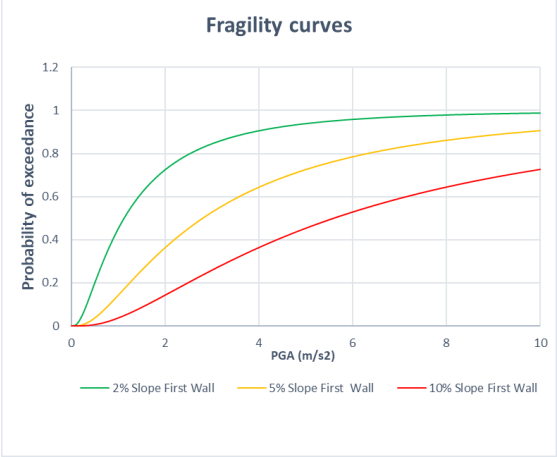

Figure 3.50 First wall slope backfills fragility curves in terms of PGA with respect to tilting angle first threshold

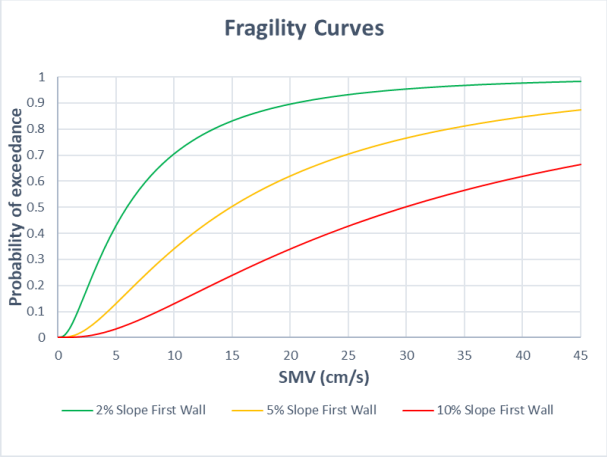

Figure 3.51 First wall slope backfills fragility curves in terms of SMV with respect to tilting angle first threshold

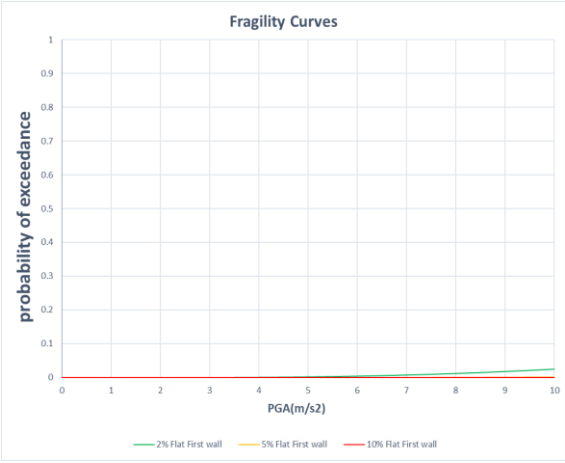

Figure 3.52 First wall flat backfills fragility curves in terms of PGA with respect to tilting angle second threshold

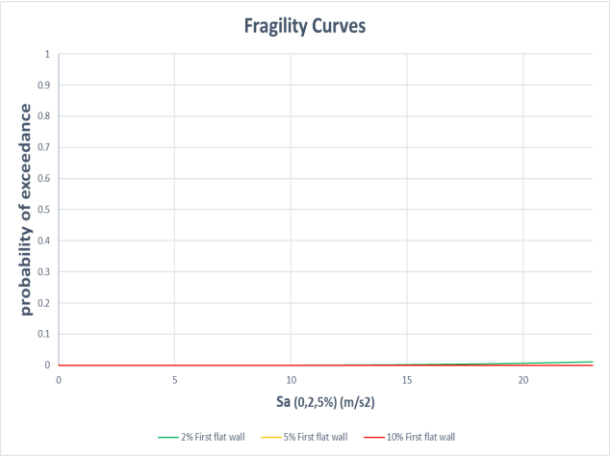

Figure 3.53 First wall flat backfills fragility curves in terms of $S_{a(0,2;5\%)}$ with respect to tilting angle second threshold

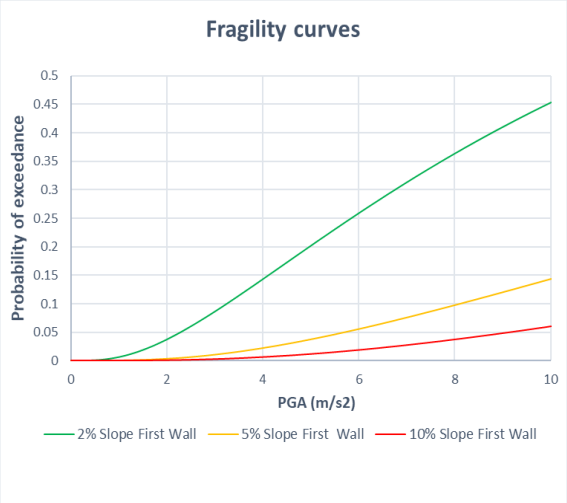

Figure 3.54 First wall slope backfills fragility curves in terms of PGA with respect to tilting angle second threshold

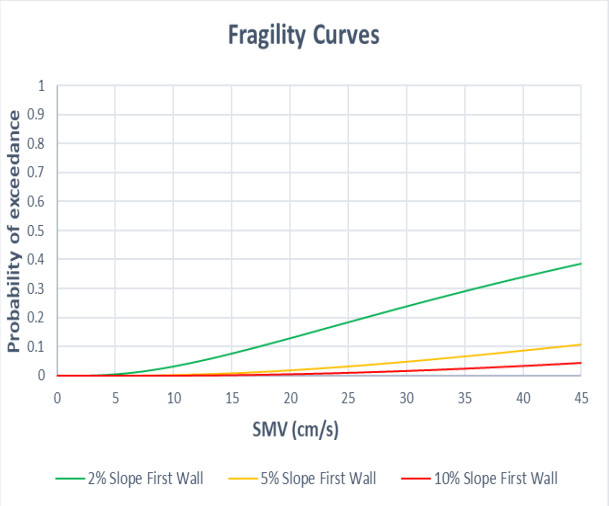

Figure 3.55 First wall flat backfills fragility curves in terms of SMV with respect to tilting angle second threshold

3.4.2 The second wall of height 4.5m according to each backfill

As the first wall, the last step was to develop the fragility curves according to each case IMs selected, which was done as written in paragraph 3.3 which in order to do it the total logarithmic standard deviation has been calculated and the logarithmic median IM with respect to the damage state values according to the threshold was also computed as shown (Appendix C Table C.15) , in order to make the cumulative lognormal function that gives the probability of exceedance according to these parameters. Surely that each fragility curves graph that are shown in Figures 3.55 to 3.66 are done for each case as mentioned in their references.

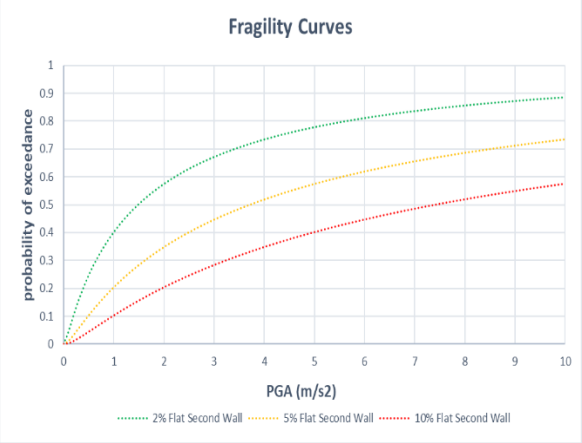

Figure 3.56 Second wall flat backfills fragility curves in terms of PGA with respect to relative horizontal displacement

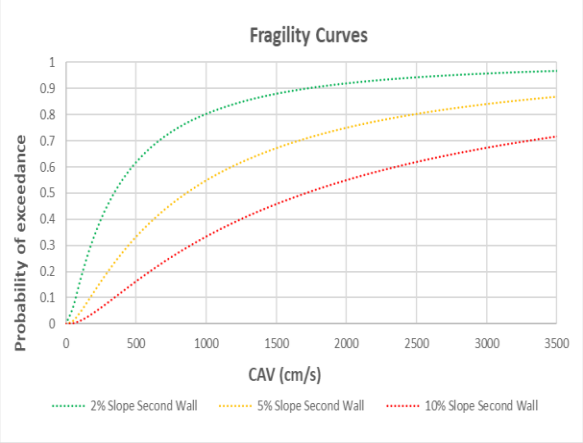

Figure 3.57 second wall flat backfills fragility curves in terms of ASI with respect to relative horizontal displacement

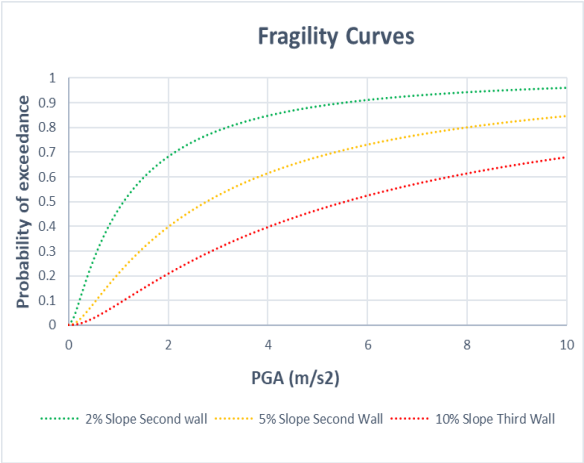

Figure 3.58 Second wall slope backfills fragility curves in terms of PGA with respect to relative horizontal displacement

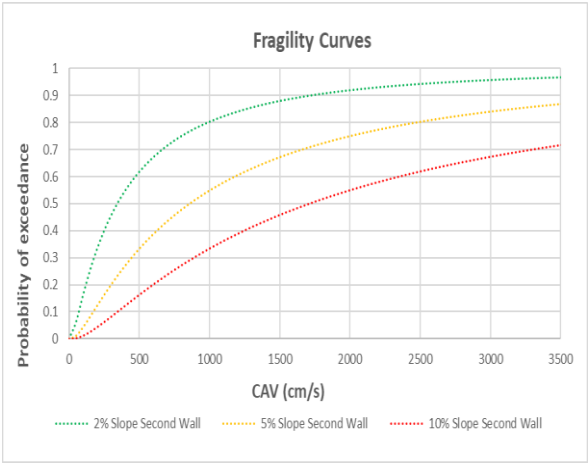

Figure 3.59 Second wall slope backfills fragility curves in terms of CAV with respect to relative horizontal displacement

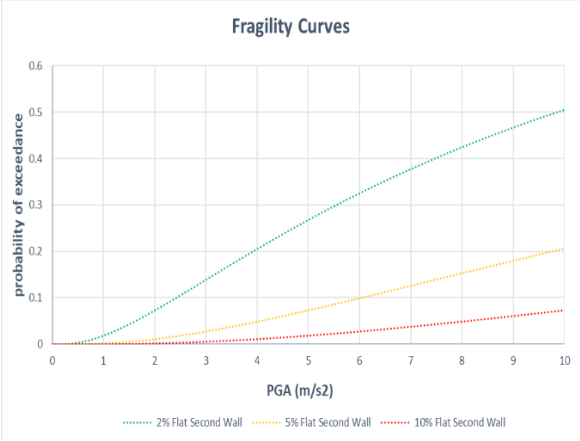

Figure 3.60 Second wall flat backfills fragility curves in terms of PGA with respect to tilting angle first threshold

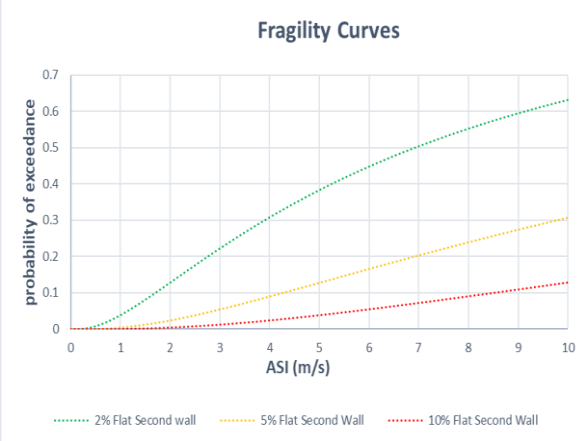

Figure 3.61 Second wall flat backfills fragility curves in terms of ASI with respect to tilting angle first threshold

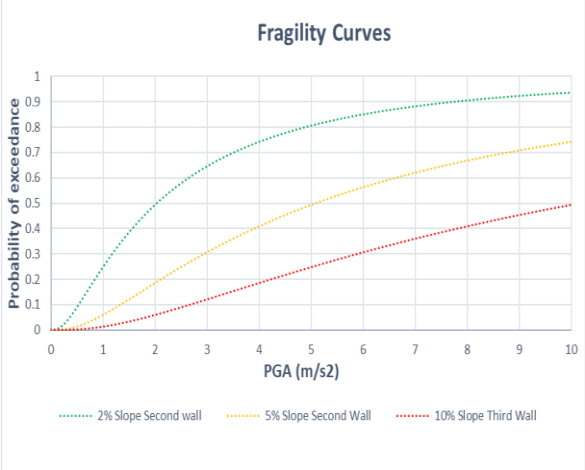

Figure 3.62 Second wall slope backfills fragility curves in terms of PGA with respect to tilting angle first threshold

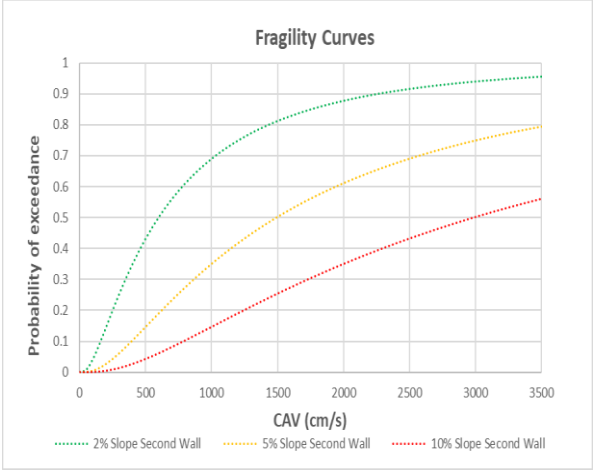

Figure 3.63 Second wall slope backfills fragility curves in terms of CAV with respect to tilting angle first threshold

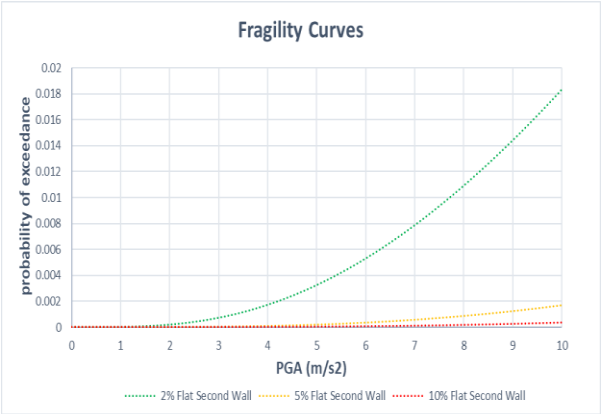

Figure 3.64 Second wall flat backfills fragility curves in terms PGA with respect to tilting angle second threshold

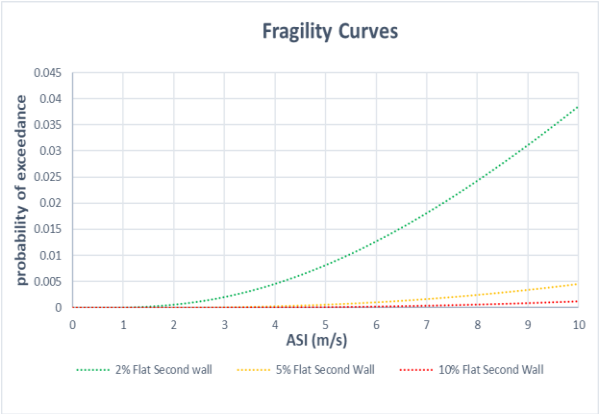

Figure 3.65 Second wall flat backfills fragility curves in terms of of ASI with respect to tilting angle second threshold

Figure 3.66 Second wall slope backfills fragility curves in terms of PGA with respect to tilting angle second threshold

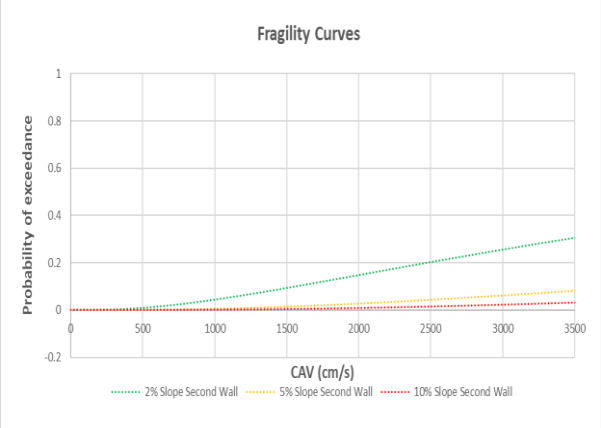

Figure 3.67 Second wall slope backfills fragility curves in terms of CAV with respect to tilting angle second threshold

3.4.3 The third wall of height 5.5m according to each backfill

After selecting the best correlated IMs the last step for the third wall was to develop the fragility curves according to each case IMs selected, which was done as written in paragraph 3.3 which in order to do it the total logarithmic standard deviation has been calculated and the logarithmic median IM with respect to the damage state values according to the threshold was also computed as shown in Appendix C Table C.16, in order to make the cumulative lognormal function that gives the probability of exceedance according to these parameters. Surely that each fragility curves graph that are shown in Figures 3.67 to 3.78are done for each case as mentioned in their references.

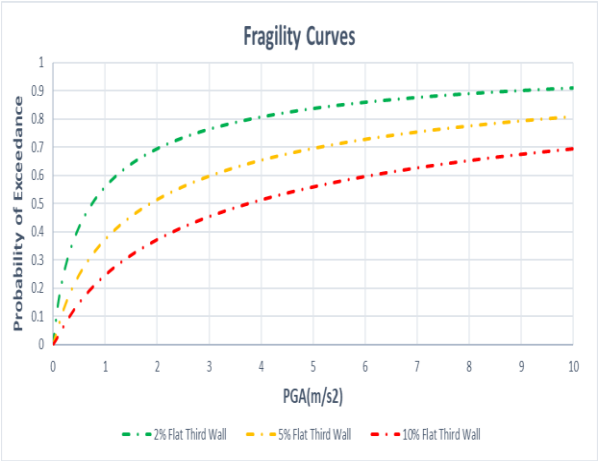

Figure 3.68 Third wall flat backfills fragility curves in terms of PGA with respect to relative horizontal displacement

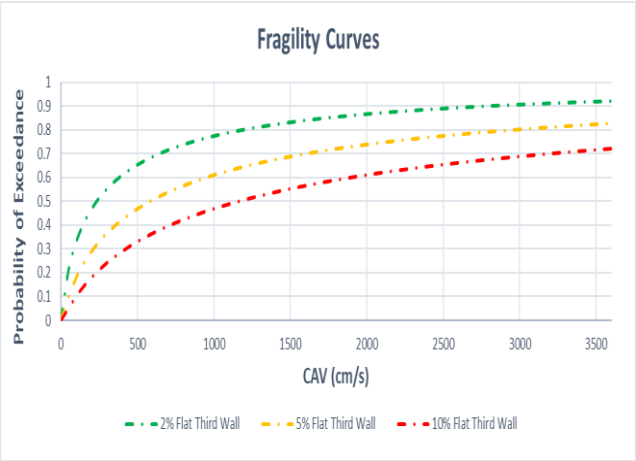

Figure 3.69 Third wall flat backfills fragility curves in terms of CAV with respect to relative horizontal displacement

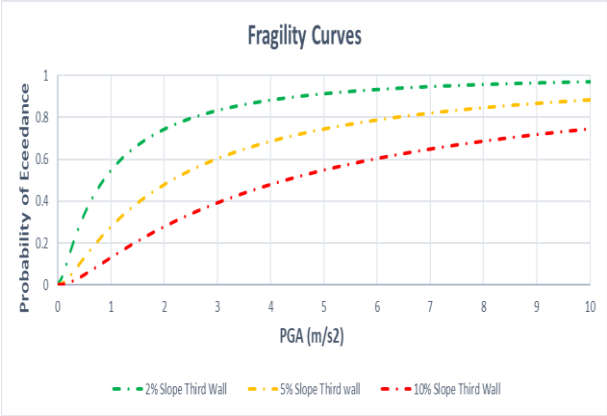

Figure 3.70 Third wall slope backfills fragility curves in terms of PGA with respect to relative horizontal displacement

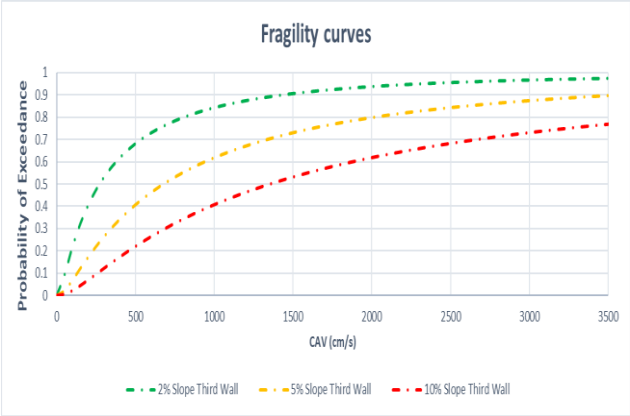

Figure 3.71 Third wall slope backfills fragility curves in terms of CAV with respect to relative horizontal displacement

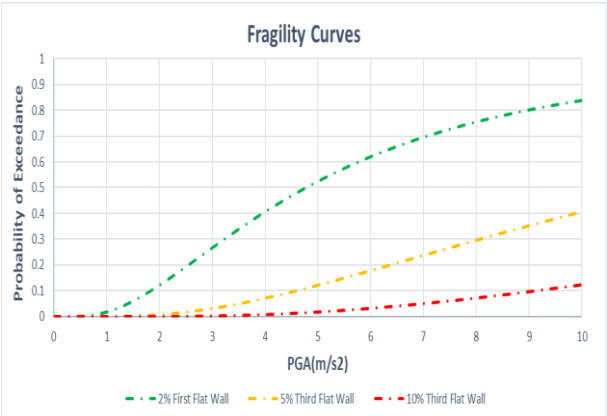

Figure 3. 72 Third wall flat backfills fragility curves in terms of PGA with respect to tilting angle first threshold

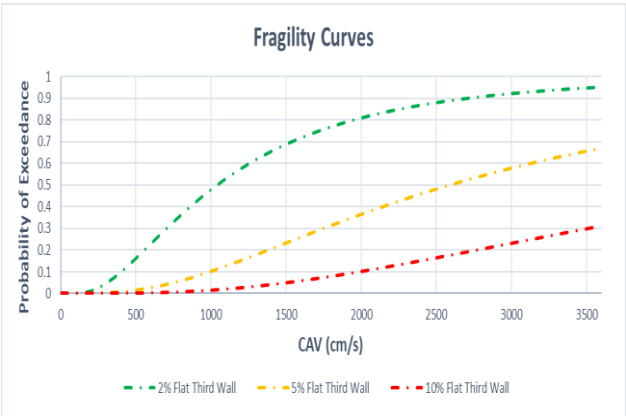

Figure 3.73 Third wall flat backfills fragility curves in terms of CAV with respect to tilting angle first threshold

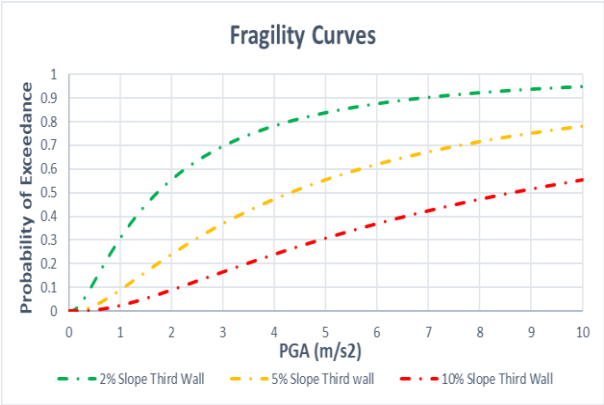

Figure 3.74 Third wall slope backfills fragility curves in terms of PGA with respect to tilting angle first threshold

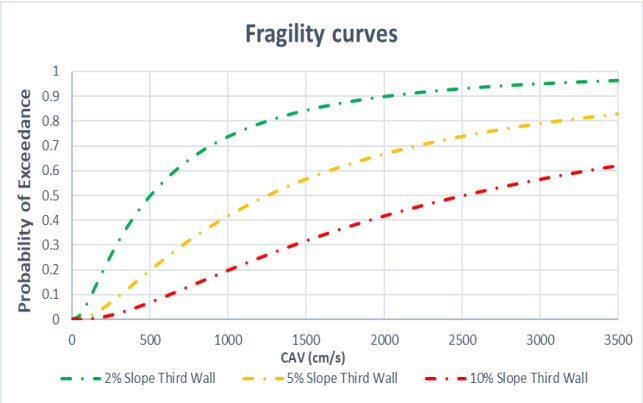

Figure 3.75 Third wall slope backfills fragility curves in terms of CAV with respect to tilting angle first threshold

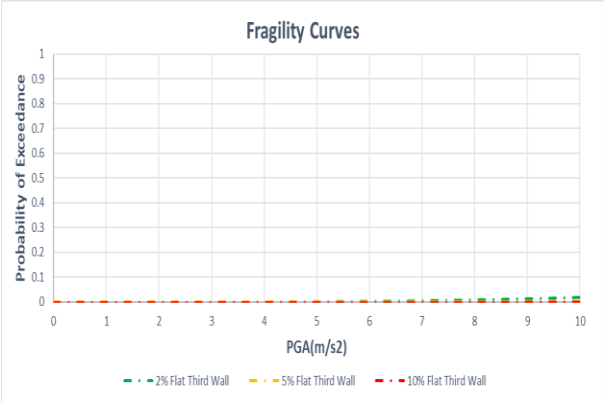

Figure 3.76 Third wall flat backfills fragility curves in terms of PGA with respect to tilting angle second threshold

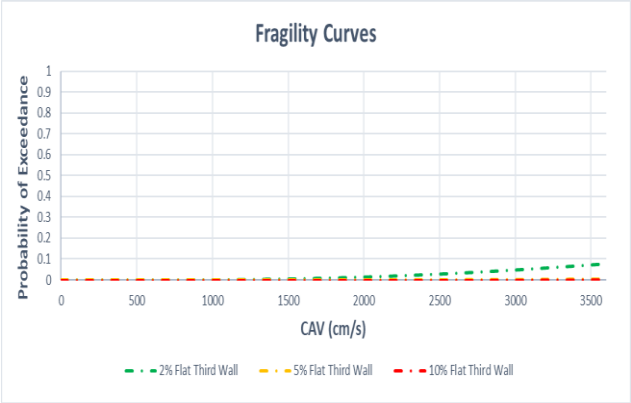

Figure 3.77 Third wall flat backfills fragility curves in terms of CAV with respect to tilting angle second threshold

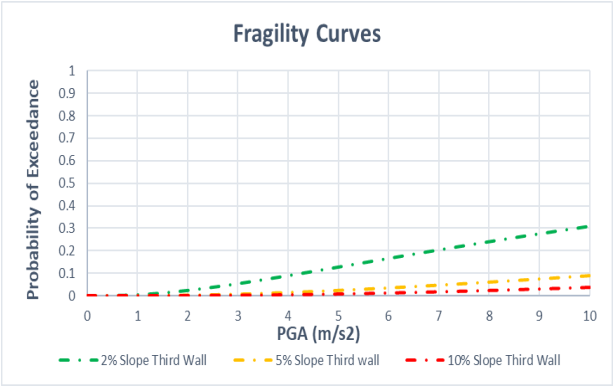

Figure 3.78 Third wall slope backfills fragility curves in terms of PGA with respect to tilting angle second threshold

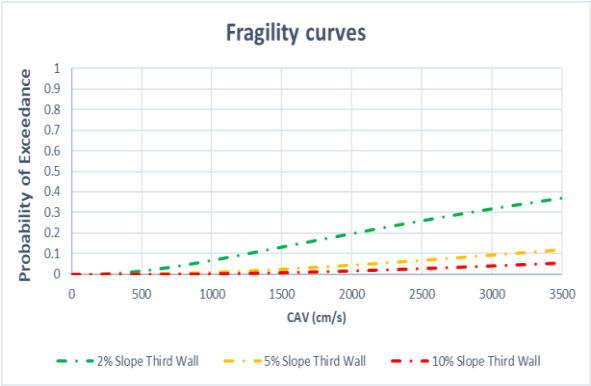

Figure 3.79 Third wall slope backfills fragility curves in terms of CAV with respect to tilting angle second threshold

3.4.4 The fourth wall of height 6.5m according to each backfill

The final usual step of developing the fragility curves, after knowing the best correlated IMs, according to each case IMs selected, which was done as written in paragraph 3.3 which in order to do it the total logarithmic standard deviation has been calculated and the logarithmic median IM with respect to the damage state values according to the threshold was also computed as shown in Appendix C Table C.17, in order to make the cumulative lognormal function that gives the probability of exceedance according to these parameters. Surely that each fragility curves graph that are shown in Figures 3.79 to 3.90 are done for each case as mentioned in their references.

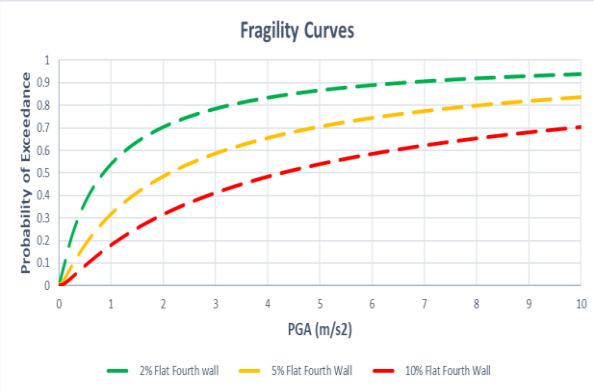

Figure 3.80 Fourth wall flat backfills fragility curves in terms of PGA with respect to relative horizontal displacement

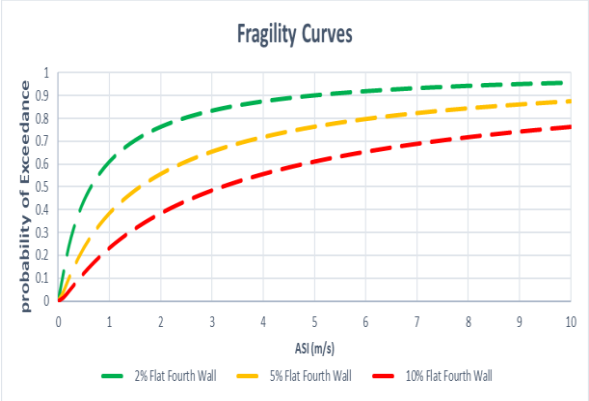

Figure 3.81 Fourth wall flat backfills fragility curves in terms of ASI with respect to relative horizontal displacement

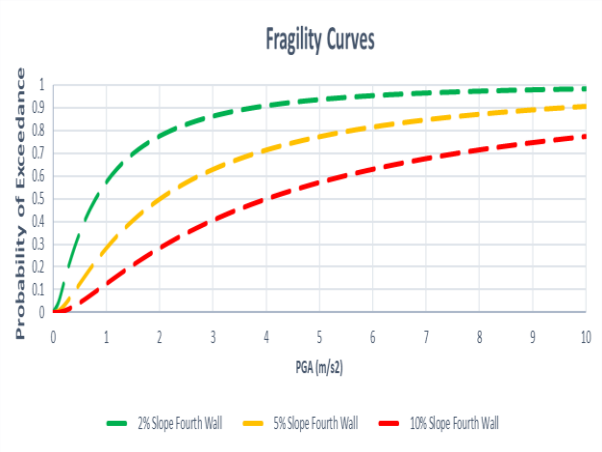

Figure 3.82 Fourth wall slope backfills fragility curves in terms of PGA with respect to relative horizontal displacement

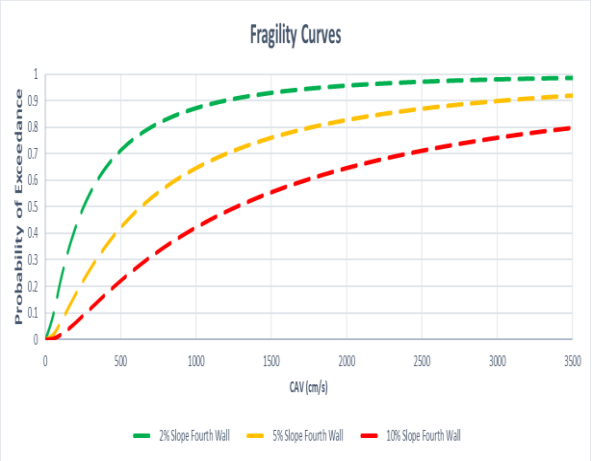

Figure 3.83 Fourth wall slope backfills fragility curves in terms of CAV with respect to relative horizontal displacement

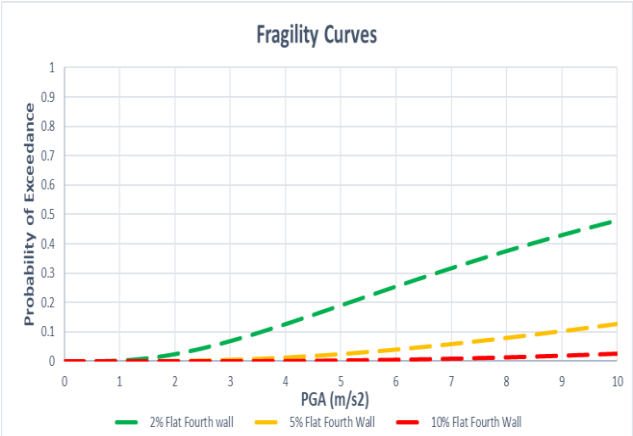

Figure 3.84 Fourth wall flat backfills fragility curves in terms of PGA with respect to tilting angle first threshold

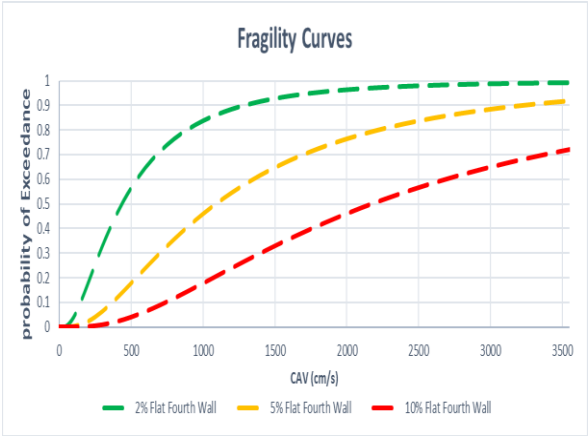

Figure 3.85 Fourth wall flat backfills fragility curves in terms of CAV with respect to tilting angle first threshold

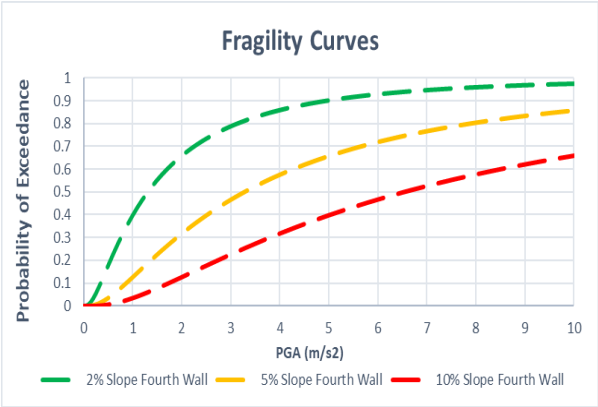

Figure 3.86 Fourth wall slope backfills fragility curves in terms of PGA with respect to tilting angle first threshold

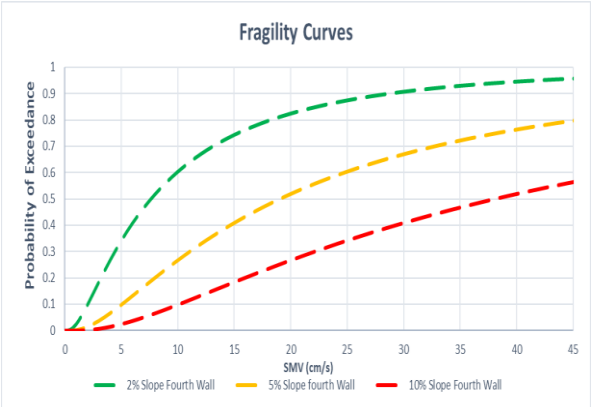

Figure 3.87 Fourth wall slope backfills fragility curves in terms of SMV with respect to tilting angle first threshold

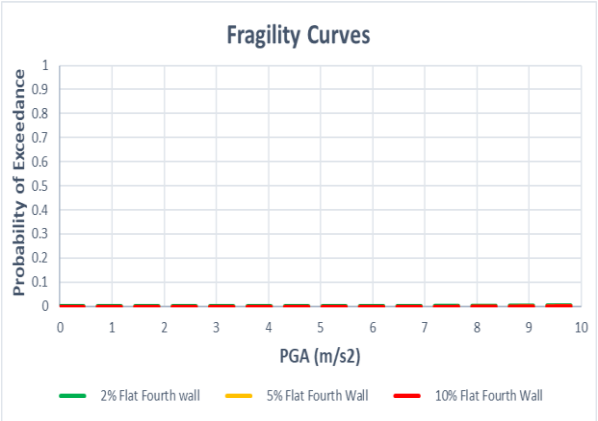

Figure 3.88 Fourth wall flat backfills fragility curves in terms of PGA with respect to tilting angle second threshold

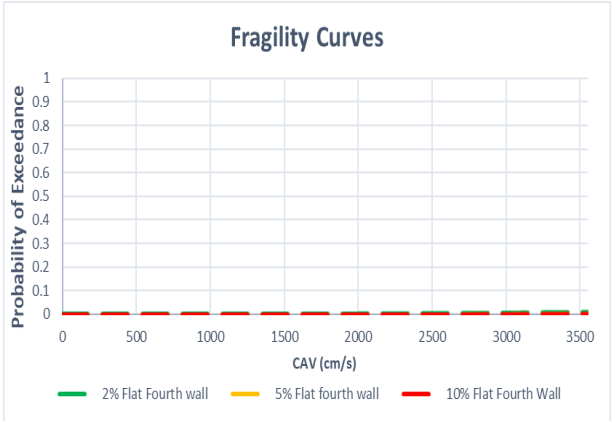

Figure 3.89 Fourth wall flat backfills fragility curves in terms of CAV with respect to tilting angle second threshold

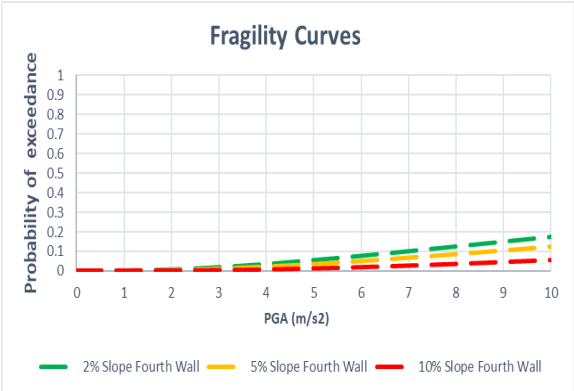

Figure 3.90 Fourth wall slope backfills fragility curves in terms of PGA with respect to tilting angle second threshold

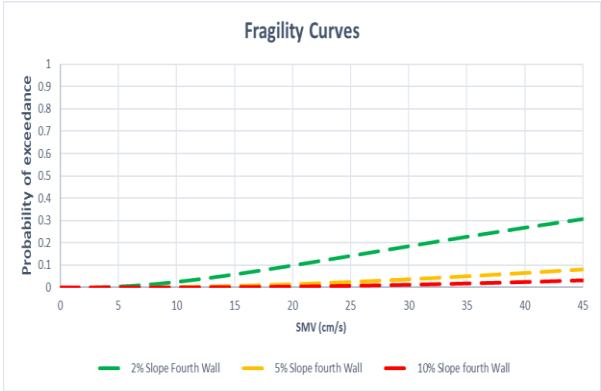

Figure 3.91 Fourth wall slope backfills fragility curves in terms of SMV with respect to tilting angle second threshold

Finally, in this part we could have a graph that represents all the fragility curves together in order that we could comment on each case and notice if there is any relationship between the geometry of the walls and the fragility curves is each case separately as shown in Figures 3.91 to 3.96 in which a nice monotonic increment in the fragility curves developed in terms of relative horizontal displacement damage state of both the backfills cases from the smallest wall to reach the fourth wall.

On the other hand, no perfect relationship could be seen for the fragility curves in terms of tilting angle for the first threshold, even if it is at least giving a good shaped curves in the slope case, which is totally not done in the case of second threshold as the value of the biggest tilting angle at the end of the numerical analysis of the dynamic load, was not more than 3 degrees, where the second threshold was enormous in terms of the specific static equilibrium angle as the smallest angle was 10 degrees in which (20%) the smallest threshold leads to 2 degrees which is too near to the reached tilting in the analysis that is why, no obvious fragility curves could be seen even, another reason was that there is no deep researches in literature about tilting threshold aspect, that made this study to be done by 2 trail values

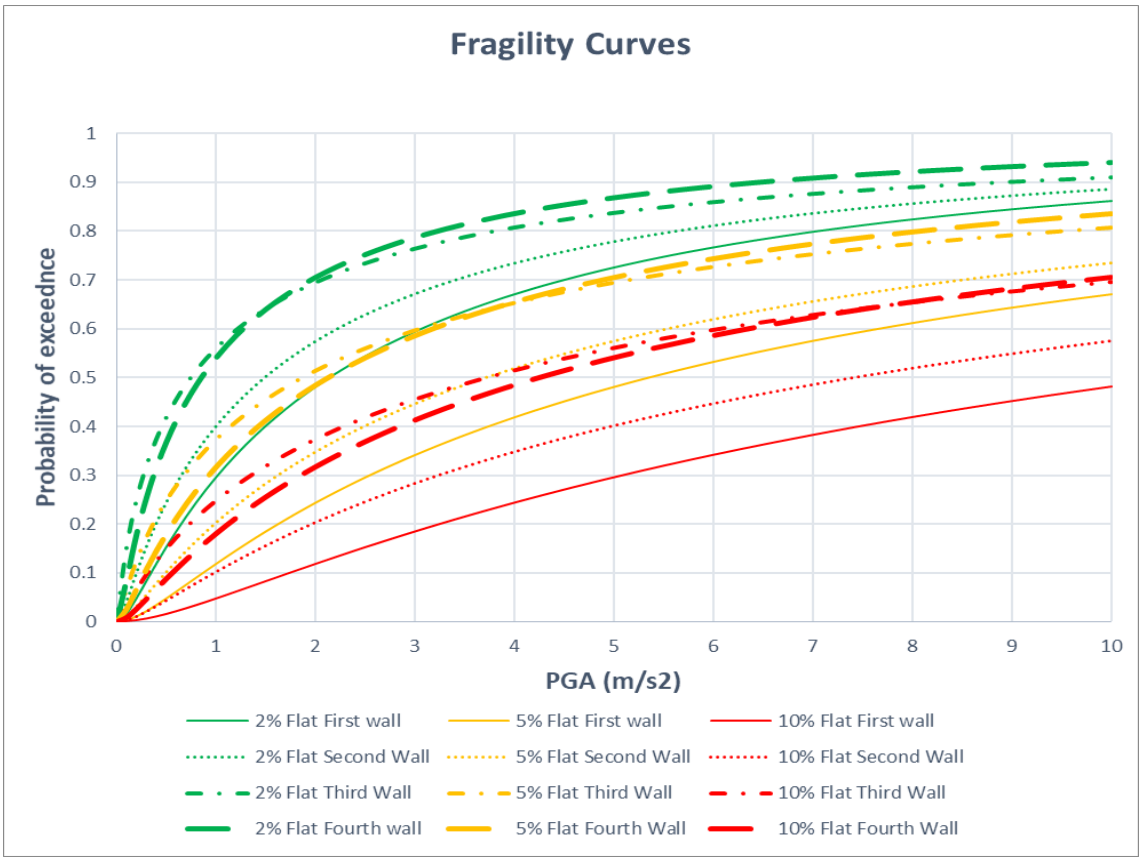

Figure 3.92 Comparison between the fragility curves of all the flat backfills walls in terms of PGA with respect to relative horizontal displacement

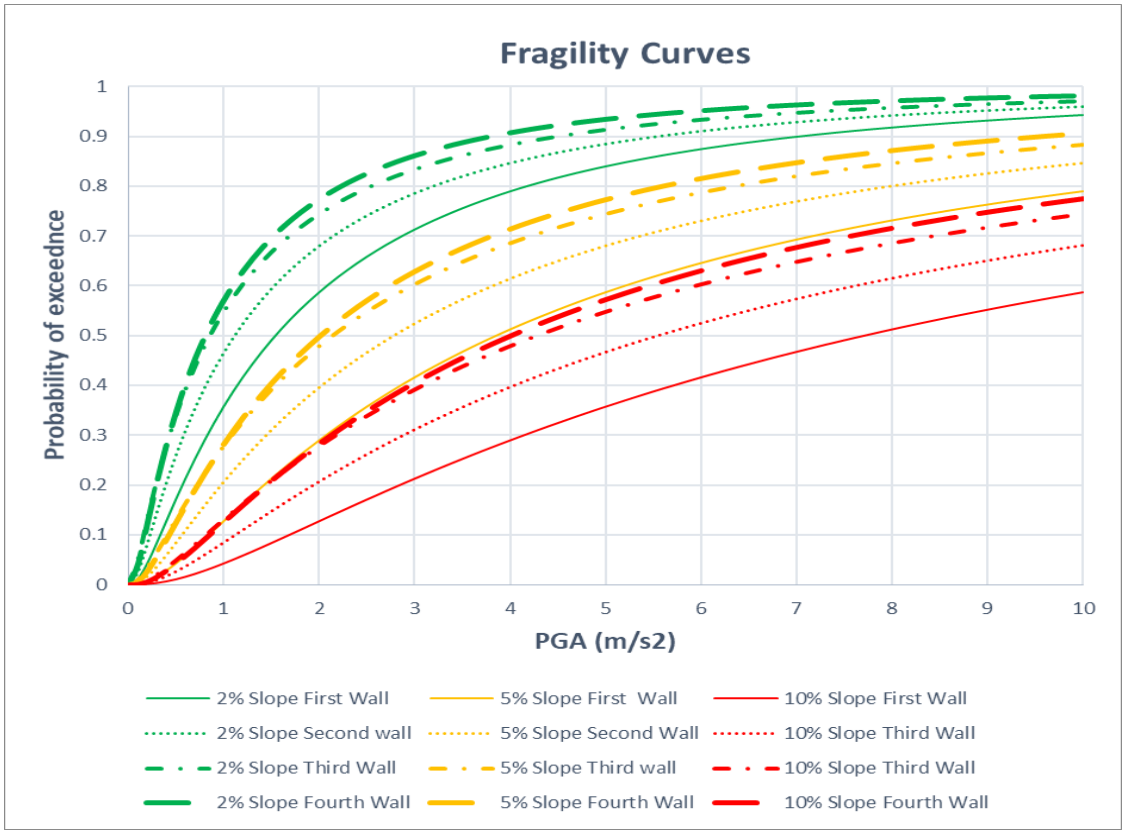

Figure 3.93 Comparison between the fragility curves of all the slope backfills walls in terms of PGA with respect to relative horizontal displacement

Figure 3.94 Comparison between the fragility curves of all the flat backfills walls in terms of PGA with respect to tilting angle first threshold

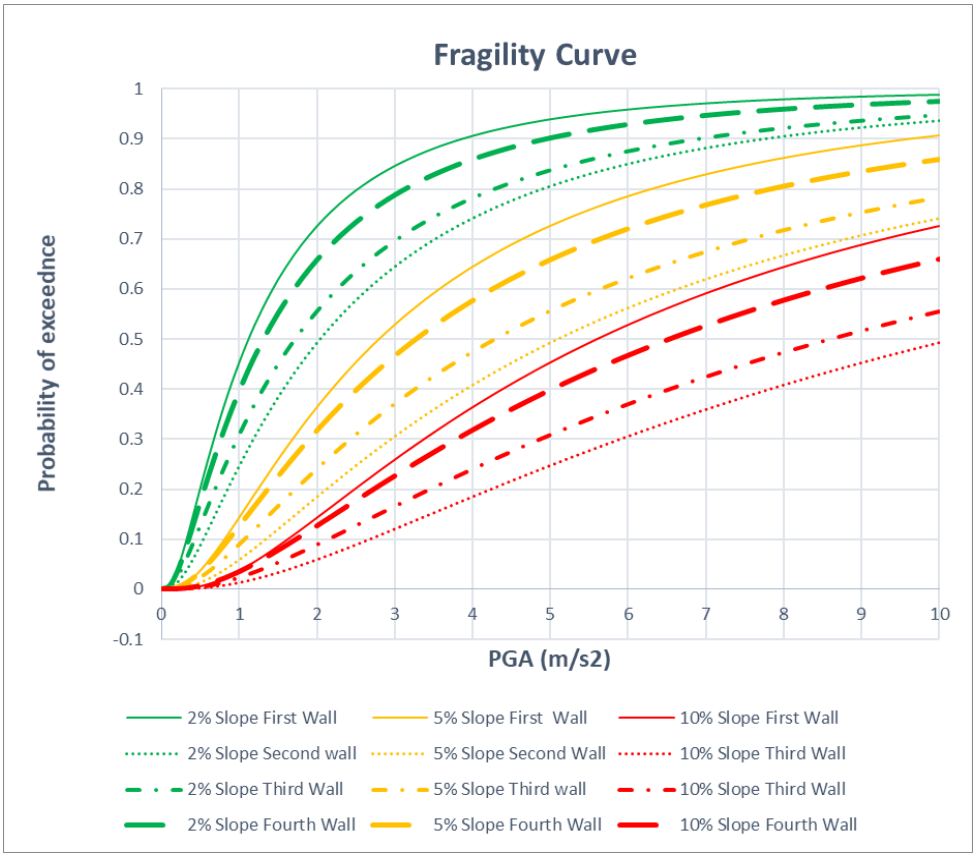

Figure 3.95 Comparison between the fragility curves of all the slope backfills walls in terms of PGA with respect to tilting angle first

threshold

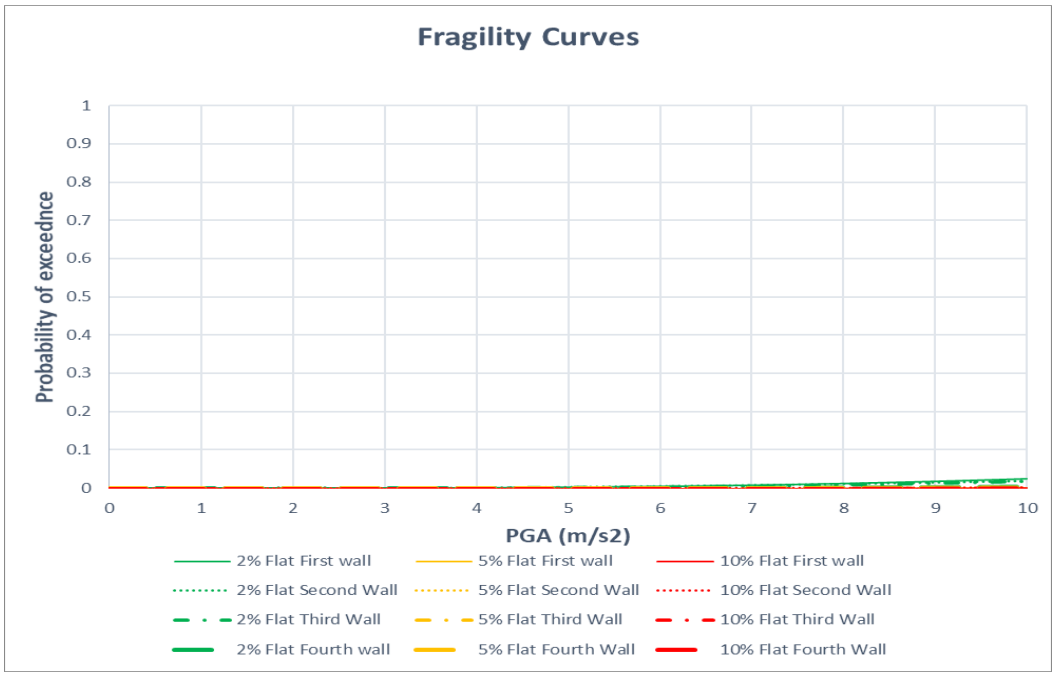

Figure 3.96 Comparison between the fragility curves of all the flat backfills walls in terms of PGA with respect to tilting angle second threshold

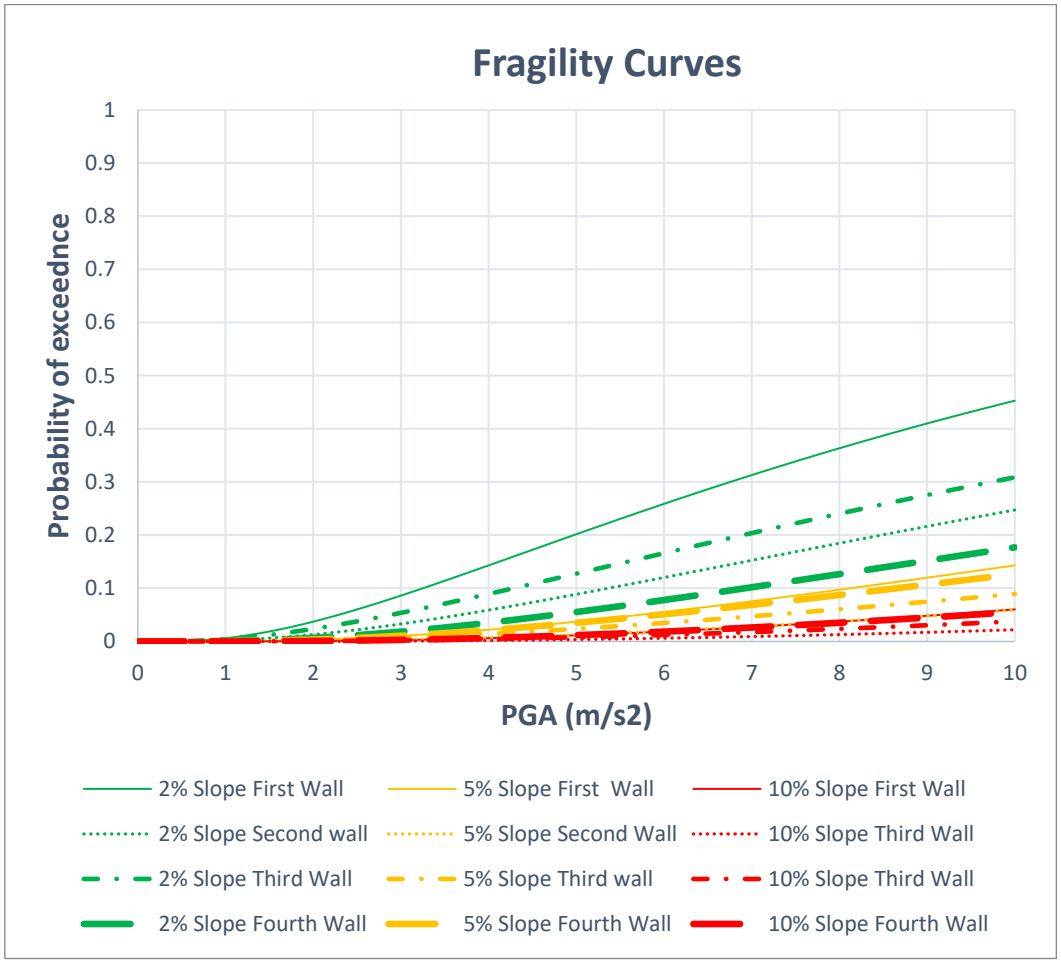

Figure 3.97 Comparison between the fragility curves of all the slope backfills walls in terms of PGA with respect to tilting angle second threshold

3.5 Combined backfills fragility curves each wall

3.5.1 The first wall of height 3.6m both backfills together

This step was done in order to see if there could be a homogenous behaviour in terms of the selected IMs, where the two cases of backfills were combined for each wall and an IM was again selected and the fragility curves were again developed in terms of this IM. In order to do that the same steps have been repeated as the first case but with fitting both the backfills results done in the numerical analysis. So, a comparison again is shown in terms of PSDM parameters studies as efficiency and proficiency.

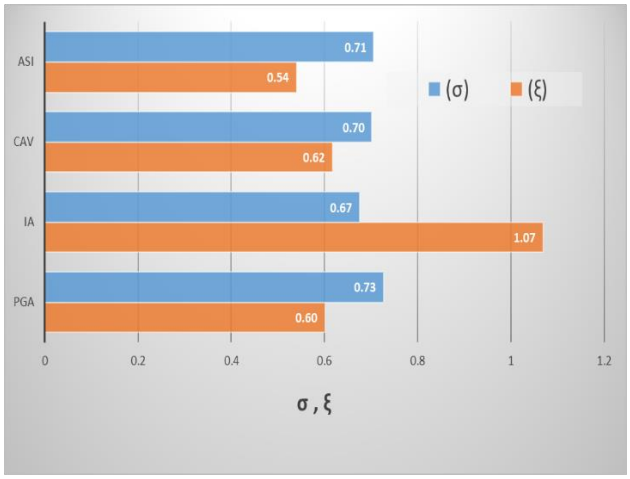

Figure 3.98 Comparing the best selected IMs for the first wall combining the backfills in terms of relative horizontal displacement with respect to efficiency (σ), and proficiency (ξ)

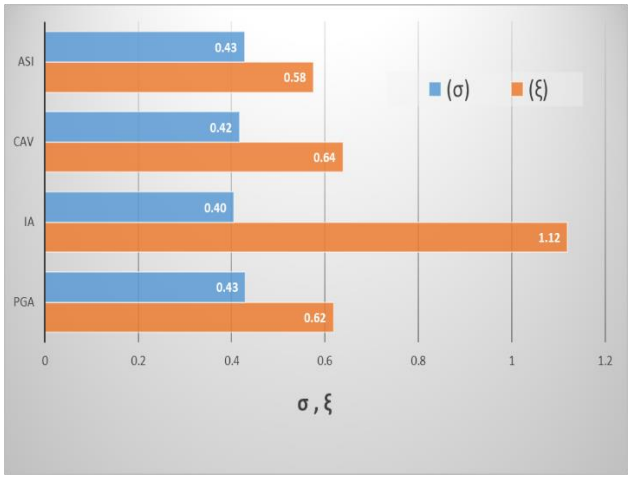

Figure 3.99 Comparing the best selected IMs for the first wall combining the backfills in terms of tilting with respect to efficiency (σ), and proficiency (ξ)

The bar chart comparison shows that the efficient IM is I_a in terms of relative horizontal displacement where looking to the combined parameter that is proficiency, it could be seen that its increasing too much, to reach a high, not preferred value to give the priority to the ASI as it has the same value as CAV while it is more efficient, the reason that lead to select the ASI intensity measure. The same overall behaviour could be seen in the other chart of the tilting damage index, which logically lead to the same selection of ASI intensity measure.

Table 3.9 Best correlated IMs for the first wall both backfills together

The best four selected IMs	Both backfills	
In terms of relative horizontal displacement	***PGA (m/s^2)***	***ASI (m/s)***
In terms of tilting	***PGA (m/s^2)***	***ASI (m/s)***

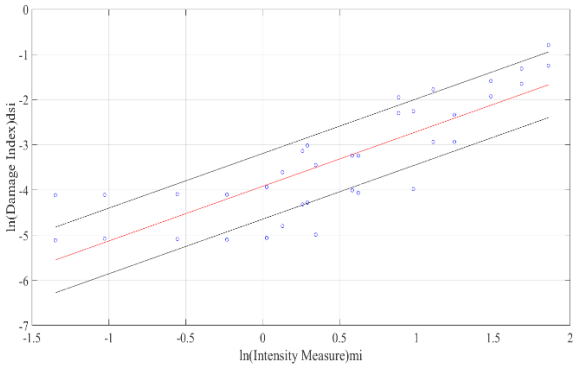

Figure 3.100 PGA both backfills relative horizontal displacement

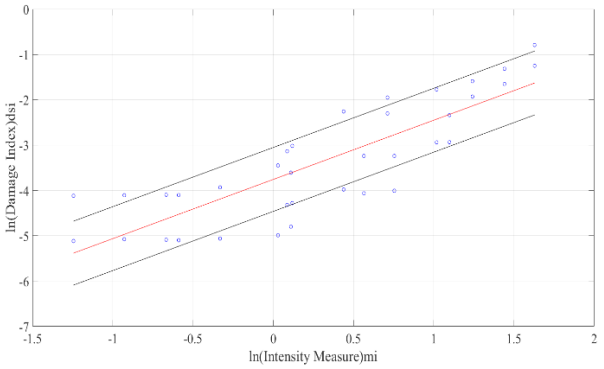

Figure 3.101 ASI both backfills relative horizontal displacement

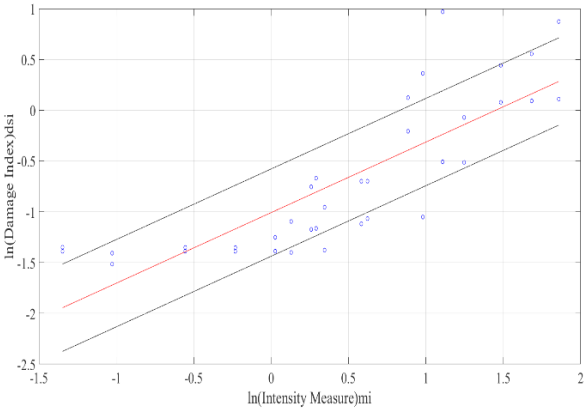

Figure 3.102 PGA both backfills Tilting

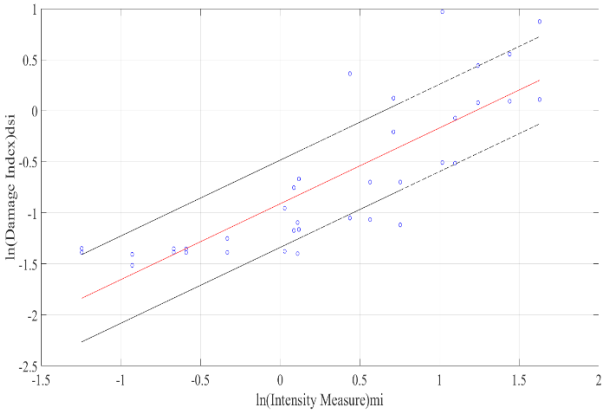

Figure 3.103 ASI both backfills Tilting

The previous graphs are the PSDM graphs of the first wall with combined backfills results,

Then the fragility curves were drawn with respect to the selected IM, as shown for the three thresholds in which the threshold of the tilting angle was the average of the two backfills angles (Figures 3.103,3,108).

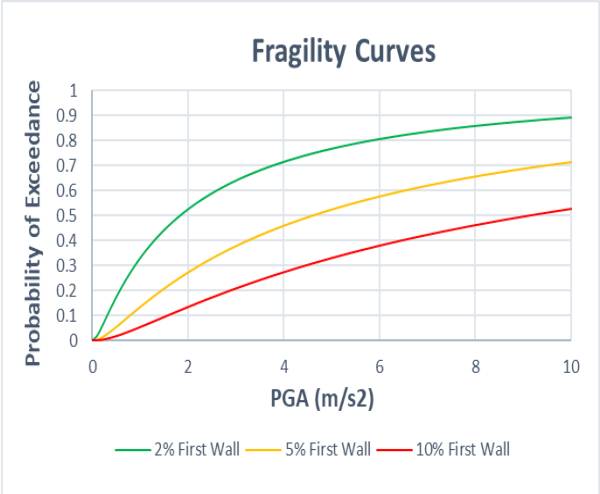

Figure 3.104 First wall both backfills fragility curves in terms of PGA with respect to relative horizontal displacement

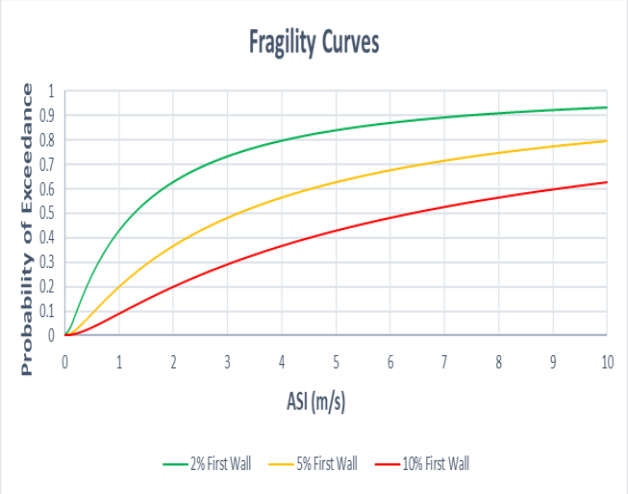

Figure 3.105 First wall both backfills fragility curves in terms of ASI with respect to relative horizontal displacement

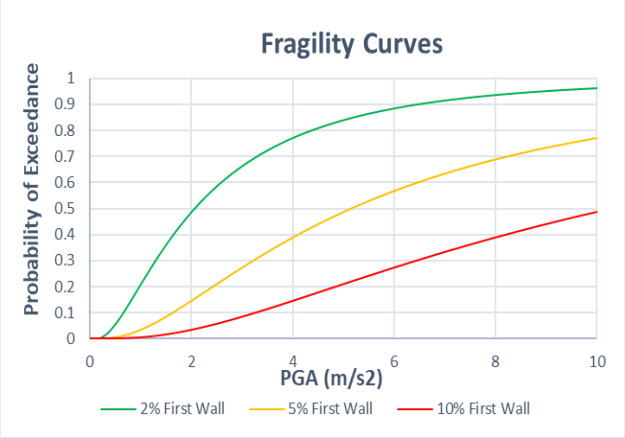

Figure 3.106 First wall both backfills fragility curves in terms of PGA with respect to tilting angle first threshold

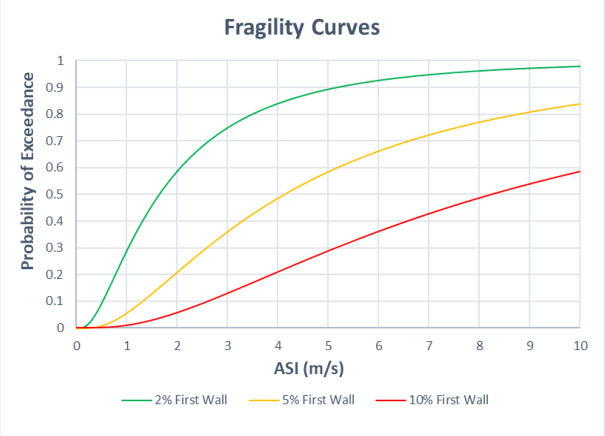

Figure 3.107 First wall both backfills fragility curves in terms of ASI with respect to tilting angle first threshold

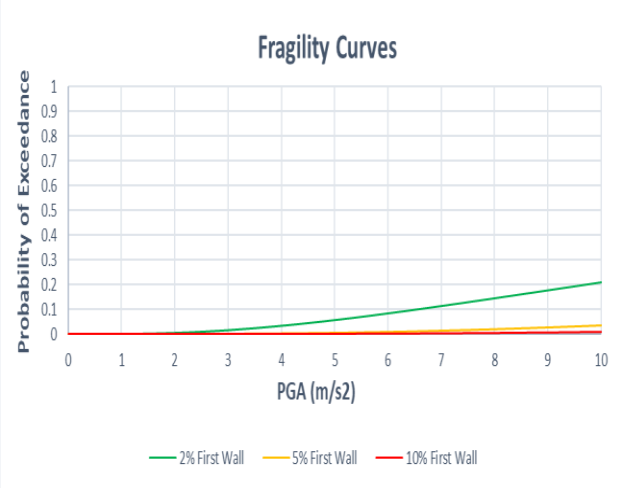

Figure 3.108 First wall both backfills fragility curves in terms of PGA with respect to tilting angle second threshold

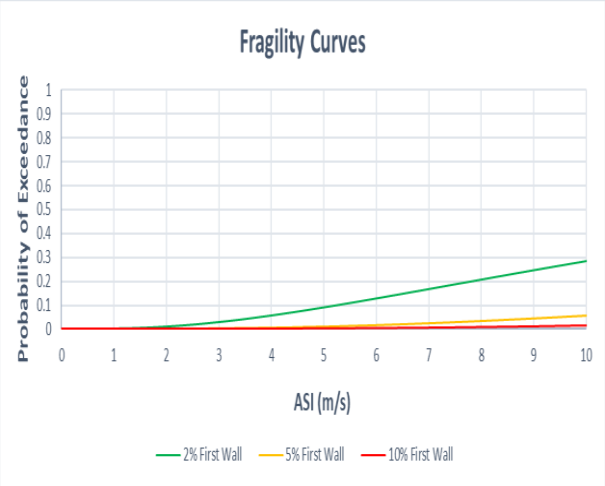

Figure 3.109 First wall both backfills fragility curves in terms of ASI with respect to tilting angle second threshold

3.5.2 The second wall of height 4.5m both backfills together

The study continues for the second wall with the same rationale but with the results of the second wall analysis for both backfills together.to have the following charts in Figures 3.109, 3.110.

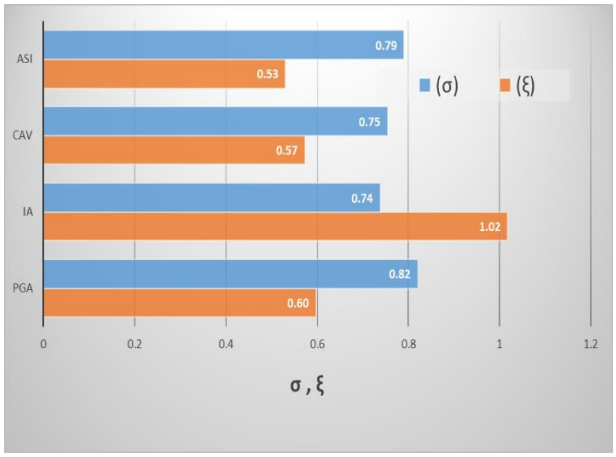

Figure 3.110 Comparing the best selected IMs for the second wall combining the backfills in terms of relative horizontal displacement with respect to efficiency (σ), and proficiency (ξ)

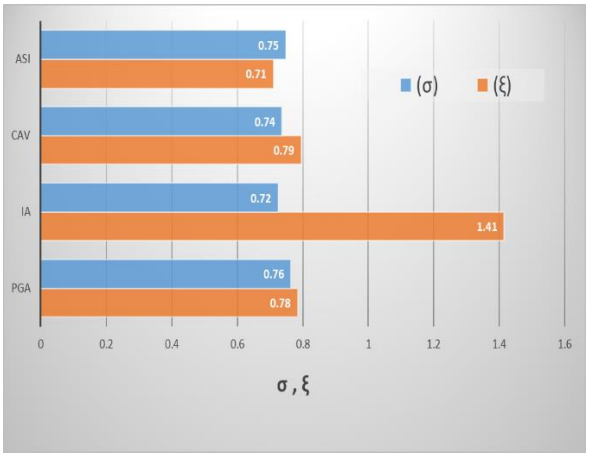

Figure 3.111 Comparing the best selected IMs for the second wall combining the backfills in terms of tilting with respect to efficiency (σ), and proficiency (ξ)

Exactly as the first wall the bar chart comparison for the second wall shows that the efficient IM is I_a in terms of relative horizontal displacement where looking to the combined parameter that is proficiency, it could be seen that its increasing too much, to reach a high, not preferred value to give the priority to the ASI as it has the same value as CAV while it is more efficient, the reason that lead to select the ASI intensity measure. The same overall behaviour could be seen in the other chart of the tilting damage index, which logically lead to the same selection of ASI intensity measure. The best selected IMs were listed in Table 3.10.

Table 3.10 Best correlated IMs for the second wall both backfills together

The best four selected IMs	Both backfills	
In terms of relative horizontal displacement	***PGA (m/s²)***	***ASI (m/s)***
In terms of tilting	***PGA (m/s²)***	***ASI (m/s)***

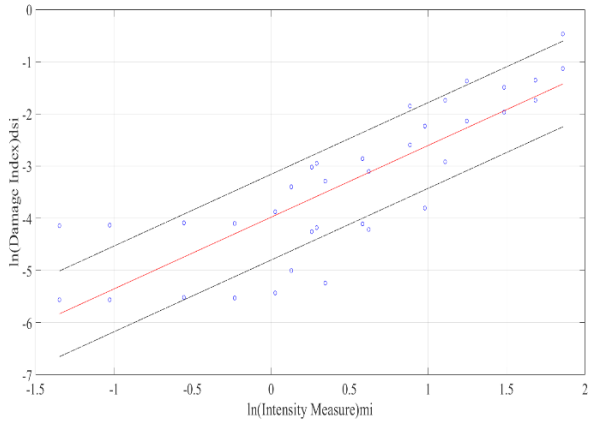

Figure 3.112 PGA both backfills relative horizontal displacement

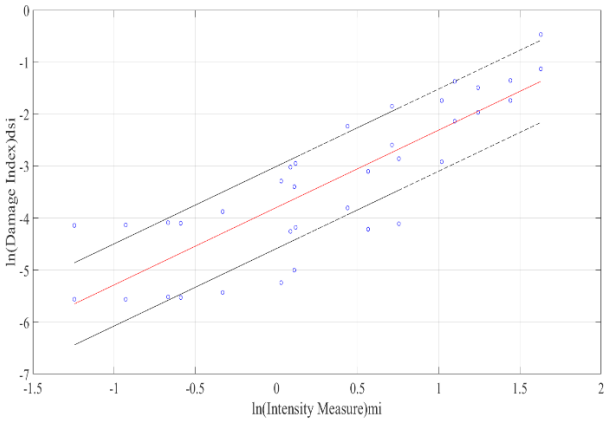

Figure 3.113 ASI both backfills relative horizontal displacement

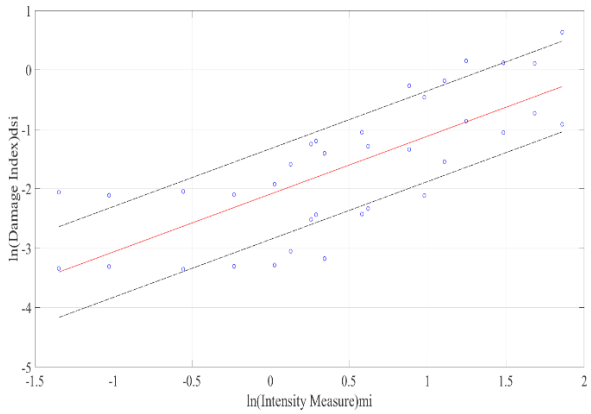

Figure 3.114 PGA both backfills Tilting

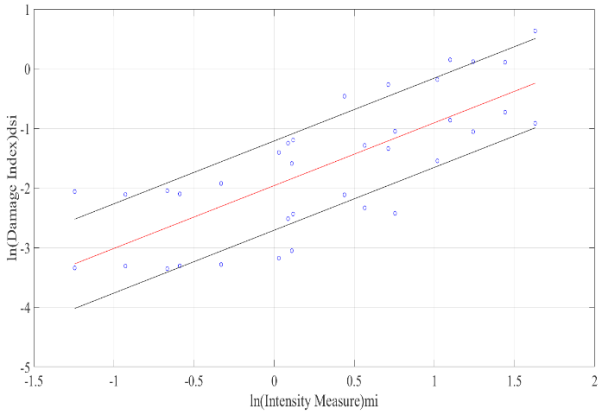

Figure 3.115 ASI both backfills Tilting

The last four graphs in Figures 3.111 to 3.114 show the selected 4 IMs in terms of both damage cases, where the threshold of the tilting angle was the average of the two backfills angles and then the fragility curves were done as shown in Figures 3.115 to 3.120.

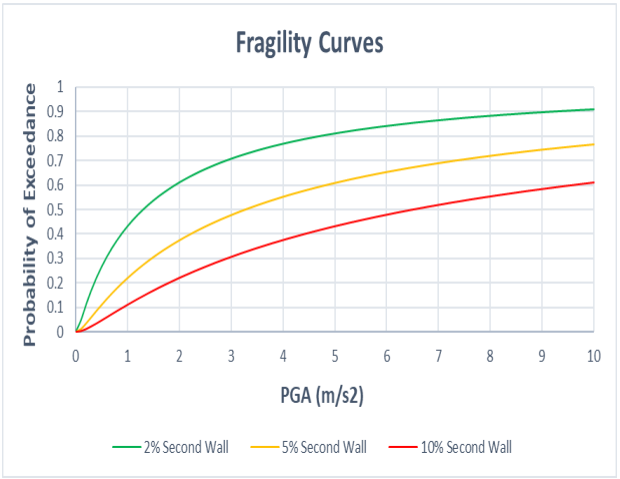

Figure 3.116 Second wall both backfills fragility curves in terms of PGA with respect to relative horizontal displacement

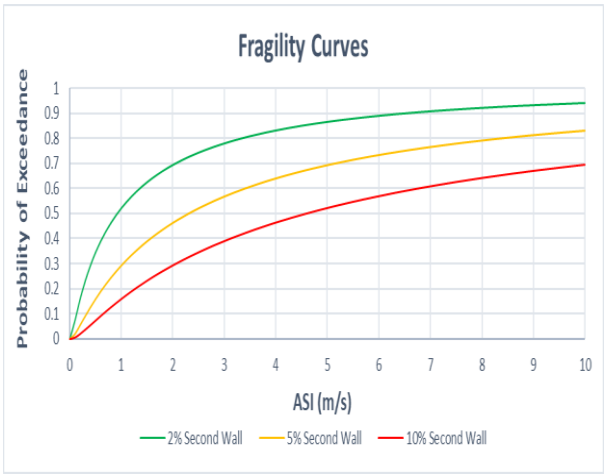

Figure 3.117 Second wall both backfills fragility curves in terms of ASI with respect to relative horizontal displacement

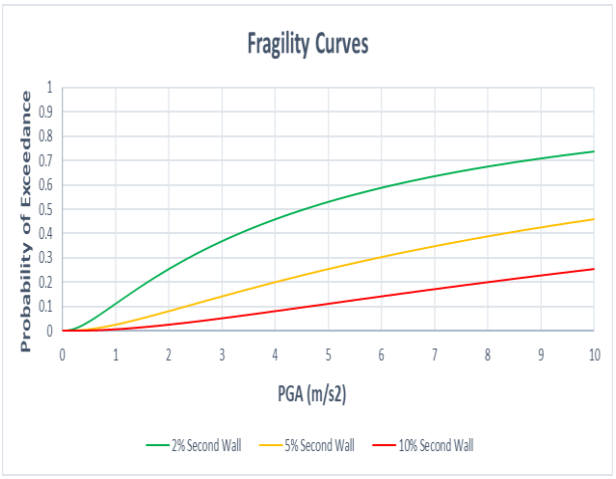

Figure 3.118 Second wall both backfills fragility curves in terms of PGA with respect to tilting angle first threshold

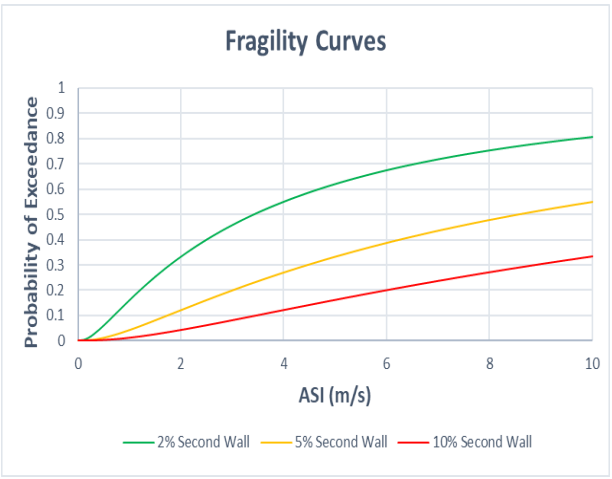

Figure 3.119 Second wall both backfills fragility curves in terms of ASI with respect tilting angle first threshold

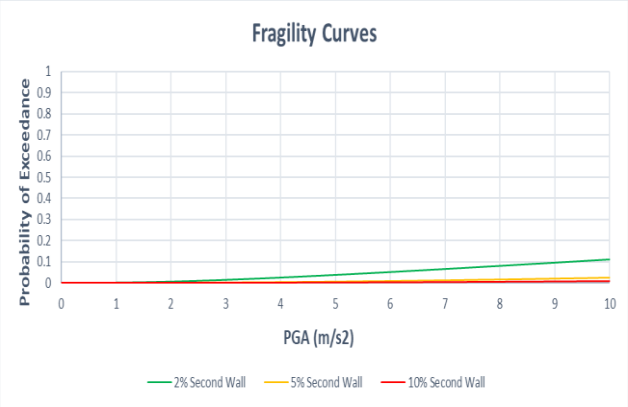

Figure 3.120 Second wall both backfills fragility curves in terms of PGA with respect to tilting angle second threshold

Figure 3.121 Second wall both backfills fragility curves in terms of ASI with respect tilting angle second threshold

3.5.3 The third wall of height 5.5m both backfills together

Similarly, the same steps were again repeated for the third wall and the comparison charts are shown in Figures 3.121, 3.122. The best selected IMs are listed in Table 3.11.

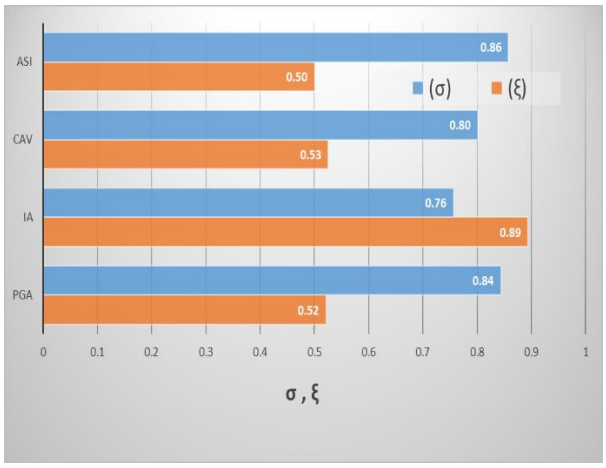

Figure 3.122 Comparing the best selected IMs for the third wall combining the backfills in terms of relative horizontal displacement with respect to efficiency (σ), and proficiency (ξ)

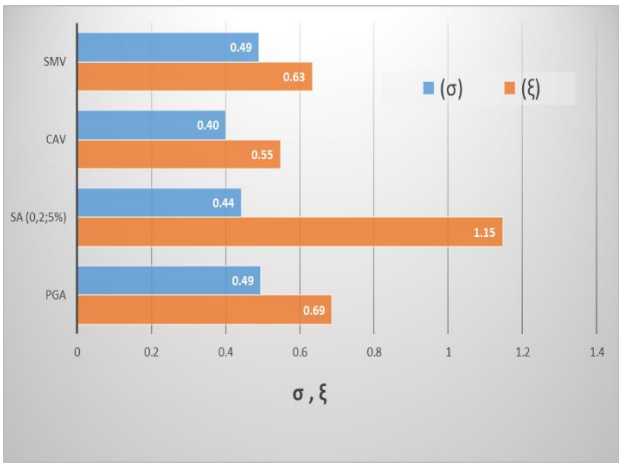

Figure 3.123 Comparing the best selected IMs for the third wall combining the backfills in terms of tilting with respect to efficiency (σ), and proficiency (ξ)

The third wall was likely the same as the previous bar charts comparison for the first and second wall shows that the efficient IM is I_a in terms of relative horizontal displacement where looking to the combined parameter that is proficiency, it could be seen that its increasing too much, to reach a high, not preferred value to give the priority to the ASI as it has the same value as CAV while it is more efficient, the reason that lead to select the ASI intensity measure. This time the behaviour of the wall could be seen in the other chart of the tilting damage index, was tending in both parameters to CAV.

Table 3.11 Best correlated IMs for the third wall both backfills together

The best four selected IMs	Both backfills	
In terms of relative horizontal displacement	***PGA (m/s^2)***	***ASI (m/s)***
In terms of tilting	***PGA (m/s^2)***	***CAV (cm/s)***

The graphs of best selected PSDM study in Figures 3.123 to 3.126.

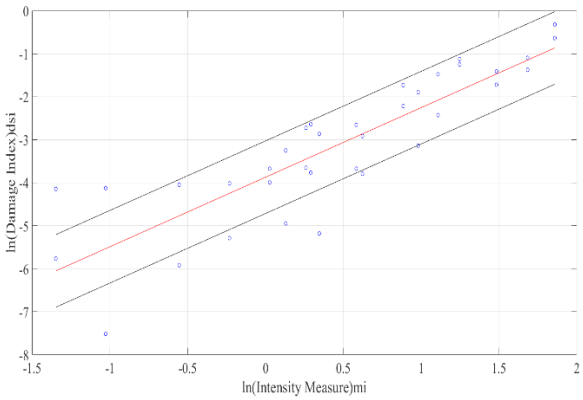

Figure 3.124 PGA both backfills relative horizontal displacement

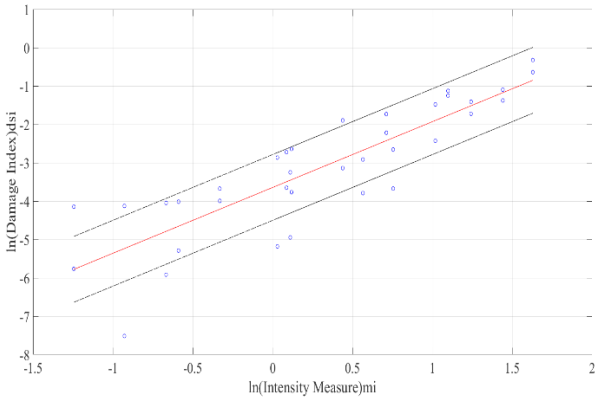

Figure 3.125 ASI *both backfills* relative *horizontal displacement*

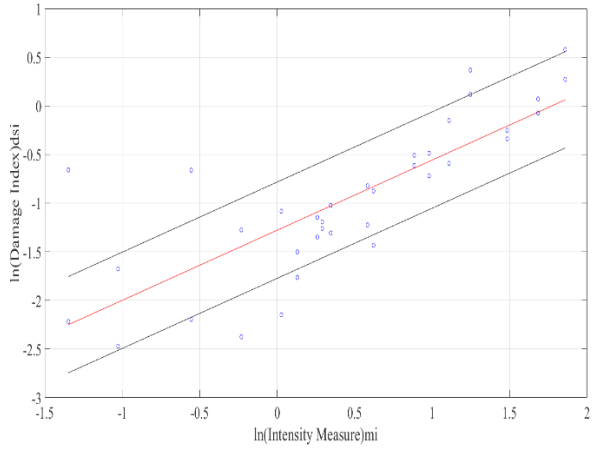

Figure 3.126 PGA both backfills Tilting

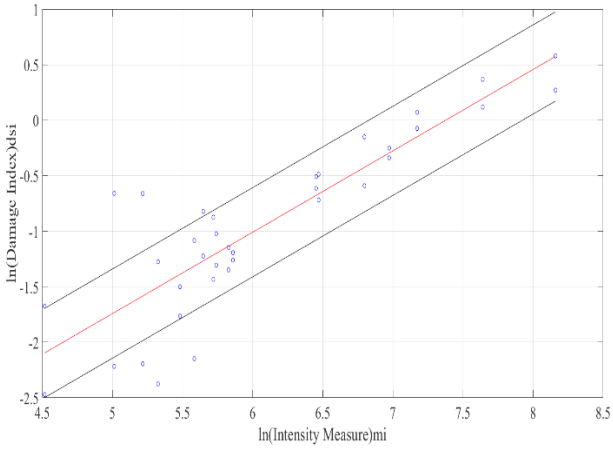

Figure 3.127 CAV both backfills Tilting

The last step as usual for each study was drawing of fragility curves where the threshold of the tilting angle was the average of the two backfills angles, and the fragility curves are shown in Figures 3.127 to 3.132.

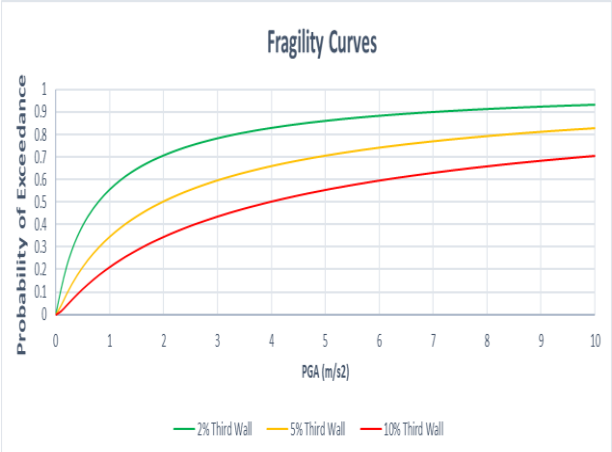

Figure 3.128 Third wall both backfills fragility curves in terms of PGA with respect to relative horizontal displacement

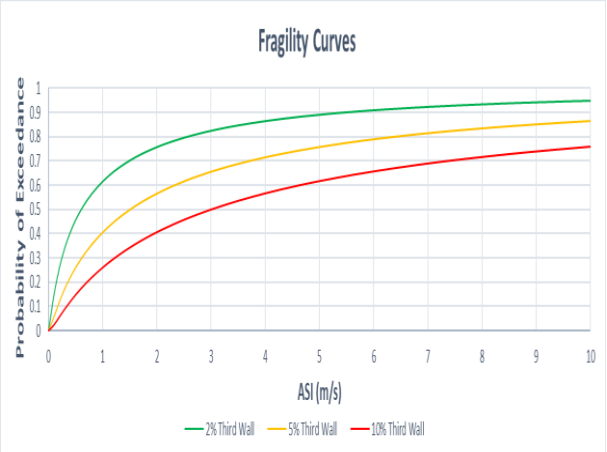

Figure 3.129 Third wall both backfills fragility curves in terms of ASI with respect to relative horizontal displacement

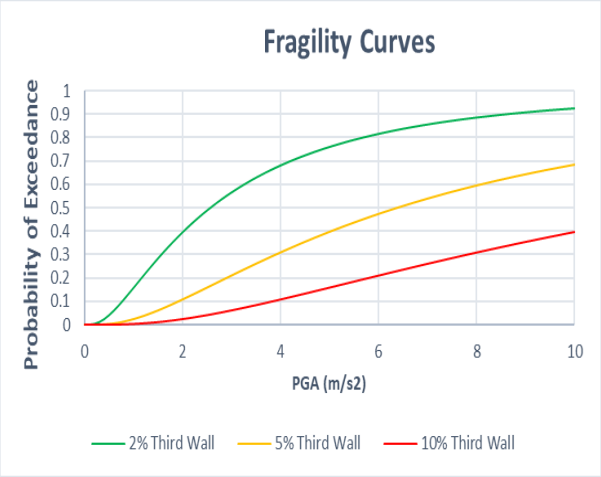

Figure 3.130 Third wall both backfills fragility curves in terms of PGA with respect to tilting angle first threshold

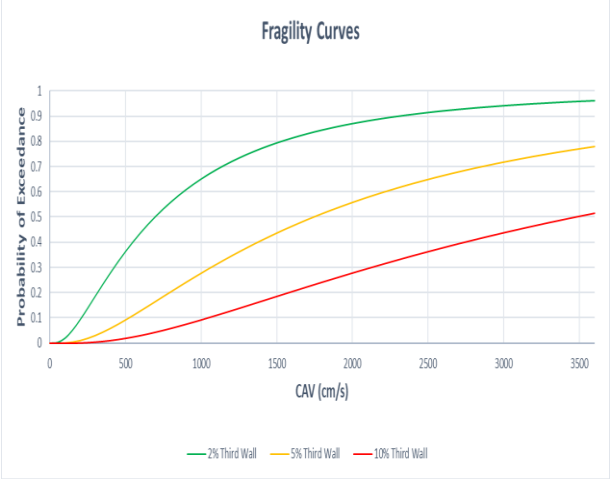

Figure 3.131 Third wall both backfills fragility curves in terms of CAV with respect to tilting angle first threshold

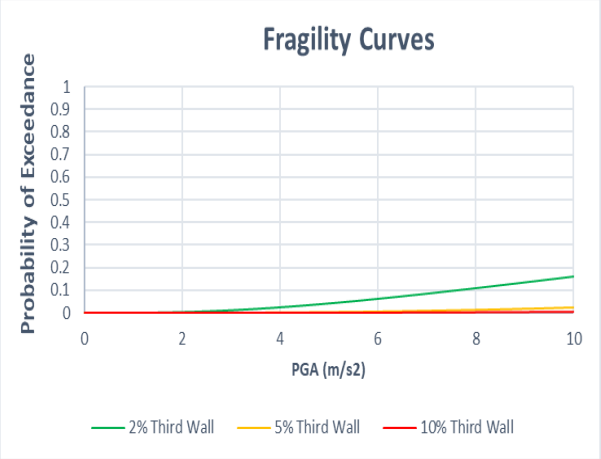

Figure 3.132 Third wall both backfills fragility curves in terms of PGA with respect to tilting angle second threshold

Figure 3.133 Third wall both backfills fragility curves in terms of CAV with respect to tilting angle second threshold

3.5.4 The fourth wall of height 6.5m both backfills together

Last wall backfills were also combined as the other walls and the charts of best IMs comparison are shown in Figure 3.133,3.134.

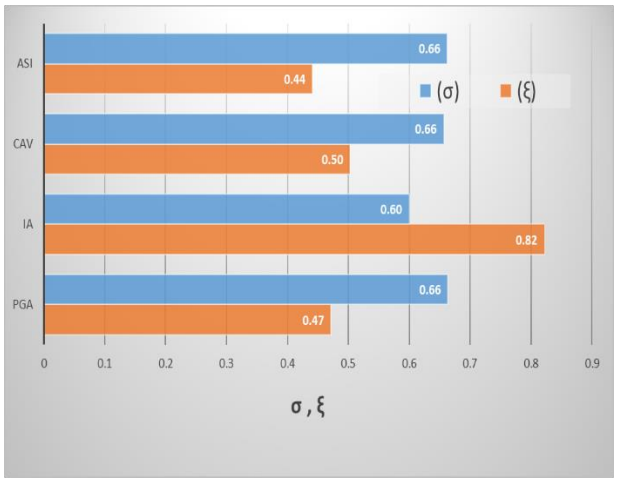

Figure 3.134 Comparing the best selected IMs for the fourth wall combining the backfills in terms of relative horizontal displacement with respect to efficiency (σ), and proficiency (ξ)

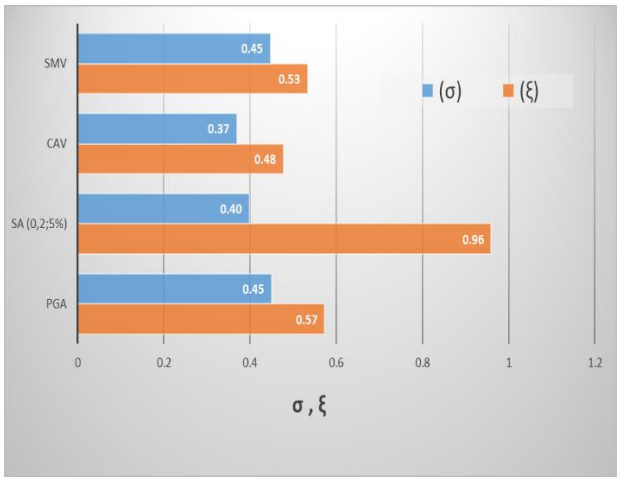

Figure 3.135 Comparing the best selected IMs for the fourth wall combining the backfills in terms of tilting with respect to efficiency (σ), and proficiency (ξ)

The relative horizontal displacement dependent study shows again a good acceptable value for I_a efficiency but in considering all the parameters again as the previous three walls ASI fits the best, while this time in terms of tilting it shows mostly the same behaviour as the third wall, in which the CAV was also selected. The PSDM graphs are shown from Figure 3.135 to 3.138 according to the best selected IMs are listed in Table 3.12.

Table 3.12 Best correlated IMs for the fourth wall both backfills together

The best four selected IMs	Both backfills	
In terms of relative horizontal displacement	***PGA (m/s^2)***	***ASI (m/s)***
In terms of tilting	***PGA (m/s^2)***	***CAV (cm/s)***

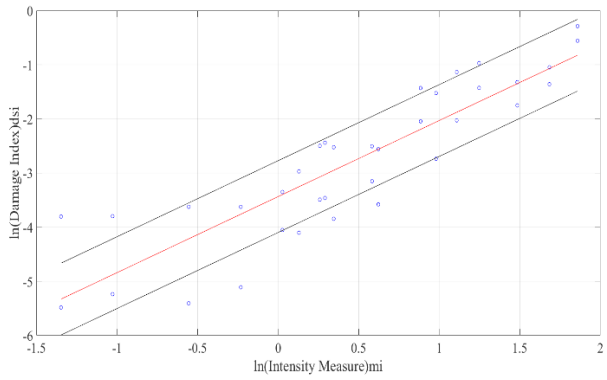

Figure 3.136 PGA both backfills relative horizontal displacement

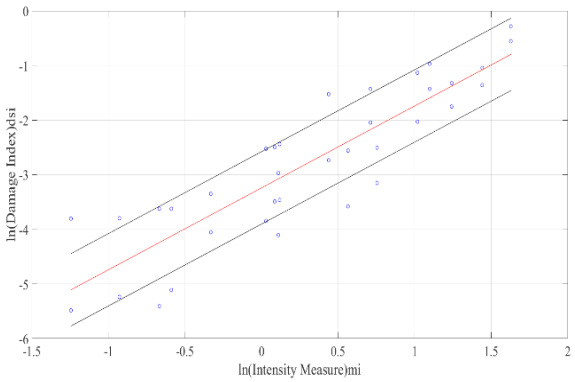

Figure 3.137 ASI *both backfills* relative *horizontal displacement*

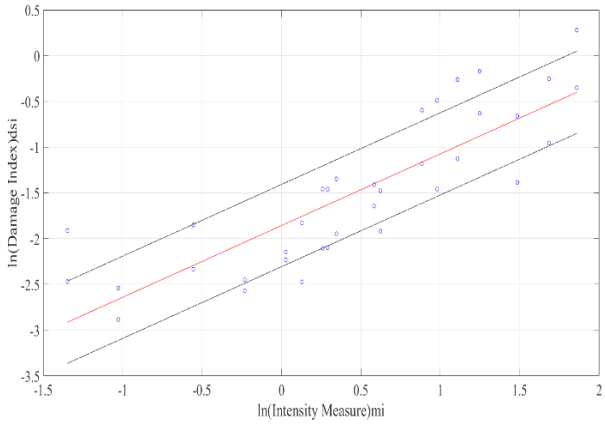

Figure 3.138 PGA both backfills Tilting

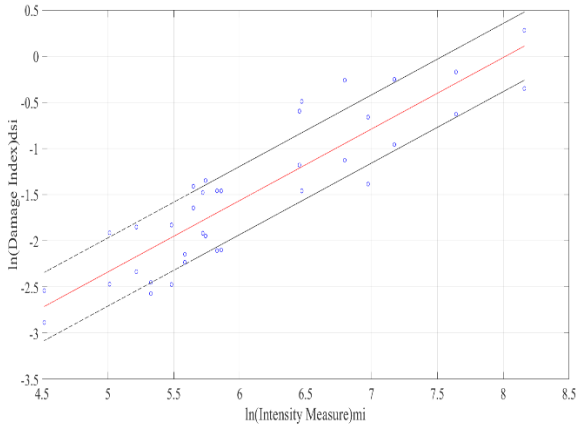

Figure 3.139 CAV both backfills Tilting

The fragility curves of this case are shown in Figures 3.139 to 3.144.

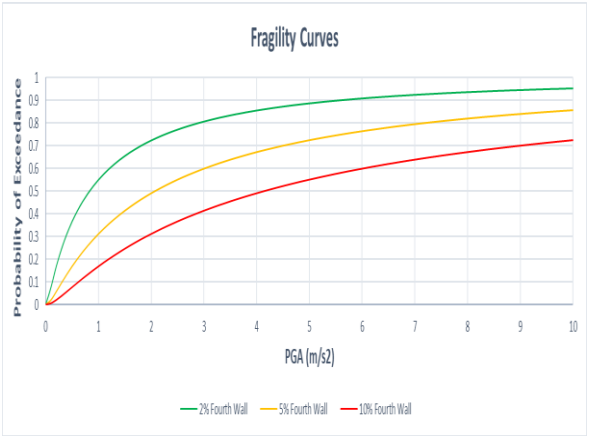

Figure 3.140 Fourth wall both backfills fragility curves in terms of PGA with respect to relative horizontal displacement

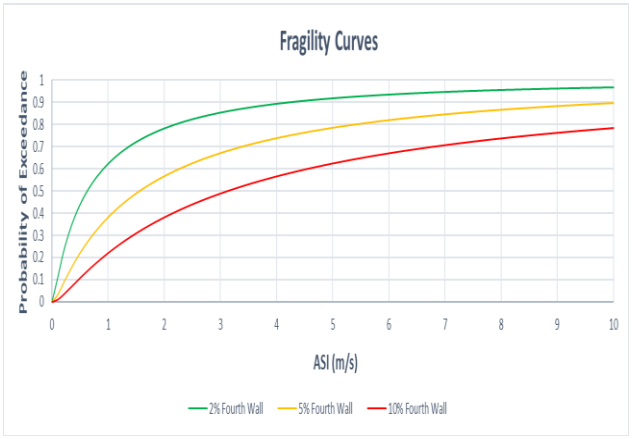

Figure 3.141 Fourth wall both backfills fragility curves in terms of ASI with respect to relative horizontal displacement

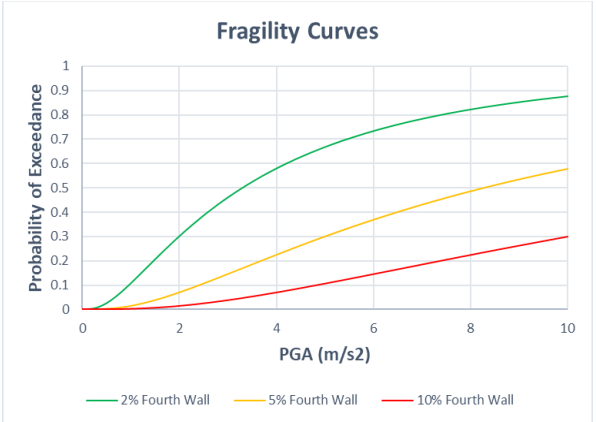

Figure 3.142 Fourth wall both backfills fragility curves in terms of PGA with respect to tilting angle first threshold

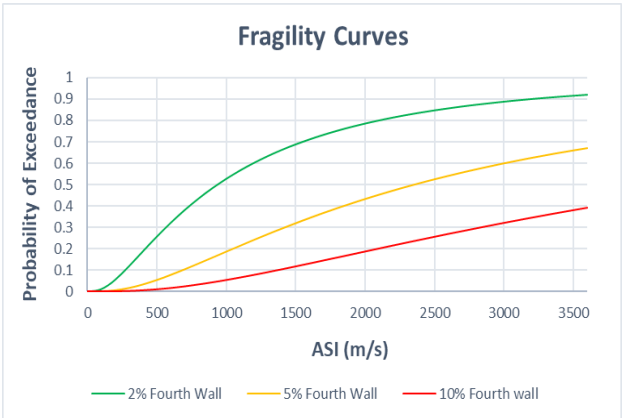

Figure 3.143 Fourth wall both backfills fragility curves in terms of ASI with respect to tilting angle first threshold

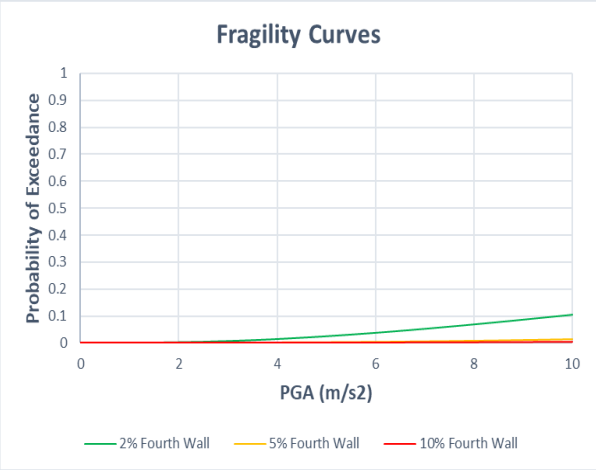

Figure 3.144 Fourth wall both backfills fragility curves in terms of PGA with respect to tilting angle second threshold

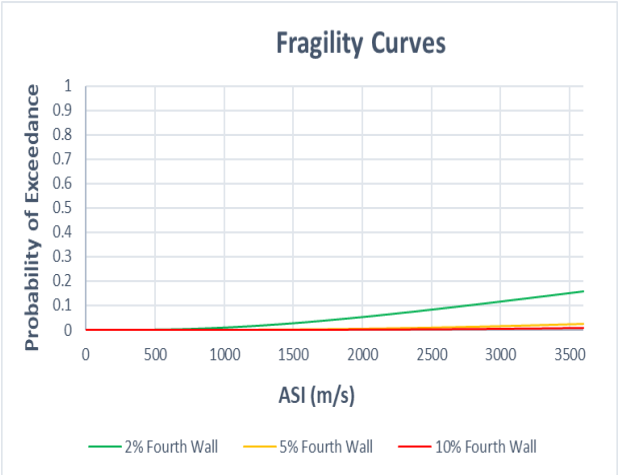

Figure 3.145 Fourth wall both backfills fragility curves in terms of ASI with respect to tilting angle second threshold

After having all the fragility curves of the combined backfills, it could be seen that our results for each wall was as an average result of separated backfills and the best IMs were mostly ASI and CAV that were also representing most of the fragility curves in the separated case.

3.6 Fragility curves of all walls combined together

The least study was done by combining all the data together in order to see overall best correlated IM and in the same steps order as all the work done before the comparison charts of this step are shown in Figures 3.145, 3.146.

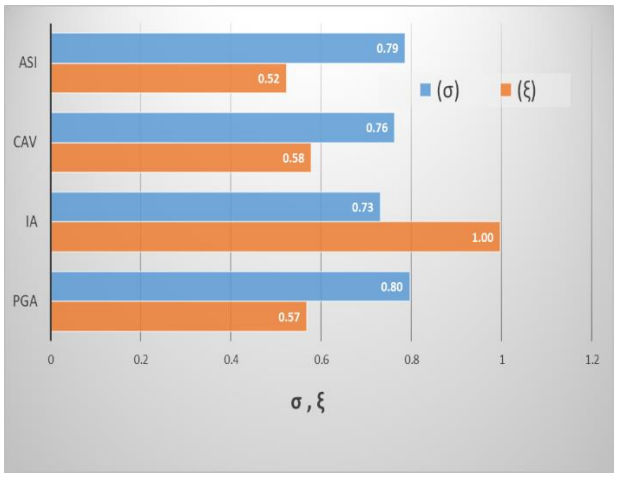

Figure 3.146 Comparing the best selected IMs for all walls combined together in terms of relative horizontal displacement with respect to efficiency (σ), and proficiency (ξ)

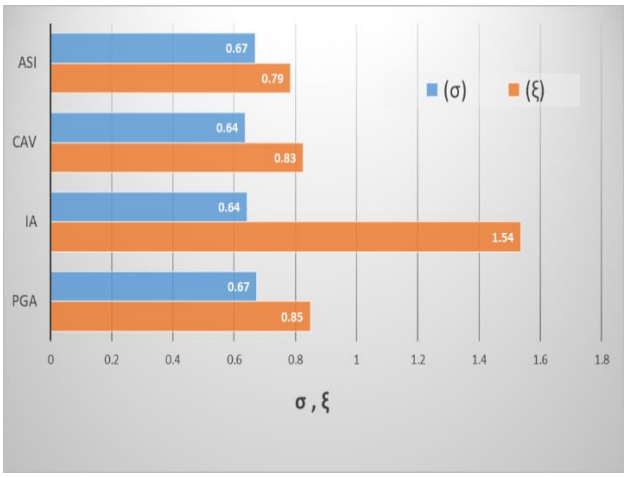

Figure 3.147 Comparing the best selected IMs for all walls combined together in terms of tilting with respect to efficiency (σ), and proficiency (ξ)

The combined case has a nearer and too close behaviour with the best correlated IMs as shown excluding the proficiency of I_a and according to the calculated results, the best correlated IM in both damage index cases can be seen as ASI, the most IM appearing in all studies that lead to a reasonable result. As all the walls cases are involved in this study, the IM fitting for them will be the IM that was selected in the previous steps.

The Table 3.13 shows the best IMs selected in this case.

Table 3.13 Best correlated IMs for all the walls together

The best four selected IMs	All walls together	
In terms of relative horizontal displacement	***PGA (m/s^2)***	***ASI (m/s)***
In terms of tilting	***PGA (m/s^2)***	***ASI (m/s)***

One important issue was having an overall tilting angle for all the walls in order to have a correct analysis and this was done by the weighted average according to the height of each wall in order not to lose the physical effect of the walls. The best IMs probabilistic seismic demand model are shown In Figures 3.147 to 3.156

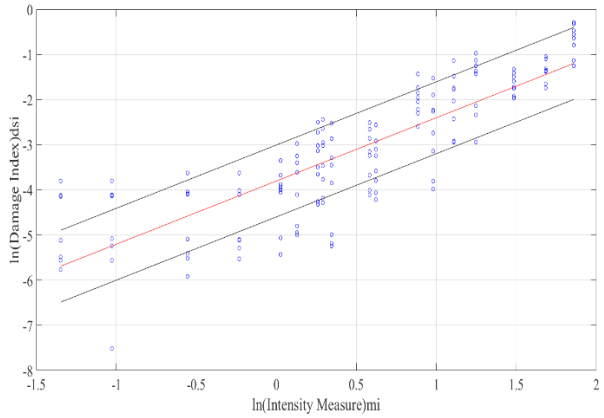

Figure 3.148 PGA all walls relative horizontal displacement

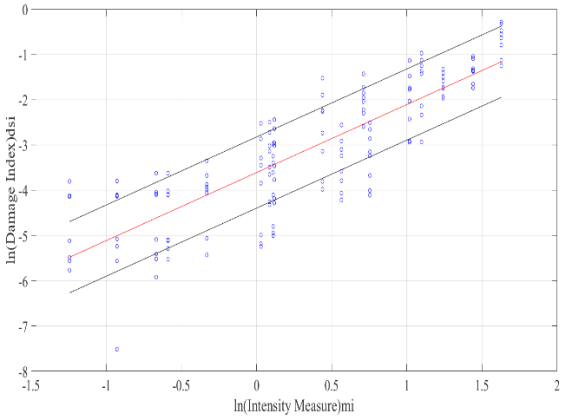

Figure 3.149 ASI all walls relative horizontal displacement

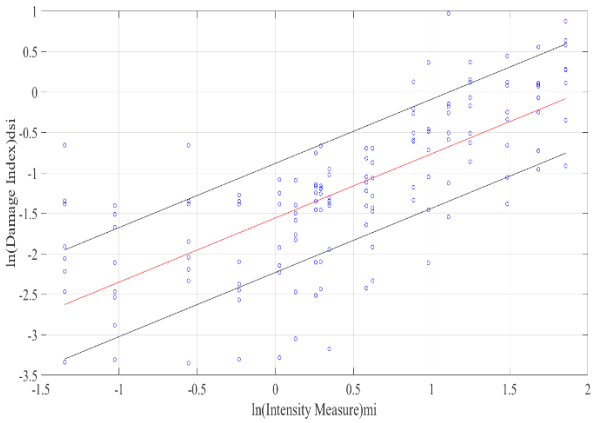

Figure 3.150 PGA all walls Tilting

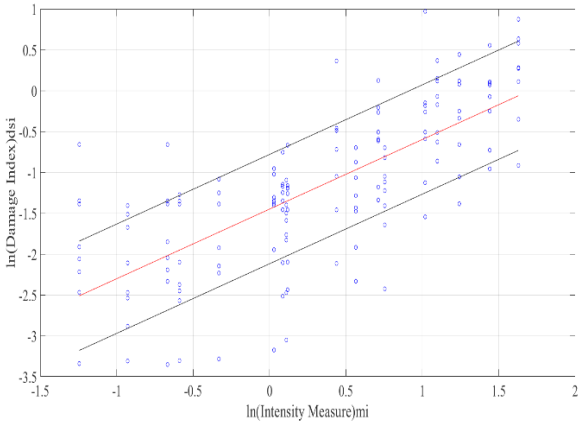

Figure 3.151 ASI all walls Tilting

The fragility curves of this composite situation are shown in Figures 3.151 to 3.156.

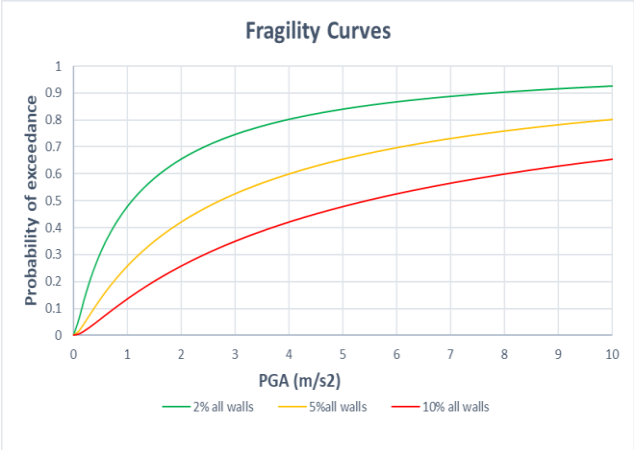

Figure 3.152 All walls combined together fragility curves in terms of PGA with respect to relative horizontal displacement

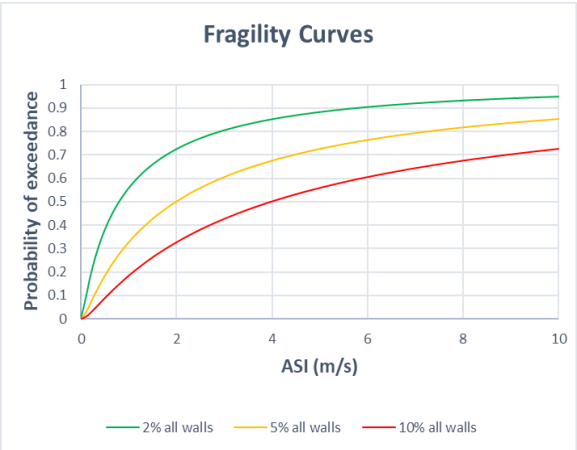

Figure 3.153 All walls combined together fragility curves in terms of ASI with respect to relative horizontal displacement

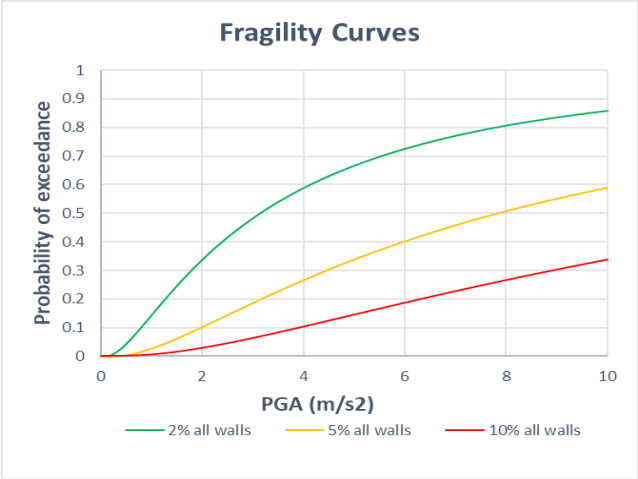

Figure 3.154 All walls fragility curves in terms of PGA with respect to tilting angle first threshold

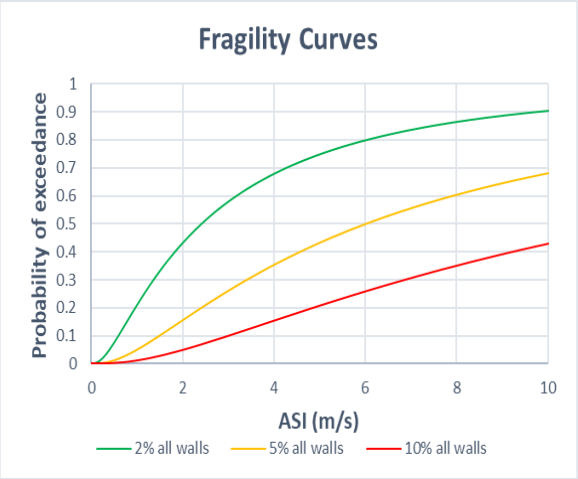

Figure 3.155 All walls fragility curves in terms of ASI with respect to tilting angle first threshold

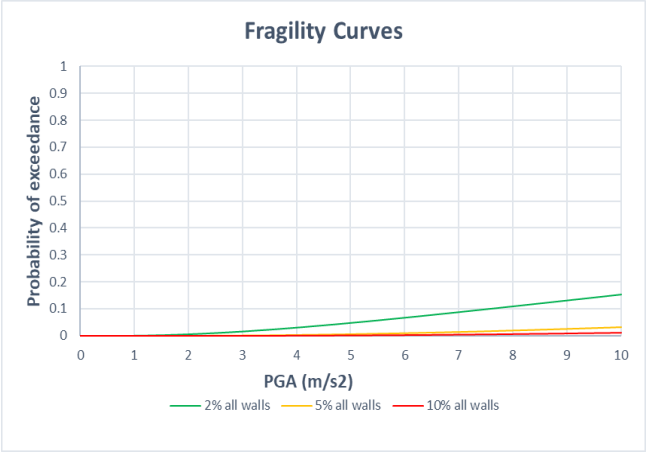

Figure 3.156 All walls combined together fragility curves in terms of PGA with respect to tilting angle second threshold

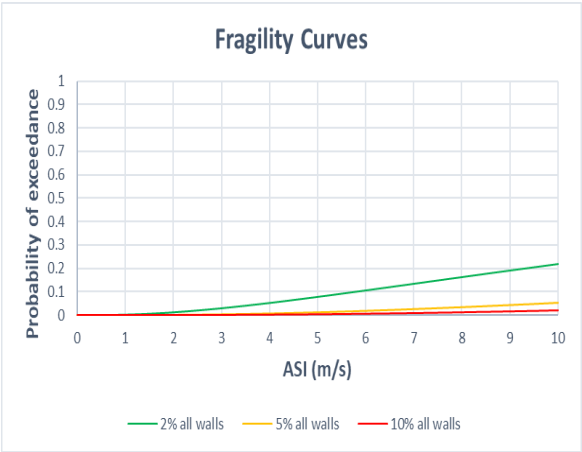

Figure 3.157 All walls combined together fragility curves in terms of ASI with respect to tilting angle second threshold

The last comment on this fully combined case study of fragility curves is that it could be seen that the curves were mostly representing the average of all the walls separately.

Conclusion and further developments

The aim of this study was to develop the fragility curves in terms of the best intensity measure according to several geometries and backfill cases and of earth retaining walls according to the damage index of these walls in terms of relative horizontal displacement and tilting of the walls that were gotten from a numerical analysis based on FLAC software, in which specific characteristics were applied in order to have these analysis values.

The results were then contributed with the several intensity measures (IMs) of a given input motions in a probabilistic seismic demand model (PSDM) study, were the best correlated IMs were selected for each case according to PSDM studies, in which they were used to build the fragility curves that were compared and arranged according to a well-known reference that was HUANG et,2009 in terms of horizontal displacement.
In which the result was a clear monotonic increment in the fragility curves according to damage state levels with the increasing magnitude of the geometry of all walls for both backfill cases. That leads us that the approach that was used, is fulfilling the requirements of studying the relationship between the best IM selected and the damage states in term of horizontal displacement.
According to these results also, we can say that the numerical analysis of the walls, done by FLAC are almost right as they lead us to find a valid relation between the geometries of the walls and the fragility curves.

Another approach was tried, in terms of tilting damage states in which two thresholds were used, that none of them lead us to a perfect or clear relationship.
Then the walls were combined in several ways to have a deeper view in terms of IMs, and how they will change in terms of combination and the best overall IM in the case of combining all the walls together.
As a conclusion in our study we can say that our study mostly fits with ASI intensity measure as it was the most appearing IM in all the cases and specially the combined ones.

Developing this study could be done in various ways, starting by the general shape of the wall that was selected in this study as a gravity retaining wall, where there are a lot of other shapes and types of retaining walls that could be studied.
The study was done with a numerical analysis program in which there are a lot of deep concepts and models that could be an alternate for our choices, another main issue that has been ignored in this

study was the polarity of the dynamic load in which all the loads were applied in the same direction, because the numerical dynamic analysis consumes a lot of time, no time was available for having the analysis of both polar.

Another lack of information that could be developed was in term of damage state according to tilting, in which no clear or affordable reference was mentioning this aspect, as a lot of efforts could be done in this aspect.

APPENDIXES

APPENDIX-A

In the coming tables the formulas that are used are according to the Italian code and according to the Italian partial coefficients for actions and resistance as shown in tables (3.1), (4.1), (5.1), (6.1) and the calculations Hs been done for both flat and slope cases according to the geometry of second, third and fourth walls.

The second wall:

Wall Geometry	(m)
Stem Width (t_s)	0.65
H	4.5
B	2.8
Toe Height (t_b)	0.75
Toe Width (t_w)	0.5
γ interaction soil	17(kN/m^3)
γ soil under wall	20(kN/m^3)

Table A.1 Second wall geometry

Table A.2 Actions of second wall

effect of actions	Formula	Flat(β=0)		Slope(β=25°)		unit
		A1=1.3	A1=1	A1=1.3	A1=1	
Appropriate earth pressure coefficient	$K_{a,\beta}=\left(\frac{cos\beta-\sqrt{cos^2\beta-cos^2\varphi}}{cos\beta+\sqrt{cos^2\beta-cos^2\varphi}}\right)cos\beta$	0.33	0.41	0.49	0.82	-
Design friction angle	$\varphi_d = atan\left(\frac{\tan(\varphi_k)}{\gamma_\varphi}\right)$	0.52 30	0.43 24.79	0.52 30	0.43 24.79	Rad °
Design thrust from earth pressure	$E_{a,Gd} = \gamma_G K_{a\beta,d}\left(\frac{1}{2}\gamma_k H^2\right)$	74.59	70.42	108.62	141.63	(kN/m)
Horizontal component of design thrust	$H_{Ed} = E_{a,d}\cos(\beta)$	74.59	70.42	98.74	128.74	(kN/m)
Stem weight of the wall	$W_{stem,Gk}=\gamma_{c,k}.t_s$.H	50.40	50.40	50.40	50.40	(kN/m)
base weight of the wall	$W_{base,Gk}=\gamma_{c,k}.t_b$.B	58.50	58.50	58.50	58.50	(kN/m)
Triangle area weight of the wall	$W_{traingle,Gk}=\gamma_{c,k}.\frac{1}{2}$.(H - t_b).(B - t_s- t_w)	74.25	74.25	74.25	74.25	(kN/m)
Total weight of wall	$W_{total,Gk} = W_{stem,Gk} + W_{base,Gk} + W_{traingle,Gk}$	183.15	183.15	183.15	183.15	(kN/m)
Moments about wall toe - Design overturning moments (destabilizing) about wall toe	$M_{Gd}=\frac{1}{3}E_{a,Gd}$H cos(β)	110.76	104.58	146.62	191.18	(kN.m/m)
Centroid of wall on x-axis from the toe	$\bar{X} = \frac{\bar{x_s}A_{stem} + \bar{x_b}A_{base} + \bar{x_{tra}}A_{traingle}}{A_{total}}$	1.82	1.82	1.82	1.82	(m)
Design restoring moments (stabilizing) about wall toe	$M_{Rd}=\bar{X}.W_{Gk}$	434.39	334.15	434.39	334.15	(kN.m/m)
Line of action of resultant force is a distance from the toe	$X=\frac{M_{Rd}-M_{Gd}}{N_{Ed}}$	1.36	0.96	1.02	0.50	(m)
Eccentricity of actions from centre line of base	$e_d=\frac{B}{2}-X$	0.04	0.44	0.38	0.90	(m)
Effective width of base	$B'_d = B - 2e_d$	2.72	1.93	2.03	1.01	(m)
Design bearing capacity factors	$N_{q,d} = e^{\pi\tan(\varphi_d)}\left(tan\left(45° + \frac{\varphi_d}{2}\right)\right)^2$	18.17	10.33	18.18	10.33	-
	$N_{\gamma,d} = 2\left(N_{q,d} - 1\right)tan(\varphi_d)$	19.83	8.62	19.83	8.62	-
Shape factors (for an infinitely	s_q	1	1.00	1.00	1.00	-

long footing)	s_γ	1	1.00	1.00	1.00	-
Inclination factors: (using m_B= 2 for an infinitely long footing)	$i_q=\left(1-\frac{H_{Ed}}{N_{Ed}-Ac'_d\cot(\varphi_d)}\right)^{m_B}$	0.461	0.37	0.42	0.22	-
	$i_\gamma = i_q^{\frac{m_B+1}{m_B}}$	0.313	0.22	0.28	0.10	-
Design bearing resistance from overburden	$q_{Rvq,d} = \gamma_k t_b N_{q,d} s_q i_q$	91.85	41.93	115.76	61.20	(kN/m^2)
Design bearing resistance from body-mass	$q_{Rv\gamma,d} = \frac{1}{2} B'_d \gamma_k N_{\gamma,d} s_\gamma i_\gamma$	385.14	118.70	402.84	156.52	(kN/m^2)
Total design bearing resistance	$q_{lim} = q_{Rvq,d} + q_{Rv\gamma,d}$	476.99	160.63	518.60	217.72	(kN/m^2)
Characteristic bearing resistance (in terms of force)	$N_{Rd} = q_{lim} B'_d$	1296.70	309.76	1053.27	219.69	(kN/m)
Vertical/normal component of design weight and thrust	$N_{Ed}=\gamma_G W_{Gk} + E_{a,d}\sin(\beta)$	238.10	183.15	283.38	242.19	(kN/m)
Design sliding resistance	$H_{Rd} = \gamma_{G1,fav} N_{Ed} \tan(\delta_d)$	168.57	133.19	188.43	159.73	(kN/m)

Table A.3 Verifications of second wall

Verifications	Overdesign factor	Flat		Slope	
Verification of resistance to sliding	ODF = $\frac{H_{Rd}}{\gamma_R H_{Ed}}$	2.05	1.72	1.73	1.13
Verification of overturning resistance	ODF = $\frac{M_{Rd}}{\gamma_R M_{Gd}}$	3.41	2.78	2.58	1.52
Verification of bearing resistance	ODF = $\frac{N_{Rd}}{\gamma_R N_{Ed}}$	3.89	2.62	2.65	1.27

The third wall:

Wall Geometry	(m)
Stem Width (t_s)	0.75
H	5.5
B	3.35
Toe Height (t_b)	0.8
Toe Width (t_w)	0.6
γ interaction soil	17(kN/m^3)
γ soil under wall	20(kN/m^3)

Table A.4 Third wall geometry

Table A.5 Actions of third wall

effect of actions	Formula	Flat(β=0)		Slope(β=25°)		unit
		A1=1.3	A1=1	A1=1.3	A1=1	
Appropriate earth pressure coefficient	$K_{a,\beta}=\left(\frac{\cos\beta-\sqrt{\cos^2\beta-\cos^2\varphi}}{\cos\beta+\sqrt{\cos^2\beta-\cos^2\varphi}}\right)\cos\beta$	0.33	0.41	0.49	0.82	-
Design friction angle	$\varphi_d = atan\left(\frac{\tan(\varphi_k)}{\gamma_\varphi}\right)$	0.52 30	0.43 24.79	0.52 30	0.43 24.79	Rad °
Design thrust from earth pressure	$E_{a,Gd} = \gamma_G K_{a\beta,d}\left(\frac{1}{2}\gamma_k H^2\right)$	111.42	105.20	162.27	211.58	(kN/m)
Horizontal component of design thrust	$H_{Ed} = E_{a,d}\cos(\beta)$	111.42	105.20	147.49	192.31	(kN/m)

Stem weight of the wall	$W_{stem,Gk}=\gamma_{c,k}.t_s$.H	64.32	64.32	64.32	64.32	(kN/m)
base weight of the wall	$W_{base,Gk}=\gamma_{c,k}.t_b$.B	84.60	84.60	84.60	84.60	(kN/m)
Triangle area weight of the wall	$W_{traingle,Gk}=\gamma_{c,k}.\frac{1}{2}$.(H - t_b).(B - t_s- t_w)	112.80	112.80	112.80	112.80	(kN/m)
Total weight of wall	$W_{total,Gk} = W_{stem,Gk} + W_{base,Gk} + W_{traingle,Gk}$	261.72	261.72	261.72	261.72	(kN/m)
Moments about wall toe - Design overturning moments (destabilizing) about wall toe	$M_{Gd}=\frac{1}{3}E_{a,Gd}$H cos(β)	202.23	190.93	267.70	349.05	(kN.m/m)
Centroid of wall on x-axis from the toe	$\bar{X}=\frac{\overline{x_s}A_{stem}+\overline{x_b}A_{base}+\overline{x_{tra}}A_{traingle}}{A_{total}}$	2.21	2.21	2.21	2.21	(m)
Design restoring moments (stabilizing) about wall toe	$M_{Rd}=\bar{X}.W_{Gk}$	750.75	577.50	750.75	577.50	(kN.m/m)
Line of action of resultant force is a distance from the toe	$X=\frac{M_{Rd}-M_{Gd}}{N_{Ed}}$	1.61	1.14	1.18	0.56	(m)
Eccentricity of actions from centre line of base	$e_d=\frac{B}{2}-X$	0.06	0.54	0.49	1.11	(m)
Effective width of base	$B'_d=B-2e_d$	3.22	2.27	2.37	1.12	(m)
Design bearing capacity factors	$N_{q,d}=e^{\pi\tan(\varphi_d)}\left(tan\left(45°+\frac{\varphi_d}{2}\right)\right)^2$	18.17	10.33	18.18	10.33	-
	$N_{\gamma,d}=2\left(N_{q,d}-1\right)tan(\varphi_d)$	19.83	8.62	19.83	8.62	-
Shape factors (for an infinitely long footing)	s_q	1	1.00	1.00	1.00	-
	s_γ	1	1.00	1.00	1.00	-
Inclination factors: (using m_B= 2 for an infinitely long footing)	$i_q=\left(1-\frac{H_{Ed}}{N_{Ed}-Ac'_d\cot(\varphi_d)}\right)^{m_B}$	0.461	0.37	0.42	0.21	-
	$i_\gamma=i_q^{\frac{m_B+1}{m_B}}$	0.313	0.22	0.27	0.10	-
Design bearing resistance from overburden	$q_{Rvq,d}=\gamma_k t_b N_{q,d}s_q i_q$	93.96	42.22	118.53	60.35	(kN/m^2)
Design bearing resistance from body-mass	$q_{R\nu\gamma,d}=\frac{1}{2}B'_d\gamma_k N_{\gamma,d}s_\gamma i_\gamma$	456.81	139.88	469.80	173.76	(kN/m^2)
Total design bearing resistance	$q_{lim}=q_{Rvq,d}+q_{R\nu\gamma,d}$	550.77	182.10	588.33	234.11	(kN/m^2)
Characteristic bearing resistance (in terms of force)	$N_{Rd}=q_{lim}B'_d$	1775.89	413.79	1393.50	262.25	(kN/m)
Vertical/normal component of design weight and thrust	$N_{Ed}=\gamma_G W_{Gk}+E_{a,d}\sin(\beta)$	340.24	261.72	407.88	349.92	(kN/m)
Design sliding resistance	$H_{Rd}=\gamma_{G1,fav}N_{Ed}\tan(\delta_d)$	233.83	184.54	266.20	227.75	(kN/m)

Table A.6 Verifications of third wall

Verifications	Overdesign factor	Flat		Slope	
Verification of resistance to sliding	ODF = $\frac{H_{Rd}}{\gamma_R H_{Ed}}$	1.91	1.59	1.64	1.08
Verification of overturning resistance	ODF = $\frac{M_{Rd}}{\gamma_R M_{Gd}}$	3.23	2.63	2.44	1.44
Verification of bearing resistance	ODF = $\frac{N_{Rd}}{\gamma_R N_{Ed}}$	3.73	2.21	2.44	1.05

The fourth wall:

Wall Geometry	(m)
Stem Width (t_s)	0.8
H	6.5
B	4
Toe Height (t_b)	0.8
Toe Width (t_w)	0.8
γ interaction soil	17(kN/m^3)
γ soil under wall	20(kN/m^3)

Table A. 7 Fourth wall geometry

Table A.8 Actions of fourth wall

effect of actions	Formula	Flat(β=0)		Slope(β=25°)		unit
		A1=1.3	A1=1	A1=1.3	A1=1	
Appropriate earth pressure coefficient	$K_{a,\beta}=\left(\frac{cos\beta-\sqrt{cos^2\beta-cos^2\varphi}}{cos\beta+\sqrt{cos^2\beta-cos^2\varphi}}\right)cos\beta$	0.33	0.41	0.49	0.82	-
Design friction angle	$\varphi_d = atan\left(\frac{\tan(\varphi_k)}{\gamma_\varphi}\right)$	0.52 30	0.43 24.79	0.52 30	0.43 24.79	Rad °
Design thrust from earth pressure	$E_{a,Gd} = \gamma_G K_{a\beta,d}\left(\frac{1}{2}\gamma_k H^2\right)$	155.62	146.93	226.64	295.51	(kN/m)
Horizontal component of design thrust	$H_{Ed} = E_{a,d}\cos(\beta)$	155.62	146.93	206.00	268.61	(kN/m)
Stem weight of the wall	$W_{stem,Gk}=\gamma_{c,k}.t_s.\mathrm{H}$	76.80	76.80	76.80	76.80	(kN/m)
base weight of the wall	$W_{base,Gk}=\gamma_{c,k}.t_b.\mathrm{B}$	109.44	109.44	109.44	109.44	(kN/m)
Triangle area weight of the wall	$W_{traingle,Gk}=\gamma_{c,k}.\frac{1}{2}.(\mathrm{H}-t_b).(\mathrm{B}-t_s-t_w)$	164.16	164.16	164.16	164.16	(kN/m)
Total weight of wall	$W_{total,Gk} = W_{stem,Gk} + W_{base,Gk} + W_{traingle,Gk}$	350.40	350.40	350.40	350.40	(kN/m)
Moments about wall toe - Design overturning moments (destabilizing) about wall toe	$M_{Gd}=\frac{1}{3}E_{a,Gd}\mathrm{H}\cos(\beta)$	333.81	315.16	441.88	576.16	(kN.m/m)
Centroid of wall on x-axis from the toe	$\bar{X} = \frac{\bar{x_s}A_{stem} + \bar{x_b}A_{base} + \bar{x_{tra}}A_{traingle}}{A_{total}}$	2.69	2.69	2.69	2.69	(m)
Design restoring moments (stabilizing) about wall toe	$M_{Rd}=\bar{X}.W_{Gk}$	1224.0	941.57	1224.0	941.57	(kN.m/m)
Line of action of resultant force is a distance from the toe	$\mathrm{X}=\frac{M_{Rd}-M_{Gd}}{N_{Ed}}$	1.95	1.38	1.42	0.66	(m)
Eccentricity of actions from centre line of base	$e_d=\frac{B}{2}-X$	0.05	0.62	0.58	1.34	(m)
Effective width of base	$B'_d = B - 2e_d$	3.91	2.75	2.84	1.33	(m)
Design bearing capacity factors	$N_{q,d} = e^{\pi\tan(\varphi_d)}\left(tan\left(45° + \frac{\varphi_d}{2}\right)\right)^2$	18.17	10.33	18.18	10.33	-
	$N_{\gamma,d} = 2\left(N_{q,d}-1\right)tan(\varphi_d)$	19.83	8.62	19.83	8.62	-
Shape factors (for an infinitely long footing)	s_q	1	1.00	1.00	1.00	-
	s_γ	1	1.00	1.00	1.00	-
Inclination factors: (using	$i_q=\left(1-\frac{H_{Ed}}{N_{Ed}-Ac'_d\cot(\varphi_d)}\right)^{m_B}$	0.461	0.37	0.42	0.21	-

m_B= 2 for an infinitely long footing)	$i_\gamma = i_q^{\frac{m_B+1}{m_B}}$	0.313	0.22	0.27	0.10	-
Design bearing resistance from overburden	$q_{Rvq,d} = \gamma_k t_b N_{q,d} s_q i_q$	90.04	39.80	113.77	55.73	(kN/m^2)
Design bearing resistance from body-mass	$q_{Rv\gamma,d} = \frac{1}{2} B'_d \gamma_k N_{\gamma,d} s_\gamma i_\gamma$	553.76	169.30	564.14	206.12	(kN/m^2)
Total design bearing resistance	$q_{lim} = q_{Rvq,d} + q_{Rv\gamma,d}$	643.80	209.10	677.91	261.85	(kN/m^2)
Characteristic bearing resistance (in terms of force)	$N_{Rd} = q_{lim} B'_d$	2516.4	575.09	1928.1	347.94	(kN/m)
Vertical/normal component of design weight and thrust	N_{Ed}=$\gamma_G W_{Gk} + E_{a,d} \sin(\beta)$	455.52	350.40	550.00	473.59	(kN/m)
Design sliding resistance	$H_{Rd} = \gamma_{G1,fav} N_{Ed} \tan(\delta_d)$	303.72	239.41	352.35	304.27	(kN/m)

Table A. 9 Verifications of fourth wall

Verifications	Overdesign factor	Flat		Slope	
Verification of resistance to sliding	ODF = $\frac{H_{Rd}}{\gamma_R H_{Ed}}$	1.77	1.48	1.55	1.03
Verification of overturning resistance	ODF = $\frac{M_{Rd}}{\gamma_R M_{Gd}}$	3.19	2.60	2.41	1.42
Verification of bearing resistance	ODF = $\frac{N_{Rd}}{\gamma_R N_{Ed}}$	3.95	2.30	2.50	1.03

APPENDIX-B

Table B.1 Intensity Measures input

Earthquake ID	A95 (m/s^2)	T_{pred} (s)	T_m (s)	PGV (cm/s)	PGD (cm)	Vrms (cm/s)	Drms (cm)	Spe ED (cm^2/s)	VSI (cm)	I_h (cm)	SMA (m/s^2)	SMV (cm/s)
Acc_100	0.254	0.34	0.40	1.757	0.391	0.328	0.146	6.452	8.596	7.242	0.208	1.627
Acc_110	0.352	0.28	0.29	2.138	0.186	0.361	0.046	2.980	7.345	5.672	0.342	1.536
Acc_120	0.564	0.20	0.48	2.413	1.735	0.653	1.084	27.182	16.223	15.630	0.297	2.400
Acc_130	0.779	0.08	0.21	3.335	1.471	0.819	0.647	20.118	13.244	11.318	0.660	2.745
Acc_140	1.009	0.08	0.21	4.318	1.905	1.061	0.838	33.710	17.144	14.651	0.855	3.553
Acc_150	1.118	0.22	0.25	6.286	1.025	1.033	0.204	26.672	26.159	17.727	1.014	5.305
Acc_160	1.286	0.18	0.27	6.617	0.589	1.086	0.150	34.156	24.734	18.142	0.997	5.286
Acc_170	1.327	0.18	0.27	6.830	0.608	1.121	0.155	36.386	25.528	18.725	1.029	5.456
Acc_180	1.395	0.36	0.65	14.102	5.016	2.815	2.127	316.421	49.000	45.681	0.845	9.021
Acc_190	1.769	0.38	0.39	13.097	3.117	1.552	0.556	96.175	59.107	43.765	1.291	10.353
Acc_200	1.840	0.20	0.29	14.576	2.925	1.336	0.681	71.262	38.534	27.595	1.290	8.289
Acc_210	2.403	0.18	0.27	12.365	1.101	2.030	0.280	119.263	46.218	33.900	1.863	9.878
Acc_220	2.631	0.54	0.83	30.885	11.581	6.147	4.551	1508.634	137.567	131.409	1.601	23.134
Acc_230	2.992	0.28	0.88	49.338	17.202	8.535	5.633	2909.378	202.500	196.537	2.383	30.349
Acc_240	3.347	0.10	0.30	32.016	9.718	3.854	4.292	1188.351	90.181	82.514	3.344	21.044
Acc_250	4.355	0.20	0.26	24.700	5.572	3.174	1.069	371.430	107.991	80.156	4.211	17.810
Acc_260	5.316	0.20	0.26	30.149	6.802	3.874	1.305	553.422	131.819	97.842	5.141	21.740
Acc_270	6.267	0.14	0.57	54.907	21.075	6.436	2.722	9857.804	275.289	270.415	5.943	45.964

Table B.2 Intensity Measures input

Earthquake ID	$S_{a(0.2;5\%)}$ (m/s^2)	$S_{pv(0.2;5\%)}$ (m/s^2)	$S_{d(0.4;5\%)}$ (m/s^2)	$S_{a(0.4;5\%)}$ (m/s^2)	$S_{pv(0.4;5\%)}$ (m/s^2)	$S_{d(0.4;5\%)}$ (m/s^2)	$S_{a(0.6;5\%)}$ (m/s^2)	$S_{pv(0.6;5\%)}$ (m/s^2)	$S_{d(0.6;5\%)}$ (m/s^2)	$S_{a(1;5\%)}$ (m/s^2)	$S_{pv(1;5\%)}$ (m/s^2)	$S_{d(1;5\%)}$ (m/s^2)	$S_{a(2;5\%)}$ (m/s^2)	$S_{pv(2;5\%)}$ (m/s^2)	$S_{d(0.2;5\%)}$ (m/s^2)
Acc_100	0.614	1.802	0.062	0.660	4.141	0.266	0.412	0.190	0.072	0.190	0.072	1.802	0.072	1.802	4.141
Acc_110	1.302	3.731	0.131	0.775	5.138	0.313	0.337	0.128	0.045	0.128	0.045	3.731	0.045	3.731	5.138
Acc_120	2.795	9.030	0.282	1.017	6.564	0.410	0.500	0.318	0.267	0.318	0.267	9.030	0.267	9.030	6.564
Acc_130	1.832	5.465	0.185	0.963	6.660	0.388	0.356	0.289	0.117	0.289	0.117	5.465	0.117	5.465	6.660
Acc_140	2.372	7.074	0.239	1.246	8.622	0.502	0.460	0.375	0.152	0.375	0.152	7.074	0.152	7.074	8.622
Acc_150	3.346	10.34	0.337	2.740	17.892	1.105	1.826	0.507	0.102	0.507	0.102	10.34	0.102	10.34	17.89
Acc_160	4.967	15.52	0.501	1.597	10.428	0.644	1.692	0.477	0.106	0.477	0.106	15.52	0.106	15.52	10.42
Acc_170	5.127	16.02	0.517	1.648	10.763	0.664	1.746	0.492	0.110	0.492	0.110	16.02	0.110	16.02	10.76
Acc_180	1.901	4.104	0.192	2.730	16.393	1.102	1.928	1.498	0.539	1.498	0.539	4.104	0.539	4.104	16.39
Acc_190	3.707	9.225	0.374	7.580	48.553	3.057	2.206	1.192	0.421	1.192	0.421	9.225	0.421	9.225	48.55
Acc_200	5.943	18.76	0.599	4.182	27.884	1.683	1.438	0.502	0.291	0.502	0.291	18.76	0.291	18.76	27.88
Acc_210	9.282	29.01	0.936	2.984	19.486	1.203	3.162	0.891	0.199	0.891	0.199	29.01	0.199	29.01	19.48
Acc_220	3.408	8.689	0.344	2.845	14.782	1.150	4.606	2.538	2.209	2.538	2.209	8.689	2.209	8.689	14.78
Acc_230	6.757	15.77	0.682	7.689	42.268	3.103	4.859	4.423	3.724	4.423	3.724	15.77	3.724	15.77	42.26
Acc_240	8.239	24.94	0.831	5.558	37.865	2.244	3.298	1.701	1.076	1.701	1.076	24.94	1.076	24.94	37.86
Acc_250	18.22	56.93	1.838	6.986	48.579	2.819	4.980	3.228	0.744	3.228	0.744	56.93	0.744	56.93	48.57
Acc_260	22.25	69.49	2.244	8.528	59.297	3.441	6.079	3.940	0.908	3.940	0.908	69.49	0.908	69.49	59.29
Acc_270	18.76	63.38	1.889	10.152	57.968	4.100	6.519	6.383	4.291	6.383	4.291	63.38	4.291	63.38	57.96

Appendix-C

The colours assigned for each parameter is varying according to its goodness, ranging from red for the worst values to green that are the best values passing through the yellow colour for the intermediate values, and that for practically as much the value is bigger as it is the best, while for efficiency and proficiency it is the opposite, as the smaller value is the best value, for all the tables.

Table C.1 Practically, Efficiency and Proficiency of first wall H=3.6m assuming relative horizontal displacement as damage measure of structure.

	Flat			Slope		
	(b)	(σ)	(ξ)	(b)	(σ)	(ξ)
PGA (m/s2)	1.307	0.653	0.500	1.112	0.433	0.390
PGV (cm/s)	0.975	0.806	0.827	0.878	0.495	0.564
PGD (cm)	0.618	1.058	1.714	0.572	0.769	1.346
Arms (m/s^2)	1.432	0.704	0.492	1.214	0.495	0.408
Vrms (cm/s)	1.018	0.922	0.906	0.962	0.570	0.593
Drms (cm)	0.426	1.223	2.871	0.425	0.928	2.184
Ia(m/s)	0.687	0.563	0.820	0.576	0.374	0.648
Ic (-)	0.949	0.585	0.617	0.798	0.388	0.486
Spe ED (cm^2/s)	0.460	0.889	1.934	0.424	0.563	1.328
CAV (cm/s)	1.238	0.600	0.485	1.037	0.417	0.402
ASI (m/s)	1.431	0.592	0.414	1.183	0.439	0.371
VSI (cm)	1.010	0.775	0.768	0.908	0.454	0.500
Ih (cm)	0.935	0.832	0.890	0.852	0.504	0.592
SMA (m/s^2)	1.260	0.581	0.461	1.044	0.424	0.406
SMV (cm/s)	1.075	0.762	0.709	0.963	0.446	0.463
EDA (m/s^2)	1.313	0.656	0.499	1.121	0.428	0.382
A95 (m/s^2)	1.306	0.654	0.501	1.111	0.433	0.390
Tpred (s)	0.251	1.356	5.396	0.043	1.105	25.574
Tm (S)	0.286	1.356	4.739	0.655	1.063	1.623
Sa (0,2;5%) (m/s^2)	1.260	0.555	0.440	0.996	0.506	0.508
Sa (0,4;5%) (m/s2)	1.217	0.776	0.638	1.010	0.600	0.595
Sa (0,6;5%) (m/s2)	1.081	0.740	0.685	0.964	0.426	0.442
Sa (1;5%)(m/s2)	0.940	0.774	0.824	0.841	0.464	0.552
Sa (2;5%) (m/s2)	0.669	0.987	1.475	0.624	0.675	1.082
Sv (0,2;5%) (m/S)	1.183	0.593	0.501	0.917	0.565	0.617
Sv (0,4;5%) (S)	1.243	0.768	0.618	1.007	0.626	0.621
Sv (0,6;5%) (S)	1.109	0.765	0.689	0.979	0.482	0.493
Sv (1;5%) (S)	1.044	0.744	0.713	0.923	0.452	0.490
Sv (2;5%) (S)	0.839	0.863	1.029	0.767	0.541	0.704
Sd (0,2;5%) (m/S)	1.261	0.555	0.440	0.996	0.505	0.507
Sd (0,4;5%) (S)	1.217	0.776	0.638	1.009	0.600	0.594
Sd (0,6;5%)(S)	1.081	0.740	0.685	0.965	0.426	0.442
Sd (1;5%) (S)	0.938	0.775	0.826	0.840	0.465	0.553
Sd (2;5%) (S)	0.666	0.989	1.486	0.621	0.677	1.091

Table C.2 Practically, Efficiency and Proficiency of first wall H=3.6m assuming tilting as damage measure of structure.

	Flat			Slope		
	(b)	(σ)	(ξ)	(b)	(σ)	(ξ)
PGA (m/s2)	0.560	0.315	0.562	0.829	0.389	0.469
PGV (cm/s)	0.411	0.384	0.933	0.693	0.341	0.492
PGD (cm)	0.268	0.472	1.761	0.473	0.542	1.146
Arms (m/s^2)	0.618	0.329	0.532	0.910	0.421	0.462
Vrms (cm/s)	0.435	0.422	0.969	0.782	0.366	0.468
Drms (cm)	0.192	0.537	2.792	0.379	0.664	1.754
Ia(m/s)	0.295	0.278	0.940	0.427	0.361	0.845
Ic (-)	0.409	0.285	0.697	0.594	0.364	0.613
Spe ED (cm^2/s)	0.196	0.410	2.088	0.338	0.388	1.146
CAV (cm/s)	0.538	0.282	0.524	0.768	0.390	0.508
ASI (m/s)	0.608	0.300	0.494	0.878	0.399	0.454
VSI (cm)	0.429	0.368	0.860	0.719	0.300	0.417
Ih (cm)	0.398	0.389	0.977	0.682	0.326	0.478
SMA (m/s^2)	0.542	0.284	0.525	0.767	0.405	0.528
SMV (cm/s)	0.454	0.367	0.808	0.755	0.313	0.415
EDA (m/s^2)	0.562	0.318	0.565	0.837	0.383	0.458
A95 (m/s^2)	0.560	0.315	0.563	0.829	0.388	0.468
Tpred (s)	0.153	0.596	3.900	0.174	0.847	4.881
Tm (S)	0.086	0.600	6.968	0.749	0.779	1.039
Sa (0,2;5%) (m/s^2)	0.547	0.264	0.482	0.706	0.491	0.696
Sa (0,4;5%) (m/s2)	0.512	0.374	0.730	0.768	0.477	0.621
Sa (0,6;5%) (m/s2)	0.457	0.359	0.785	0.736	0.347	0.472
Sa (1;5%)(m/s2)	0.406	0.357	0.878	0.658	0.333	0.506
Sa (2;5%) (m/s2)	0.287	0.447	1.560	0.519	0.442	0.851
Sv (0,2;5%) (m/S)	0.515	0.277	0.539	0.636	0.540	0.849
Sv (0,4;5%) (S)	0.526	0.367	0.698	0.754	0.510	0.677
Sv (0,6;5%) (S)	0.465	0.372	0.802	0.742	0.396	0.534
Sv (1;5%) (S)	0.447	0.350	0.783	0.718	0.333	0.464
Sv (2;5%) (S)	0.355	0.403	1.136	0.621	0.342	0.551
Sd (0,2;5%) (m/S)	0.548	0.264	0.482	0.706	0.491	0.695
Sd (0,4;5%) (S)	0.512	0.374	0.730	0.768	0.477	0.621
Sd (0,6;5%)(S)	0.457	0.359	0.785	0.736	0.347	0.472
Sd (1;5%) (S)	0.406	0.357	0.880	0.657	0.333	0.506
Sd (2;5%) (S)	0.285	0.448	1.572	0.517	0.444	0.858

Table C.3 Practically, Efficiency and Proficiency of second wall H=4.5m assuming relative horizontal displacement as damage measure of structure.

	Flat			Slope		
	(b)	(σ)	(ξ)	(b)	(σ)	(ξ)
PGA (m/s2)	1.537	0.646	0.420	1.210	0.417	0.344
PGV (cm/s)	1.174	0.804	0.685	0.964	0.471	0.489
PGD (cm)	0.748	1.147	1.534	0.635	0.789	1.242
Arms (m/s^2)	1.693	0.702	0.415	1.318	0.498	0.377
Vrms (cm/s)	1.229	0.965	0.785	1.039	0.594	0.572
Drms (cm)	0.543	1.345	2.478	0.484	0.966	1.995
Ia(m/s)	0.814	0.482	0.593	0.637	0.278	0.437
Ic (-)	1.124	0.521	0.464	0.878	0.324	0.369
Spe ED (cm^2/s)	0.555	0.920	1.658	0.466	0.556	1.194
CAV (cm/s)	1.477	0.515	0.349	1.156	0.312	0.270
ASI (m/s)	1.676	0.573	0.342	1.303	0.388	0.298
VSI (cm)	1.195	0.797	0.666	0.981	0.465	0.474
Ih (cm)	1.112	0.864	0.777	0.922	0.517	0.560
SMA (m/s^2)	1.475	0.560	0.379	1.142	0.391	0.342
SMV (cm/s)	1.287	0.752	0.584	1.054	0.417	0.395
EDA (m/s^2)	1.548	0.644	0.416	1.221	0.410	0.336
A95 (m/s^2)	1.534	0.650	0.424	1.209	0.420	0.348
Tpred (s)	0.310	1.539	4.966	0.076	1.183	15.621
Tm (S)	0.412	1.536	3.731	0.643	1.145	1.782
Sa (0,2;5%) (m/s^2)	1.438	0.615	0.428	1.063	0.547	0.514
Sa (0,4;5%)(m/s2)	1.421	0.828	0.583	1.123	0.577	0.514
Sa (0,6;5%) (m/s2)	1.284	0.743	0.579	1.038	0.441	0.425
Sa (1;5%)(m/s2)	1.097	0.825	0.752	0.899	0.501	0.557
Sa (2;5%) (m/s2)	0.801	1.063	1.327	0.676	0.705	1.043
Sv (0,2;5%) (m/S)	1.345	0.671	0.499	0.978	0.610	0.623
Sv (0,4;5%) (S)	1.447	0.824	0.570	1.126	0.600	0.533
Sv (0,6;5%) (S)	1.323	0.766	0.579	1.068	0.470	0.440
Sv (1;5%) (S)	1.221	0.781	0.640	0.994	0.467	0.469
Sv (2;5%) (S)	0.995	0.910	0.915	0.827	0.566	0.685
Sd (0,2;5%) (m/S)	1.438	0.615	0.428	1.063	0.547	0.514
Sd (0,4;5%) (S)	1.421	0.828	0.583	1.123	0.577	0.514
Sd (0,6;5%)(S)	1.284	0.743	0.579	1.038	0.441	0.425
Sd (1;5%) (S)	1.096	0.825	0.753	0.898	0.501	0.558
Sd (2;5%) (S)	0.797	1.065	1.336	0.674	0.708	1.051

Table C.4 Practically, Efficiency and Proficiency of second wall H=4.5m assuming tilting as damage measure of structure.

	Flat			slope		
	(b)	(σ)	(ξ)	(b)	(σ)	(ξ)
PGA (m/s2)	0.987	0.438	0.444	0.961	0.336	0.350
PGV (cm/s)	0.760	0.525	0.691	0.770	0.366	0.475
PGD (cm)	0.476	0.755	1.587	0.510	0.620	1.217
Arms (m/s^2)	1.111	0.434	0.391	1.050	0.393	0.375
Vrms (cm/s)	0.793	0.631	0.796	0.833	0.461	0.554
Drms (cm)	0.356	0.869	2.439	0.395	0.757	1.916
Ia(m/s)	0.521	0.350	0.672	0.503	0.243	0.484
Ic (-)	0.724	0.354	0.488	0.695	0.270	0.388
Spe ED (cm^2/s)	0.350	0.625	1.786	0.370	0.442	1.193
CAV (cm/s)	0.939	0.383	0.407	0.913	0.269	0.295
ASI (m/s)	1.076	0.393	0.366	1.032	0.319	0.310
VSI (cm)	0.760	0.543	0.715	0.783	0.362	0.462
Ih (cm)	0.705	0.588	0.834	0.736	0.403	0.548
SMA (m/s^2)	0.947	0.387	0.409	0.902	0.326	0.361
SMV (cm/s)	0.824	0.508	0.616	0.840	0.326	0.388
EDA (m/s^2)	0.996	0.433	0.435	0.969	0.330	0.341
A95 (m/s^2)	0.985	0.441	0.447	0.959	0.339	0.353
Tpred (s)	0.187	0.999	5.329	-0.002	0.941	445.784
Tm (S)	0.211	0.999	4.741	0.538	0.907	1.686
Sa (0,2;5%) (m/s^2)	0.921	0.425	0.462	0.836	0.451	0.540
Sa (0,4;5%) (m/s2)	0.910	0.554	0.609	0.892	0.461	0.517
Sa (0,6;5%) (m/s2)	0.826	0.495	0.599	0.830	0.338	0.407
Sa (1;5%)(m/s2)	0.693	0.569	0.821	0.718	0.389	0.542
Sa (2;5%) (m/s2)	0.506	0.709	1.400	0.543	0.552	1.017
Sv (0,2;5%) (m/S)	0.858	0.465	0.541	0.766	0.504	0.658
Sv (0,4;5%) (S)	0.930	0.546	0.587	0.894	0.480	0.537
Sv (0,6;5%) (S)	0.852	0.507	0.595	0.854	0.364	0.426
Sv (1;5%) (S)	0.774	0.540	0.698	0.792	0.368	0.465
Sv (2;5%) (S)	0.628	0.620	0.986	0.659	0.446	0.677
Sd (0,2;5%) (m/S)	0.921	0.425	0.462	0.836	0.451	0.540
Sd (0,4;5%) (S)	0.910	0.554	0.609	0.891	0.461	0.517
Sd (0,6;5%)(S)	0.826	0.495	0.599	0.830	0.338	0.407
Sd (1;5%) (S)	0.692	0.569	0.823	0.717	0.389	0.542
Sd (2;5%) (S)	0.504	0.710	1.410	0.540	0.554	1.026

Table C.5 Practically, Efficiency and Proficiency of third wall H=5.5m assuming relative horizontal displacement as damage measure of structure.

	Flat			Slope		
	(b)	(σ)	(ξ)	(b)	(σ)	(ξ)
PGA (m/s2)	1.962	0.679	0.346	1.273	0.386	0.303
PGV (cm/s)	1.480	0.951	0.643	1.022	0.424	0.415
PGD (cm)	1.018	1.297	1.274	0.674	0.792	1.175
Arms (m/s^2)	2.170	0.748	0.345	1.388	0.478	0.345
Vrms (cm/s)	1.604	1.090	0.679	1.112	0.554	0.498
Drms (cm)	0.810	1.541	1.904	0.523	0.980	1.873
Ia(m/s)	1.030	0.472	0.459	0.663	0.264	0.398
Ic (-)	1.427	0.509	0.356	0.917	0.301	0.328
Spe ED (cm^2/s)	0.713	1.058	1.483	0.492	0.533	1.082
CAV (cm/s)	1.851	0.585	0.316	1.197	0.329	0.275
ASI (m/s)	2.071	0.726	0.351	1.359	0.381	0.281
VSI (cm)	1.496	0.962	0.643	1.034	0.435	0.421
Ih (cm)	1.398	1.039	0.743	0.973	0.494	0.508
SMA (m/s^2)	1.844	0.656	0.356	1.190	0.388	0.326
SMV (cm/s)	1.629	0.868	0.533	1.114	0.370	0.332
EDA (m/s^2)	1.971	0.688	0.349	1.285	0.374	0.291
A95 (m/s^2)	1.959	0.685	0.349	1.271	0.389	0.306
Tpred (s)	0.785	1.873	2.385	0.033	1.227	37.608
Tm (S)	0.389	1.911	4.909	0.734	1.179	1.605
Sa (0,2;5%) (m/s^2)	1.724	0.885	0.513	1.093	0.584	0.534
Sa (0,4;5%) (m/s2)	1.740	1.060	0.609	1.173	0.584	0.497
Sa (0,6;5%) (m/s2)	1.568	0.966	0.616	1.097	0.398	0.362
Sa (1;5%)(m/s2)	1.367	1.011	0.739	0.947	0.477	0.504
Sa (2;5%) (m/s2)	1.013	1.288	1.271	0.713	0.710	0.996
Sv (0,2;5%) (m/S)	1.607	0.953	0.593	0.999	0.659	0.660
Sv (0,4;5%) (S)	1.771	1.055	0.596	1.174	0.613	0.523
Sv (0,6;5%) (S)	1.634	0.961	0.588	1.130	0.431	0.381
Sv (1;5%) (S)	1.532	0.936	0.611	1.048	0.439	0.419
Sv (2;5%) (S)	1.249	1.104	0.884	0.870	0.557	0.641
Sd (0,2;5%) (m/S)	1.725	0.885	0.513	1.093	0.584	0.534
Sd (0,4;5%) (S)	1.739	1.060	0.610	1.173	0.583	0.497
Sd (0,6;5%)(S)	1.568	0.966	0.616	1.098	0.398	0.362
Sd (1;5%) (S)	1.365	1.012	0.742	0.946	0.478	0.505
Sd (2;5%) (S)	1.009	1.291	1.280	0.710	0.713	1.004

Table C.6 Practically, Efficiency and Proficiency of third wall H=5.5m assuming tilting as damage measure of structure.

	Flat			Slope		
	(b)	(σ)	(ξ)	(b)	(σ)	(ξ)
PGA (m/s2)	0.430	0.415	0.964	1.011	0.357	0.353
PGV (cm/s)	0.345	0.420	1.218	0.829	0.335	0.404
PGD (cm)	0.296	0.397	1.339	0.560	0.615	1.097
Arms (m/s^2)	0.414	0.462	1.117	1.094	0.437	0.400
Vrms (cm/s)	0.372	0.439	1.177	0.908	0.430	0.474
Drms (cm)	0.269	0.427	1.589	0.449	0.763	1.700
Ia(m/s)	0.243	0.365	1.501	0.529	0.266	0.503
Ic (-)	0.318	0.396	1.247	0.729	0.301	0.413
Spe ED (cm^2/s)	0.192	0.375	1.951	0.404	0.401	0.991
CAV (cm/s)	0.500	0.289	0.578	0.966	0.272	0.281
ASI (m/s)	0.466	0.409	0.879	1.081	0.352	0.326
VSI (cm)	0.368	0.400	1.087	0.843	0.331	0.393
Ih (cm)	0.362	0.390	1.075	0.798	0.369	0.463
SMA (m/s^2)	0.399	0.418	1.046	0.938	0.378	0.403
SMV (cm/s)	0.387	0.402	1.039	0.903	0.291	0.322
EDA (m/s^2)	0.431	0.416	0.966	1.023	0.346	0.338
A95 (m/s^2)	0.428	0.417	0.975	1.010	0.360	0.357
Tpred (s)	-0.160	0.565	3.532	0.063	0.992	15.815
Tm (S)	0.318	0.552	1.737	0.721	0.934	1.297
Sa (0,2;5%) (m/s^2)	0.377	0.434	1.149	0.856	0.520	0.607
Sa (0,4;5%) (m/s2)	0.409	0.431	1.053	0.942	0.483	0.512
Sa (0,6;5%) (m/s2)	0.342	0.443	1.296	0.888	0.319	0.359
Sa (1;5%)(m/s2)	0.344	0.398	1.158	0.773	0.365	0.473
Sa (2;5%) (m/s2)	0.302	0.384	1.274	0.595	0.535	0.900
Sv (0,2;5%) (m/S)	0.356	0.437	1.230	0.778	0.578	0.744
Sv (0,4;5%) (S)	0.414	0.432	1.044	0.938	0.513	0.546
Sv (0,6;5%) (S)	0.356	0.442	1.242	0.912	0.354	0.388
Sv (1;5%) (S)	0.377	0.396	1.049	0.852	0.342	0.402
Sv (2;5%) (S)	0.321	0.405	1.263	0.712	0.428	0.601
Sd (0,2;5%) (m/S)	0.378	0.434	1.148	0.856	0.519	0.607
Sd (0,4;5%) (S)	0.409	0.431	1.054	0.942	0.482	0.512
Sd (0,6;5%)(S)	0.342	0.443	1.296	0.888	0.318	0.358
Sd (1;5%) (S)	0.344	0.398	1.157	0.772	0.365	0.473
Sd (2;5%) (S)	0.301	0.384	1.276	0.592	0.537	0.907

Table C.7 Practically, Efficiency and Proficiency of first wall H=6.5massuming relative horizontal displacement as damage measure of structure.

	Flat			Slope		
	(b)	(σ)	(ξ)	(b)	(σ)	(ξ)
PGA (m/s2)	1.630	0.436	0.267	1.182	0.366	0.310
PGV (cm/s)	1.278	0.582	0.455	0.961	0.360	0.375
PGD (cm)	0.833	1.036	1.244	0.643	0.711	1.106
Arms (m/s^2)	1.802	0.511	0.283	1.286	0.454	0.353
Vrms (cm/s)	1.377	0.758	0.551	1.058	0.467	0.441
Drms (cm)	0.633	1.270	2.006	0.512	0.883	1.725
Ia(m/s)	0.846	0.281	0.332	0.614	0.269	0.439
Ic (-)	1.176	0.297	0.252	0.849	0.300	0.353
Spe ED (cm^2/s)	0.604	0.760	1.258	0.467	0.455	0.974
CAV (cm/s)	1.502	0.462	0.308	1.110	0.319	0.287
ASI (m/s)	1.746	0.413	0.236	1.254	0.382	0.305
VSI (cm)	1.280	0.629	0.491	0.971	0.377	0.388
Ih (cm)	1.195	0.713	0.597	0.918	0.425	0.463
SMA (m/s^2)	1.539	0.384	0.250	1.096	0.394	0.360
SMV (cm/s)	1.389	0.531	0.382	1.045	0.313	0.299
EDA (m/s^2)	1.641	0.431	0.262	1.195	0.351	0.294
A95 (m/s^2)	1.628	0.440	0.270	1.180	0.369	0.313
Tpred (s)	0.253	1.547	6.113	0.003	1.142	389.775
Tm (S)	0.621	1.527	2.457	0.785	1.082	1.378
Sa (0,2;5%) (m/s^2)	1.411	0.686	0.486	1.000	0.572	0.572
Sa (0,4;5%) (m/s2)	1.504	0.706	0.470	1.082	0.560	0.518
Sa (0,6;5%) (m/s2)	1.358	0.590	0.434	1.023	0.365	0.357
Sa (1;5%)(m/s2)	1.171	0.677	0.578	0.885	0.433	0.489
Sa (2;5%) (m/s2)	0.862	0.974	1.130	0.680	0.626	0.922
Sv (0,2;5%) (m/S)	1.294	0.783	0.605	0.910	0.643	0.707
Sv (0,4;5%) (S)	1.519	0.722	0.476	1.076	0.594	0.552
Sv (0,6;5%) (S)	1.412	0.595	0.422	1.051	0.402	0.382
Sv (1;5%) (S)	1.306	0.612	0.469	0.979	0.397	0.406
Sv (2;5%) (S)	1.069	0.780	0.730	0.822	0.486	0.591
Sd (0,2;5%) (m/S)	1.412	0.685	0.485	1.001	0.572	0.571
Sd (0,4;5%) (S)	1.504	0.706	0.469	1.081	0.559	0.517
Sd (0,6;5%)(S)	1.359	0.590	0.435	1.023	0.365	0.357
Sd (1;5%) (S)	1.170	0.678	0.580	0.884	0.433	0.490
Sd (2;5%) (S)	0.858	0.977	1.139	0.677	0.629	0.929

Table C.8 Practically, Efficiency and Proficiency of first wall H=6.5m assuming tilting as damage measure of structure.

	Flat			Slope		
	(b)	(σ)	(ξ)	(b)	(σ)	(ξ)
PGA (m/s2)	0.610	0.414	0.679	0.958	0.332	0.347
PGV (cm/s)	0.503	0.403	0.801	0.796	0.271	0.340
PGD (cm)	0.393	0.431	1.098	0.538	0.566	1.052
Arms (m/s^2)	0.613	0.484	0.790	1.036	0.408	0.394
Vrms (cm/s)	0.557	0.428	0.768	0.881	0.354	0.401
Drms (cm)	0.342	0.500	1.464	0.437	0.705	1.616
Ia(m/s)	0.333	0.347	1.042	0.496	0.274	0.553
Ic (-)	0.444	0.389	0.876	0.685	0.296	0.432
Spe ED (cm^2/s)	0.269	0.345	1.282	0.388	0.347	0.894
CAV (cm/s)	0.650	0.266	0.410	0.898	0.302	0.337
ASI (m/s)	0.660	0.403	0.611	1.016	0.344	0.339
VSI (cm)	0.531	0.369	0.694	0.804	0.286	0.356
Ih (cm)	0.517	0.358	0.692	0.762	0.321	0.421
SMA (m/s^2)	0.556	0.433	0.780	0.878	0.374	0.425
SMV (cm/s)	0.561	0.369	0.659	0.863	0.234	0.271
EDA (m/s^2)	0.615	0.413	0.671	0.970	0.316	0.326
A95 (m/s^2)	0.608	0.417	0.685	0.956	0.334	0.349
Tpred (s)	-0.055	0.695	12.744	0.106	0.935	8.788
Tm (S)	0.567	0.644	1.135	0.764	0.868	1.135
Sa (0,2;5%) (m/s^2)	0.516	0.473	0.916	0.791	0.518	0.654
Sa (0,4;5%) (m/s2)	0.584	0.441	0.756	0.886	0.463	0.522
Sa (0,6;5%) (m/s2)	0.518	0.428	0.825	0.845	0.281	0.332
Sa (1;5%)(m/s2)	0.488	0.380	0.780	0.730	0.343	0.470
Sa (2;5%) (m/s2)	0.412	0.384	0.932	0.570	0.487	0.854
Sv (0,2;5%) (m/S)	0.475	0.491	1.035	0.713	0.575	0.807
Sv (0,4;5%) (S)	0.580	0.455	0.785	0.876	0.499	0.569
Sv (0,6;5%) (S)	0.534	0.435	0.814	0.869	0.313	0.360
Sv (1;5%) (S)	0.536	0.373	0.696	0.807	0.316	0.392
Sv (2;5%) (S)	0.462	0.382	0.828	0.682	0.377	0.553
Sd (0,2;5%) (m/S)	0.516	0.473	0.915	0.791	0.517	0.654
Sd (0,4;5%) (S)	0.584	0.441	0.756	0.886	0.462	0.522
Sd (0,6;5%)(S)	0.518	0.428	0.825	0.845	0.281	0.332
Sd (1;5%) (S)	0.487	0.380	0.780	0.730	0.344	0.471
Sd (2;5%) (S)	0.411	0.385	0.936	0.568	0.489	0.861

Table C.9 Practically, Efficiency and Proficiency of first wall H=3.6m both backfills combined both damages (relative horizontal displacement, tilting).

	Relative horizontal displacement			Tilting		
	(b)	(σ)	(ξ)	(b)	(σ)	(ξ)
PGA (m/s2)	1.209	0.726	0.601	0.695	0.430	0.619
PGV (cm/s)	0.926	0.809	0.874	0.552	0.448	0.811
PGD (cm)	0.595	1.019	1.714	0.371	0.561	1.514
Arms (m/s2)	1.323	0.766	0.579	0.764	0.448	0.586
Vrms (cm/s)	0.990	0.886	0.895	0.609	0.476	0.783
Drms (cm)	0.425	1.158	2.721	0.285	0.642	2.249
Ia(m/s)	0.631	0.675	1.069	0.361	0.405	1.120
Ic (-)	0.874	0.687	0.787	0.501	0.409	0.815
Spe ED (cm2/s)	0.442	0.868	1.965	0.267	0.476	1.781
CAV (cm/s)	1.138	0.701	0.617	0.653	0.417	0.638
ASI (m/s)	1.307	0.705	0.540	0.743	0.427	0.575
VSI (cm)	0.959	0.784	0.817	0.574	0.428	0.746
Ih (cm)	0.894	0.824	0.922	0.540	0.446	0.826
SMA (m/s2)	1.152	0.696	0.605	0.654	0.424	0.647
SMV (cm/s)	1.019	0.775	0.761	0.604	0.431	0.713
EDA (m/s2)	1.217	0.726	0.597	0.700	0.429	0.613
A95 (m/s2)	1.209	0.727	0.601	0.694	0.430	0.619
Tpred (s)	0.104	1.295	12.450	0.010	0.752	72.349
Tm (S)	0.471	1.279	2.717	0.418	0.728	1.742
Sa (0,2;5%) (m/s2)	1.128	0.716	0.635	0.627	0.452	0.722
Sa (0,4;5%) (m/s2)	1.113	0.832	0.748	0.640	0.488	0.763
Sa (0,6;5%) (m/s2)	1.023	0.760	0.743	0.596	0.437	0.732
Sa (1;5%)(m/s2)	0.890	0.786	0.883	0.532	0.431	0.811
Sa (2;5%) (m/s2)	0.646	0.951	1.472	0.403	0.514	1.275
Sv (0,2;5%) (m/S)	1.050	0.752	0.716	0.576	0.479	0.833
Sv (0,4;5%) (S)	1.125	0.839	0.746	0.640	0.499	0.779
Sv (0,6;5%) (S)	1.044	0.787	0.754	0.604	0.459	0.761
Sv (1;5%) (S)	0.983	0.769	0.782	0.582	0.428	0.735
Sv (2;5%) (S)	0.803	0.849	1.058	0.488	0.459	0.941
Sd (0,2;5%) (m/S)	1.128	0.716	0.634	0.627	0.452	0.722
Sd (0,4;5%) (S)	1.113	0.832	0.748	0.640	0.488	0.763
Sd (0,6;5%) (S)	1.023	0.761	0.743	0.596	0.437	0.732
Sd (1;5%) (S)	0.889	0.787	0.885	0.531	0.431	0.812
Sd (2;5%) (S)	0.643	0.953	1.482	0.401	0.515	1.284

Table C.10 Practically, Efficiency and Proficiency of second wall H=4.5m both backfills combined both damages (relative horizontal displacement, tilting).

	Relative horizontal displacement			tilting		
	(b)	(σ)	(ξ)	(b)	(σ)	(ξ)
PGA (m/s2)	1.374	0.821	0.598	0.974	0.763	0.784
PGV (cm/s)	1.069	0.893	0.835	0.765	0.795	1.039
PGD (cm)	0.691	1.137	1.644	0.493	0.943	1.913
Arms (m/s2)	1.506	0.863	0.573	1.081	0.775	0.717
Vrms (cm/s)	1.134	0.994	0.876	0.813	0.853	1.049
Drms (cm)	0.513	1.291	2.515	0.376	1.032	2.746
Ia(m/s)	0.725	0.738	1.018	0.512	0.724	1.415
Ic (-)	1.001	0.759	0.758	0.710	0.730	1.028
Spe ED (cm2/s)	0.510	0.963	1.888	0.360	0.846	2.348
CAV (cm/s)	1.317	0.755	0.573	0.926	0.736	0.795
ASI (m/s)	1.489	0.790	0.531	1.054	0.748	0.710
VSI (cm)	1.088	0.888	0.816	0.772	0.800	1.036
Ih (cm)	1.017	0.929	0.914	0.721	0.824	1.143
SMA (m/s2)	1.309	0.787	0.601	0.925	0.748	0.809
SMV (cm/s)	1.171	0.858	0.733	0.832	0.781	0.939
EDA (m/s2)	1.384	0.819	0.591	0.982	0.761	0.774
A95 (m/s2)	1.371	0.823	0.600	0.972	0.764	0.786
Tpred (s)	0.193	1.467	7.608	0.095	1.152	12.158
Tm (S)	0.527	1.451	2.752	0.374	1.141	3.046
Sa (0,2;5%) (m/s2)	1.250	0.852	0.682	0.878	0.788	0.898
Sa (0,4;5%) (m/s2)	1.272	0.934	0.734	0.901	0.827	0.918
Sa (0,6;5%) (m/s2)	1.161	0.861	0.742	0.828	0.780	0.942
Sa (1;5%)(m/s2)	0.998	0.909	0.911	0.706	0.814	1.154
Sa (2;5%) (m/s2)	0.739	1.071	1.450	0.524	0.905	1.726
Sv (0,2;5%) (m/S)	1.162	0.892	0.768	0.812	0.814	1.002
Sv (0,4;5%) (S)	1.286	0.940	0.731	0.912	0.829	0.910
Sv (0,6;5%) (S)	1.196	0.878	0.734	0.853	0.789	0.924
Sv (1;5%) (S)	1.108	0.883	0.797	0.783	0.800	1.022
Sv (2;5%) (S)	0.911	0.963	1.057	0.644	0.845	1.313
Sd (0,2;5%) (m/S)	1.251	0.852	0.681	0.879	0.788	0.897
Sd (0,4;5%) (S)	1.272	0.934	0.734	0.901	0.827	0.918
Sd (0,6;5%)(S)	1.161	0.862	0.742	0.828	0.780	0.942
Sd (1;5%) (S)	0.997	0.909	0.912	0.705	0.814	1.155
Sd (2;5%) (S)	0.735	1.073	1.460	0.522	0.906	1.736

Table C.11 Practically, Efficiency and Proficiency of third wall H=5.5m both backfills combined both damages (relative horizontal displacement, tilting).

	Relative horizontal displacement			tilting		
	(b)	(σ)	(ξ)	(b)	(σ)	(ξ)
PGA (m/s2)	1.617	0.844	0.522	0.721	0.495	0.687
PGV (cm/s)	1.251	0.951	0.760	0.587	0.493	0.840
PGD (cm)	0.846	1.214	1.434	0.428	0.567	1.323
Arms (m/s^2)	1.779	0.893	0.502	0.754	0.548	0.727
Vrms (cm/s)	1.358	1.044	0.769	0.640	0.529	0.827
Drms (cm)	0.666	1.393	2.090	0.359	0.642	1.789
Ia(m/s)	0.846	0.757	0.894	0.386	0.443	1.147
Ic (-)	1.172	0.774	0.660	0.523	0.470	0.898
Spe ED (cm^2/s)	0.603	1.025	1.699	0.298	0.482	1.617
CAV (cm/s)	1.524	0.801	0.526	0.733	0.402	0.548
ASI (m/s)	1.715	0.858	0.500	0.773	0.490	0.634
VSI (cm)	1.265	0.958	0.758	0.605	0.479	0.792
Ih (cm)	1.185	1.006	0.848	0.580	0.482	0.831
SMA (m/s^2)	1.517	0.837	0.552	0.669	0.502	0.751
SMV (cm/s)	1.371	0.905	0.660	0.645	0.471	0.731
EDA (m/s^2)	1.628	0.843	0.518	0.727	0.493	0.679
A95 (m/s^2)	1.615	0.846	0.524	0.719	0.497	0.692
Tpred (s)	0.409	1.652	4.040	0.049	0.809	16.612
Tm (S)	0.562	1.646	2.930	0.519	0.775	1.491
Sa (0,2;5%) (m/s^2)	1.409	0.976	0.693	0.617	0.553	0.896
Sa (0,4;5%) (m/s2)	1.457	1.041	0.715	0.676	0.539	0.798
Sa (0,6;5%) (m/s2)	1.333	0.950	0.713	0.615	0.506	0.823
Sa (1;5%)(m/s2)	1.157	0.989	0.855	0.558	0.486	0.871
Sa (2;5%) (m/s2)	0.863	1.179	1.367	0.448	0.530	1.184
Sv (0,2;5%) (m/S)	1.303	1.028	0.789	0.567	0.574	1.014
Sv (0,4;5%) (S)	1.472	1.049	0.713	0.676	0.549	0.813
Sv (0,6;5%) (S)	1.382	0.957	0.692	0.634	0.513	0.810
Sv (1;5%) (S)	1.290	0.949	0.736	0.614	0.479	0.779
Sv (2;5%) (S)	1.059	1.051	0.993	0.516	0.508	0.983
Sd (0,2;5%) (m/S)	1.409	0.976	0.692	0.617	0.553	0.896
Sd (0,4;5%) (S)	1.456	1.041	0.715	0.675	0.539	0.798
Sd (0,6;5%)(S)	1.333	0.950	0.713	0.615	0.506	0.823
Sd (1;5%) (S)	1.156	0.990	0.857	0.558	0.486	0.871
Sd (2;5%) (S)	0.859	1.182	1.376	0.447	0.531	1.190

Table C.12 Practically, Efficiency and Proficiency of fourth wall H=6.5m both backfills combined both damages (relative horizontal displacement, tilting).

	Relative horizontal displacement			tilting		
	(b)	(σ)	(ξ)	(b)	(σ)	(ξ)
PGA (m/s2)	1.406	0.663	0.472	0.784	0.449	0.573
PGV (cm/s)	1.120	0.706	0.630	0.650	0.427	0.657
PGD (cm)	0.738	1.004	1.360	0.465	0.542	1.164
Arms (m/s^2)	1.544	0.713	0.462	0.824	0.512	0.621
Vrms (cm/s)	1.217	0.802	0.659	0.719	0.463	0.645
Drms (cm)	0.573	1.175	2.052	0.389	0.634	1.629
Ia(m/s)	0.730	0.600	0.822	0.415	0.398	0.959
Ic (-)	1.013	0.611	0.604	0.565	0.426	0.754
Spe ED (cm^2/s)	0.535	0.799	1.494	0.328	0.418	1.274
CAV (cm/s)	1.306	0.657	0.503	0.774	0.369	0.477
ASI (m/s)	1.500	0.662	0.442	0.838	0.447	0.533
VSI (cm)	1.125	0.727	0.646	0.668	0.412	0.617
Ih (cm)	1.056	0.772	0.731	0.639	0.416	0.651
SMA (m/s^2)	1.317	0.659	0.501	0.717	0.472	0.659
SMV (cm/s)	1.217	0.676	0.556	0.712	0.400	0.561
EDA (m/s^2)	1.418	0.657	0.464	0.793	0.444	0.561
A95 (m/s^2)	1.404	0.665	0.474	0.782	0.451	0.577
Tpred (s)	0.125	1.412	11.284	0.026	0.828	31.915
Tm (S)	0.703	1.377	1.958	0.666	0.773	1.161
Sa (0,2;5%) (m/s^2)	1.206	0.814	0.675	0.654	0.543	0.830
Sa (0,4;5%) (m/s2)	1.293	0.816	0.631	0.735	0.506	0.689
Sa (0,6;5%) (m/s2)	1.191	0.710	0.597	0.682	0.444	0.651
Sa (1;5%)(m/s2)	1.028	0.761	0.740	0.609	0.435	0.714
Sa (2;5%) (m/s2)	0.771	0.946	1.227	0.491	0.488	0.994
Sv (0,2;5%) (m/S)	1.102	0.876	0.795	0.594	0.574	0.966
Sv (0,4;5%) (S)	1.297	0.835	0.644	0.728	0.526	0.723
Sv (0,6;5%) (S)	1.231	0.722	0.587	0.701	0.456	0.650
Sv (1;5%) (S)	1.142	0.727	0.636	0.671	0.423	0.630
Sv (2;5%) (S)	0.945	0.817	0.865	0.572	0.447	0.781
Sd (0,2;5%) (m/S)	1.206	0.813	0.674	0.654	0.542	0.829
Sd (0,4;5%) (S)	1.293	0.816	0.631	0.735	0.506	0.689
Sd (0,6;5%)(S)	1.191	0.710	0.597	0.682	0.444	0.651
Sd (1;5%) (S)	1.027	0.762	0.741	0.609	0.435	0.714
Sd (2;5%) (S)	0.767	0.948	1.236	0.489	0.489	1.000

Table C.13 Practically, Efficiency and Proficiency both damages (relative horizontal displacement, tilting).all the walls combined together

	Relative horizontal displacement			tilting		
	(b)	(σ)	(ξ)	(b)	(σ)	(ξ)
PGA (m/s2)	1.401	0.796	0.568	0.793	0.674	0.850
PGV (cm/s)	1.091	0.868	0.795	0.638	0.680	1.066
PGD (cm)	0.717	1.105	1.540	0.439	0.770	1.754
Arms (m/s^2)	1.538	0.838	0.545	0.856	0.701	0.819
Vrms (cm/s)	1.175	0.954	0.812	0.695	0.712	1.024
Drms (cm)	0.544	1.258	2.311	0.352	0.840	2.385
Ia(m/s)	0.733	0.731	0.997	0.419	0.643	1.537
Ic (-)	1.015	0.745	0.734	0.575	0.654	1.138
Spe ED (cm^2/s)	0.522	0.936	1.792	0.313	0.695	2.217
CAV (cm/s)	1.321	0.763	0.578	0.771	0.637	0.826
ASI (m/s)	1.503	0.786	0.523	0.852	0.669	0.785
VSI (cm)	1.109	0.866	0.781	0.655	0.673	1.029
Ih (cm)	1.038	0.907	0.873	0.620	0.684	1.102
SMA (m/s^2)	1.324	0.778	0.588	0.741	0.675	0.910
SMV (cm/s)	1.195	0.835	0.699	0.698	0.666	0.954
EDA (m/s^2)	1.412	0.794	0.563	0.800	0.672	0.840
A95 (m/s^2)	1.400	0.798	0.570	0.792	0.675	0.852
Tpred (s)	0.208	1.451	6.987	-0.027	0.964	36.000
Tm (S)	0.566	1.433	2.534	0.494	0.939	1.900
Sa (0,2;5%) (m/s^2)	1.248	0.864	0.692	0.694	0.711	1.025
Sa (0,4;5%) (m/s2)	1.284	0.927	0.722	0.738	0.717	0.971
Sa (0,6;5%) (m/s2)	1.177	0.848	0.721	0.680	0.680	1.000
Sa (1;5%)(m/s2)	1.018	0.886	0.870	0.601	0.682	1.134
Sa (2;5%) (m/s2)	0.755	1.051	1.392	0.467	0.736	1.578
Sv (0,2;5%) (m/S)	1.154	0.909	0.788	0.637	0.732	1.149
Sv (0,4;5%) (S)	1.295	0.936	0.723	0.739	0.725	0.981
Sv (0,6;5%) (S)	1.213	0.863	0.712	0.698	0.689	0.988
Sv (1;5%) (S)	1.131	0.859	0.760	0.663	0.675	1.018
Sv (2;5%) (S)	0.930	0.941	1.012	0.555	0.700	1.262
Sd (0,2;5%) (m/S)	1.249	0.864	0.692	0.694	0.711	1.025
Sd (0,4;5%) (S)	1.283	0.927	0.722	0.738	0.717	0.972
Sd (0,6;5%)(S)	1.177	0.849	0.721	0.680	0.680	1.000
Sd (1;5%) (S)	1.017	0.887	0.872	0.601	0.682	1.135
Sd (2;5%) (S)	0.751	1.053	1.401	0.465	0.737	1.586

Table C.14 Lognormal parameters of fragility curves for different damage state assumed for wall H=3.6m

Damage state	Relative horizontal displacement						
	Flat backfill						
	1st threshold	Median 1st IM	Median 2nd IM	β_{tot}			
Minor	2%. H	0.761	0.348	1.41			
Moderate	5%. H	1.67	1.265	1.41			
Extensive	10%. H	2.370	1.958	1.41			
	Slope backfill						
	1st threshold	Median 1st IM	Median 2nd IM	β_{tot}			
Minor	2%. H	0.434	0.118	1.18			
Moderate	5%. H	1.351	1.034	1.18			
Extensive	10%. H	2.04	1.728	1.18			
Damage state	Tilting						
	Flat backfill						
	1st threshold	Median 1st IM	Median 2nd IM	2nd threshold	Median 1st IM	Median 2nd IM	β_{tot}
Minor	2%. θ	1.513	2.580	20%. θ	3.816	4.882	0.77
Moderate	5%. θ	2.429	3.496	50%. θ	4.732	5.799	0.77
Extensive	10%. θ	3.122	4.189	80%. θ	5.202	6.269	0.77
	Slope backfill						
	1st threshold	Median 1st IM	Median 2nd IM	2nd threshold	Median 1st IM	Median 2nd IM	β_{tot}
Minor	2%. θ	0.114	1.785	20%. θ	2.416828	4.088	0.97
Moderate	5%. θ	1.030	2.701	50%. θ	3.333118	5.004	0.97
Extensive	10%. θ	1.723	3.394	80%. θ	3.803122	5.474	0.97

Table C.15 Lognormal parameters of fragility curves for different damage state assumed for wall H=4.5m

Damage state	Relative horizontal displacement						
	Flat backfill						
	1st threshold	Median 1st IM	Median 2nd IM	β_{tot}			
Minor	2%. H	0.395	0.0237	1.58			
Moderate	5%. H	1.312	0.940	1.58			
Extensive	10%. H	2.005	1.633	1.58			
	Slope backfill						
	1st threshold	Median 1st IM	Median 2nd IM	β_{tot}			
Minor	2%. H	0.102	5.836	1.25			
Moderate	5%. H	1.018	6.752	1.25			
Extensive	10%. H	1.712	7.445	1.25			
Damage state	Tilting						
	Flat backfill						
	1st threshold	Median 1st IM	Median 2nd IM	2nd threshold	Median 1st IM	Median 2nd IM	β_{tot}
Minor	2%. θ	2.286	1.935	20%. θ	4.589	4.237	1.09
Moderate	5%. θ	3.202	2.851	50%. θ	5.505	5.153	1.09
Extensive	10%. θ	3.895	3.544	80%. θ	5.975	5.623	1.09
	Slope backfill						
	1st threshold	Median 1st IM	Median 2nd IM	2nd threshold	Median 1st IM	Median 2nd IM	β_{tot}
Minor	2%. θ	0.71	6.39	20%. θ	3.013	8.693	1.04
Moderate	5%. θ	1.626	7.307	50%. θ	3.929	9.609	1.04
Extensive	10%. θ	2.32	8.001	80%. θ	4.3995	10.079	1.04

Table C.16 Lognormal parameters of fragility curves for different damage state assumed for wall H=5.5m

Damage state	Relative horizontal displacement						
	Flat backfill						
	1st threshold	Median 1st IM	Median 2nd IM	β_{tot}			
Minor	2%. H	-0.291	5.447	1.93			
Moderate	5%. H	0.625	6.364	1.93			
Extensive	10%. H	1.319	7.057	1.93			
	Slope backfill						
	1st threshold	Median 1st IM	Median 2nd IM	β_{tot}			
Minor	2%. H	-0.155	-0.155	1.29			
Moderate	5%. H	0.762	0.762	1.29			
Extensive	10%. H	1.455	1.455	1.29			
Damage state	Tilting						
	Flat backfill						
	1st threshold	Median 1st IM	Median 2nd IM	2nd threshold	Median 1st IM	Median 2nd IM	β_{tot}
Minor	2%. θ	1.563	6.944	20%. θ	3.865	9.246	0.75
Moderate	5%. θ	2.479	7.861	50%. θ	4.781	10.163	0.75
Extensive	10%. θ	3.172	8.554	80%. θ	5.251	10.633	0.75
	Slope backfill						
	1st threshold	Median 1st IM	Median 2nd IM	2nd threshold	Median 1st IM	Median 2nd IM	β_{tot}
Minor	2%. θ	0.542	6.220	20%. θ	2.844	8.523	1.08
Moderate	5%. θ	1.458	7.136	50%. θ	3.760	9.439	1.08
Extensive	10%. θ	2.151	7.830	80%. θ	4.230	9.909	1.08

Table C.17 Lognormal parameters of fragility curves for different damage state assumed for wall H=6.5m

Damage state	Relative horizontal displacement						
	Flat backfill						
	1st threshold	Median 1st IM	Median 2nd IM	β_{tot}			
Minor	2%. H	-0.161	-0.454	1.59			
Moderate	5%. H	0.755	0.462	1.59			
Extensive	10%. H	1.448	1.152	1.59			
	Slope backfill						
	1st threshold	Median 1st IM	Median 2nd IM	β_{tot}			
Minor	2%. H	-0.220	5.531	1.22			
Moderate	5%. H	0.696	6.448	1.22			
Extensive	10%. H	1.389	7.141	1.22			
Damage state	Tilting						
	Flat backfill						
	1st threshold	Median 1st IM	Median 2nd IM	2nd threshold	Median 1st IM	Median 2nd IM	β_{tot}
Minor	2%. θ	2.345	6.076	20%. θ	4.647	10.103	0.84
Moderate	5%. θ	3.261	6.992	50%. θ	5.564	11.019	0.84
Extensive	10%. θ	3.954	7.686	80%. θ	6.034	11.489	0.84
	Slope backfill						
	1st threshold	Median 1st IM	Median 2nd IM	2nd threshold	Median 1st IM	Median 2nd IM	β_{tot}
Minor	2%. θ	0.268	5.532	20%. θ	3.264	4.333	1.04
Moderate	5%. θ	1.185	6.448	50%. θ	3.487	5.250	1.04
Extensive	10%. θ	1.878	7.141	80%. θ	3.957	5.720	1.04

Table C.18 Lognormal parameters of fragility curves for different damage state assumed for wall H=3.6m combined backfills

Damage state	Relative horizontal displacement						
	Both backfills						
	1st threshold	Median 1st IM	Median 2nd IM	β_{tot}			
Minor	2%. H	0.611	0.245	1.37			
Moderate	5%. H	1.527	1.161	1.37			
Extensive	10%. H	2.220	1.854	1.37			
Damage state	Tilting						
	Both backfills						
	1st threshold	Median 1st IM	Median 2nd IM	2nd threshold	Median 1st IM	Median 2nd IM	β_{tot}
Minor	2%. θ	0.725	0.502	20%. θ	3.027	2.804	0.89
Moderate	5%. θ	1.641	1.418	50%. θ	3.944	3.720	0.89
Extensive	10%. θ	2.334	2.111	80%. θ	4.414	4.191	0.89

Table C.19 Lognormal parameters of fragility curves for different damage state assumed for wall H=4.5m combined backfills

Damage state	Relative horizontal displacement						
	Both backfills						
	1st threshold	Median 1st IM	Median 2nd IM	β_{tot}			
Minor	2%. H	0.266	-0.082	1.44			
Moderate	5%. H	1.183	0.834	1.44			
Extensive	10%. H	1.876	1.528	1.44			
Damage state	Tilting						
	Both backfills						
	1st threshold	Median 1st IM	Median 2nd IM	2nd threshold	Median 1st IM	Median 2nd IM	β_{tot}
Minor	2%. θ	1.518	1.231	20%. θ	3.821	3.533	1.24
Moderate	5%. θ	2.434	2.147	50%. θ	4.737	4.450	1.24
Extensive	10%. θ	3.128	2.840	80%. θ	5.207	4.920	1.24

Table C.20 Lognormal parameters of fragility curves for different damage state assumed for wall H=5.5m combined backfills

Damage state	Relative horizontal displacement						
	Both backfills						
	1st threshold	Median 1st IM		Median 2nd IM		β_{tot}	
Minor	2%. H	-0.237		-0.506		1.72	
Moderate	5%. H	0.679		0.410		1.72	
Extensive	10%. H	1.372		1.103		1.72	
Damage state	Tilting						
	Both backfills						
	1st threshold	Median 1st IM	Median 2nd IM	2nd threshold	Median 1st IM	Median 2nd IM	β_{tot}
Minor	2%. θ	0.941	6.546	20%. θ	3.244	8.849	0.94
Moderate	5%. θ	1.858	7.462	50%. θ	4.160	9.765	0.94
Extensive	10%. θ	2.551	8.155	80%. θ	4.630	10.235	0.94

Table C. 21 Lognormal parameters of fragility curves for different damage state assumed for wall H=6.5m combined backfills

Damage state	Relative horizontal displacement						
	Both backfills						
	1st threshold	Median 1st IM		Median 2nd IM		β_{tot}	
Minor	2%. H	-0.186		-0.470		1.48	
Moderate	5%. H	0.730		0.447		1.48	
Extensive	10%. H	1.423		1.140		1.48	
Damage state	Tilting						
	Both backfills						
	1st threshold	Median 1st IM	Median 2nd IM	2nd threshold	Median 1st IM	Median 2nd IM	β_{tot}
Minor	2%. θ	1.196	6.846	20%. θ	3.498	9.148834	0.96
Moderate	5%. θ	2.112	7.763	50%. θ	4.415	10.06512	0.96
Extensive	10%. θ	2.805	8.456	80%. θ	4.885	10.53513	0.96

Table C.22 Lognormal parameters of fragility curves for different damage state assumed for all walls combined together

Damage state	Relative horizontal displacement						
	Both backfills						
	1st threshold	Median 1st IM	Median 2nd IM	β_{tot}			
Minor	2%. H	0.082	-0.229	1.53			
Moderate	5%. H	0.998	0.688	1.53			
Extensive	10%. H	1.691	1.381	1.53			
Damage state	Tilting						
	Both backfills						
	1st threshold	Median 1st IM	Median 2nd IM	2nd threshold	Median 1st IM	Median 2nd IM	β_{tot}
Minor	2%. θ	1.145	0.882	20%. θ	3.498	3.412	1.08
Moderate	5%. θ	2.061	1.798	50%. θ	4.415	4.328	1.08
Extensive	10%. θ	2.754	2.491	80%. θ	4.885	4.798	1.08

References

ARGYROUDIS, Sotirios; KAYNIA, Amir M.; PITILAKIS, Kyriazis. *Development of fragility functions for geotechnical constructions: application to cantilever retaining walls*. *Soil dynamics and earthquake engineering*, 2013, 50: 106-116.

DEYANOVA, Manya; LAI, Carlo G.; MARTINELLI, Mario. Displacement–based parametric study on the seismic response of gravity earth-retaining walls. *Soil Dynamics and Earthquake Engineering*, 2016, 80: 210-224.

GREEN, R. A.; EBELING, R. M. *Modeling the dynamic response of cantilever earth-retaining walls using FLAC*. In: *3rd International Symposium on FLAC: Numerical Modeling in Geomechanics, Sudbury, Canada*. 2003.

GREEN, Russell A.; EBELING, Robert M. *Seismic analysis of cantilever retaining walls, phase i*. MICHIGAN UNIV ANN ARBOR DEPT OF CIVIL AND ENVIRONMENTAL ENGINEERING, 2002.

KAKDERI, Kalliopi; PITILAKIS, Kyriazis. *Seismic analysis and fragility curves of gravity waterfront structures*. 2010.

ZAMIRAN, Siavash; OSOULI, Abdolreza. Fragility Analysis of Seismic Response of Cantilever Retaining Walls with Cohesive and Cohesion Less Backfill Materials. In: *IFCEE 2018*. 2018. p. 139-146.

WOTRING, Donald; ANDERSEN, Glen. Displacement-Based Design Criteria for Gravity Retaining Walls in Light of Recent Earthquakes. 2001.

MEIDANI, M., et al. Granule shape effect on the shear modulus and damping ratio of mixed gravel and clay. 2008.

Itasca Consulting Group, Inc., Minneapolis, MN, USA*, FLAC version 8.0*, 2016

PADGETT, Jamie E.; NIELSON, Bryant G.; DESROCHES, Reginald. *Selection of optimal intensity measures in probabilistic seismic demand models of highway bridge portfolios*. *Earthquake Engineering & Structural Dynamics*, 2008, 37.5: 711-725.

CHOUDHURY, D.; NIMBALKAR, S. *Seismic passive resistance by pseudo-dynamic method*. *Geotechnique*, 2005, 55.9: 699-702.

SUBBA RAO, K. S.; CHOUDHURY, Deepankar. *Seismic passive earth pressures in soils*. *Journal of Geotechnical and Geoenvironmental Engineering*, 2005, 131.1: 131-135.

FEMA. Hazus-MH 2.1 technical manual. *Multi-hazard loss estimation methodology, earthquake model*, 2013.

CHOUDHURY, Deepankar; NIMBALKAR, *Sanjay S. Pseudo-dynamic approach of seismic active earth pressure behind retaining wall*. *Geotechnical & Geological Engineering*, 2006, 24.5: 1103.

MIRAEI, M.; JAFARIAN, Y. *Fragility curves for assessing the seismic vulnerability of gravity quay walls*. In: *4th ECCOMAS Thematic Conference on Computational Methods in Structural Dynamics and Earthquake Engineering, Kos Island*. 2013.

OSOULI, Abdolreza; ZAMIRAN, Siavash. *The effect of backfill cohesion on seismic response of cantilever retaining walls using fully dynamic analysis*. *Computers and Geotechnics*, 2017, 89: 143-152.

GREEN, Russell A.; OLGUN, C. Guney; CAMERON, Wanda I. *Response and modelling of cantilever retaining walls subjected to seismic motions*. *Computer-Aided Civil and Infrastructure Engineering*, 2008, 23.4: 309-322.

SEBAALY, Graziella. *Numerical Modeling of the Characteristic Seismic Behaviour of Retaining Walls*. 2013. PhD Thesis.

ZAMIRAN, Siavash; OSOULI, Abdolreza. *Seismic motion response and fragility analyses of cantilever retaining walls with cohesive backfill*. *Soils and Foundations*, 2018, 58.2: 412-426.

SILVESTRI, Francesco; MORACI, Nicola (ed.). *Earthquake Geotechnical Engineering for Protection and Development of Environment and Constructions: Proceedings of the 7th International Conference on Earthquake Geotechnical Engineering, (ICEGE 2019), June 17-20, 2019, Rome, Italy*. CRC Press, 2019.